Mechanism of resistance to cisplatin in ovarian cancer

DISSERTATION

zur Erlangung des akademischen Grades
"Doctor rerum naturalium“
Dr. rer. nat.

Eingereicht an der
Fakultät für Mathematik, Informatik und Naturwissenschaften
der Universität Hamburg

vorgelegt von
Priyanka Nair, M. Sc.
geboren in Pune (Indien)

Hamburg
2023

Die vorgelegte Dissertation wurde von Mai 2017 bis März 2022 am Institut für Biochemie und Molekularbiologie am Fachbereich Chemie, der Fakultät für Mathematik, Informatik und Naturwissenschaften an der Universität Hamburg unter Anleitung von Prof. Dr. Zoya Ignatova angefertigt.

The submitted dissertation was conducted from May 2017 until March 2022 at the Institute of Biochemistry and Molecular Biology at the Department of Chemistry of the Faculty of Mathematics, Informatics, and Natural Sciences at the University of Hamburg under the supervision of Prof. Dr. Zoya Ignatova.

Dissertations gutachter / *dissertation reviewers*:

1. Gutachterin / *first reviewer*: **Prof. Dr. Zoya Ignatova**, Institute of Biochemistry and Molecular Biology, Universität Hamburg
2. Gutachterin / *second reviewer:* **Prof. Dr. Meliha Karsak**, Center for Molecular Neurobiology Hamburg (ZMNH), University Medical Center Hamburg-Eppendorf (UKE)

Mitglieder der Prüfungskommission (*Examination commission members*)

1) Prof Dr Zoya Ignatova, University of Hamburg,
   zoya.ignatova@uni-hamburg.de

2) Prof Dr Agnes Weiß, University of Hamburg,
   agnes.weiss@uni-hamburg.de

3) Prof Dr Peter Heisig, University of Hamburg,

   Peter.Heisig@uni-hamburg.de

Date of Oral Examination: 18.08.23

Teile dieser Arbeit wurden in folgenden Publikationen veröffentlicht:
Parts of this work are submitted in the following scientific articles:

Research articles

1. **Priyanka Nair**, Leonardo Santos, Ryder F. Whittaker Hawkins, Dörte Jechorek, Virginie Marchand, Megan C. DeWeerd, Nikhil Bharti, Moritz Freyberg, Yuri Motorin, Atanas Ignatov, Robert Rottapel and Zoya Ignatova. GCN2 activation by ribosome collisions confers cisplatin resistance in ovarian cancer. (Reviewed and under revision).

2. Thomas E Gorochowski, Irina Chelysheva, Mette Eriksen, **Priyanka Nair**, Steen Pedersen, Zoya Ignatova. Absolute quantification of translational regulation and burden using combined sequencing approaches. Molecular Systems Biology (2019)15 e8719

Contents

Table of Figures

List of Tables

List of Abbreviations

A	Adenine
A-site	Aminoacyl site
bp	Basepair
C	Cytosine
cDNA	Complementary DNA
Cis-Pt	Cisplatin
DNA	Deoxyribonucleic acid
DDAs	DNA damaging agents
eEFs	Eukaryotic elongation factors
eIFs	Eukaryotic initiation factors
EOC	Epithelial ovarian cancer
G	Guanine
GCN2	General control nonderepressible 2
ISR	Integrated stress response
JNK	c-Jun N-terminal kinase
MAPK	Mitogen-activated protein kinase
m^6A	N6-Methyladenosine
mRNA	Messenger RNA
miRNA	Micro RNA
ncRNA	Non-coding RNA
nt	Nucleotide
PIC	Preinitiation complex
PAGE	Polyacrylamide gel electrophoresis
P-site	Peptidyl site
RNA	Ribonucleic acid
RP	Ribosomal proteins
rRNA	Ribosomal RNA
T	Thymine

tRNA	Transfer RNA
Ribo-seq	Ribosome profiling
RPF	Ribosome protected fragment
RPM	Reads per million
RPKM	Reads per kilobase per million
RQC	Ribosome quality control
RSR	Ribotoxic stress response
SAPK	Stress activated protein kinase
U	Uracil
Ψ	Pseudouridine
UV	Ultraviolet

Summary

Cisplatin (cis-Pt) or cis diamminedichloroplatinum II is one of the most effective chemotherapeutic agents used in the treatment of many human malignances. But resistance to the drug is a major barrier to the successful use of the drug. Ovarian cancer, regarded as one of the most severe gynecological cancers impacting the female reproductive system, is a fatal malignancy with a low survival rate. Platinum-based drugs such as cis-Pt form the backbone of the currently available treatment offered to ovarian cancer patients. However, more than 70% of the patients relapse and develop resistance to the drug, leading to poor survival. In order to overcome this problem and maximize the benefits of the treatment, it is important to decipher the mechanism of resistance. This study aimed at understanding the underlying mechanisms involved in cis-Pt resistance. Using ovarian cancer cells, we investigated alterations to the RNA as an effect of treatment with cis-Pt. We demonstrate the activation of signaling pathways as an effect of cis-Pt induced RNA damage which leads to the resistant phenotype.

In this study, we unravel that general control non-derepressible (GCN2) mediates cis-Pt resistance in an ovarian cancer model, SKOV3 cells. We demonstrate that prolonged exposure to cis-Pt leads to ribosome collision and results in ribotoxic stress which is sensed and cascaded down by the mitogen-activated protein kinase (MAPK) pathway. In parallel, these collisions also activate the GCN2 arm of the integrated stress response (ISR). GCN2, is a regulator of the cells' stress response pathways which acts to resolve stress and aids cell survival. Under such conditions, GCN2 helps the cells mitigate the resulting stress. Depletion of GCN2 proves fatal to the cells when treated with cis-Pt and they succumb to the harmful effect of the drug emphasizing the critical role of GCN2. We show that treatment with cis-Pt activates the ZAKα - JNK axis of the MAPK signaling pathway. GCN2 acts as a protective barrier and helps the cells overcome the cis-Pt stress and acquire resistance. In absence of GCN2, the continuity and severity of the activated JNK induces apoptosis in SKOV3 cells. Our results also add to the evidence supporting the dual role of JNK in cell survival and apoptosis. We attribute activation of these signaling pathways as a result to the cis-Pt induced alteration of tRNA modification.

RNAs are decorated with vast variety of modifications and these modifications affect almost every biological process including resistance to chemotherapeutic agents. As a part of this

study, we also determined the effect of cis-Pt on the levels of the most prevalent mRNA modification, namely m^6A, and its regulators (the writers and erasers) in the ovarian cancer cell lines.

Our findings emphasize the role of RNA modifications and demands a comprehensive analysis of modifications on cellular RNAs. As a step in this direction, we also worked on a new approach to sequence tRNAs using the nanopore platform. Amongst all RNA molecules, tRNAs rank the highest for their modifications with an average of 13 modified bases in each tRNA. Commonly used sequencing methods today, however, are limited in their capacity to sequence these all so important molecules; modifications being the most important challenge affecting the outcome of these approaches. Aiming to develop more comprehensive way to analyze tRNAs, this study also dedicated efforts towards establishing a method to sequence tRNAs on the nanopore platform. The technique shows potential and will help sequence tRNAs with their modifications and will contribute to deciphering the role of dynamic modifications.

Zusammenfassung

Cisplatin (cis-Pt) oder cis-Diamindichlorplatin II ist eines der wirksamsten Chemotherapeutika zur Behandlung vieler bösartiger Tumorerkrankungen des Menschen. Die entwickelte Resistenz gegen das Medikament ist jedoch ein großes Hindernis für den erfolgreichen Einsatz. Eierstockkrebs, der als eine der schwersten gynäkologischen Krebserkrankungen des weiblichen Fortpflanzungssystems gilt ist eine tödliche bösartige Erkrankung mit einer niedrigen Überlebensrate. Medikamente auf Platinbasis wie cis-Pt bilden das Rückgrat der derzeit verfügbaren Behandlung für Eierstockkrebspatientinnen. Mehr als 70 % der Patientinnen erleiden jedoch einen Rückfall und entwickeln eine Resistenz gegen das Medikament, was zu einer niedrigen Überlebensrate führt. Um dieses Problem zu überwinden und den Nutzen der Behandlung zu maximieren, ist es wichtig den Mechanismus der Resistenz zu entschlüsseln. Ziel dieser Studie war es, die zugrunde liegenden Mechanismen der cis-Pt-Resistenz zu verstehen. Anhand von Eierstockkrebszellen untersuchten wir Veränderungen der RNA durch die Behandlung mit cis-Pt. Wir zeigen dass die Aktivierung von Signalwegen, die zu dem resistenten Phänotyp führen, durch cis-Pt induzierten RNA-Schäden ausgelöst wird.

In dieser Studie haben wir herausgefunden, dass GCN2 (General Control Non-Derepressible2) die cis-Pt-Resistenz in einem Eierstockkrebsmodell, den SKOV3-Zellen, vermittelt. Wir zeigen, dass eine längere Exposition gegenüber cis-Pt zu Ribosomenkollisionen führt und ribotoxischen Stress auslöst, der durch den Mitogen-aktivierten Proteinkinase (MAPK)-Stoffwechselweg wahrgenommen und kaskadiert wird. Parallel dazu aktivieren diese Kollisionen auch den GCN2-Arm der integrierten Stressreaktion (ISR). GCN2 ist ein Regulator der Stressreaktionswege der Zelle, der Stress entgegenwirkt und das Überleben der Zellen fördert. Unter solchen Bedingungen hilft GCN2 den Zellen, den entstehenden Stress abzumildern. Eine Erschöpfung von GCN2 erweist sich als fatal für die Zellen, wenn sie mit cis-Pt behandelt werden, und sie erliegen der schädlichen Wirkung des Medikaments, was die kritische Rolle von GCN2 unterstreicht. Wir zeigen, dass die Behandlung mit cis-Pt die ZAKα-JNK-Achse des MAPK-Signalweges aktiviert. GCN2 wirkt als schützende Barriere und hilft den Zellen, den cis-Pt-Stress zu überwinden und Resistenz zu erwerben. In Abwesenheit von GCN2 induziert die Kontinuität und Schwere der aktivierten JNK Apoptose in SKOV3-Zellen. Unsere Ergebnisse ergänzen die Belege für die doppelte Rolle von JNK beim Zellüberleben

und bei der Apoptose. Wir führen die Aktivierung dieser Signalwege auf die cis-Pt-induzierte Veränderung der tRNA-Modifikation zurück.

RNAs sind mit einer Vielzahl von Modifikationen versehen, und diese Modifikationen beeinflussen fast jeden biologischen Prozess, einschließlich der Resistenz gegen Chemotherapeutika. Im Rahmen dieser Studie haben wir auch die Auswirkungen von cis-Pt auf die Konzentrationen der am weitesten verbreiteten mRNA-Modifikation, nämlich m6A, und ihrer Regulatoren „Writers and erasers“ in den Zelllinien des Eierstockkrebses bestimmt.

Unsere Ergebnisse unterstreichen die Rolle von RNA-Modifikationen und erfordern eine umfassende Analyse von Modifikationen an zellulären RNAs. Als Schritt in diese Richtung arbeiteten wir auch an einem neuen Ansatz zur Sequenzierung von tRNAs unter Verwendung der Nanopore-Plattform. Unter allen RNA-Molekülen sind tRNAs die am stärksten modifizierten, mit durchschnittlich 13 modifizierten Basen pro tRNA. Die heute gebräuchlichen Sequenzierungsmethoden sind jedoch nur begrenzt in der Lage, diese so wichtigen Moleküle zu sequenzieren. Hierbei stellen die Modifikationen die größte Herausforderung dar, da diese das Ergebnis dieser Methoden beeinflusst. Mit dem Ziel, eine umfassendere Methode zur Analyse von tRNAs zu entwickeln, widmete sich diese Studie auch der Entwicklung einer Methode zur Sequenzierung von tRNAs auf der Nanopore-Plattform. Die Technik zeigt Potenzial und wird dazu beitragen, tRNAs mit ihren Modifikationen zu sequenzieren und die Rolle der dynamischen Modifikationen zu entschlüsseln.

1 Introduction

1.1 Cancer

Cancer, one of the most dreaded diseases in the world today, is a major cause of mortality and a barrier to achieving desirable life expectancy in most countries around the globe [1 2 3]. Having been discovered decades ago and despite immense advances in scientific knowledge and trials of promising new therapies, cancer still remains a major public health problem worldwide [2]. The Globocon estimates report 19.3 million new cases and 10 million deaths worldwide due to cancer in 2020. With the expected global cancer burden by 2040 being 28.4 million cases [1]. Cancer is a generic term used to describe a group of diseases, wherein cells from a specific part of the body grow abnormally and uncontrollably. These cancerous cells have the ability to go beyond their typical boundaries, invade adjoining parts of the body and also spread to other organs, a process known as metastasis. Unlike most other diseases, cancer is not caused by an entity that is foreign to one's body, rather the host's cells that have transformed into a pathological form [4]. Cancer can affect almost any part/ tissue of the body and is usually named by the body part where it originates even though it spreads to other parts. Breast cancer with an estimated 2.3 million new cases is the most commonly diagnosed cancer followed by lung, colorectal, prostate and stomach cancers [1].

According to World Health Organization (WHO), cancer may arise due to interaction between a person's genetic factors and 3 categories of external agents, including physical carcinogens (such as ultraviolet and ionizing radiation), chemical carcinogens (such as asbestos, tobacco smoke, aflatoxin, and arsenic) and biological carcinogens (infections from certain viruses, bacteria, or parasites) [5]. Currently, cancer diagnosis and its management is based on clinical confirmation of malignancy and on factors such as the site of origin, histotype, grade etc. [6]. Over the past decades the advances in molecular biology have dramatically changed our understanding of cancers. With increasing knowledge over the years, classification of cancer has also improved which has a strong implication on diagnosis and treatment or clinical management. Tumors are broadly classified in four ways : 1) by the tissue, organ and system 2) by the specific type, 3) by grade and 4) by the extent of spread or to stage [6]. Depending on the type and stage of cancer, treatment may involve either traditional ways such as surgery, chemotherapy, and radiation therapy or the more recently advanced therapeutic measures such

as targeted therapy, immunotherapy, hormone therapy, gene therapy etc. or even a combination of these. Despite the availability of new techniques, chemotherapy remains one of the important means to treat cancer till date. Cancer chemotherapy refers to the administration of cytotoxic chemicals, i.e. chemicals with cell killing properties, aiming to completely eradicate or at least reduce tumor [7]. It is an effective and widely used way to treat various cancers, in which one or more chemotherapeutic agents are used[5]. Chemotherapy aims to inhibit proliferation/multiplication of tumor cells and avoid metastasis. Various chemotherapeutic agents such as the alkylating agents, antimetabolites, antimicrotubular agents, antibiotics are used for chemotherapy in cancers. Among the various drugs used in chemotherapy, cisplatin, the first FDA-approved platinum compound for cancer treatment in 1978, is one of the most compelling ones [8 9].

1.2 Cisplatin - a common chemotherapeutic drug for solid cancers

Cisplatin (cis-diamminedichloroplatinum II), is a well-known drug widely employed in first-line chemotherapy treatment of various solid neoplasms such as testicular, ovarian, head and neck, bladder, lung, cervical [5 10]. The molecule was first discovered by Michele Peyrone in the 1840s [8] but it gained scientific recognition only in the 1960's after the accidental discovery by Rosenberg that it could inhibit cell division in Escherichia coli [5 8]. Thereafter they demonstrated cisplatin's ability to inhibit sarcoma and leukemia in mice [5]. Since then various studies have proven that cisplatin exerts anti-cancer activity and by the 1970s cisplatin earned a place as key ingredient in treatment of various cancers [8]. Cisplatin was the first metal based drug to be used for chemotherapeutic approaches [5] and has proven as an effective drug considered the most potential drug in the fight against cancer.

Structurally, cisplatin is a coordination compound with a square planar geometry, a small molecule composed of a platinum ion surrounded by four ligands, two adjacent chlorine and amine atoms [11 12]. The molecular structure of cisplatin determines the anticancer activity. Cisplatin is relatively stable due to its high chloride ion concentration and must be activated by a series of aquation reactions resulting in substitution of one or both the chloro groups with water molecules[10]. Once in the cytoplasm, where the chloride concentration is low, the two chlorides are readily replaced by water molecules. Being loosely bound, the water molecules can easily fall off forming a reactive species which then allows the platinum to target molecules including the sulphydryl groups on proteins and nitrogen donors on nucleic acids [10 8 13].

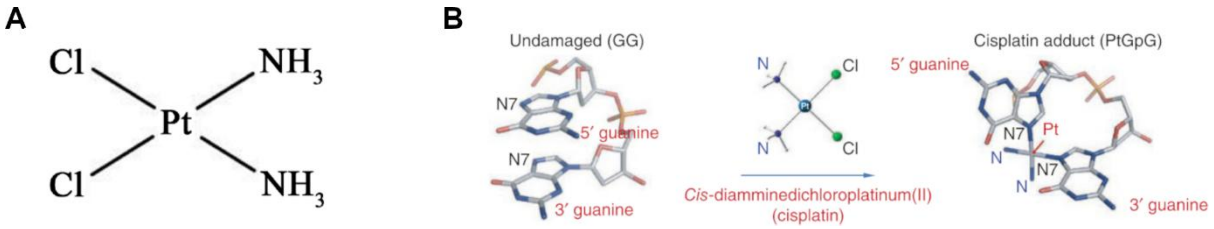

Figure 1.1 ***Cisplatin.*** *A) Structure of cis-Pt. B) Schematic depiction of an example of cisplatin binding with the N7 atoms of adjacent guanines to form a 1, 2 intrastrand crosslink. Adapted from Ummat et al., 2012* [14]

The primary target of cisplatin is considered to be DNA. The cytotoxic effect of cisplatin on cancer cells is attributed to its impediment of processes such as DNA replication and transcription, leading to cellular apoptosis. In its activated form cisplatin easily form bonds between the DNA bases which inhibits DNA synthesis and thereby growth. Cisplatin is commonly known to interact with DNA resulting in the formation of cisplatin-DNA adducts [8] [11] [15] [16] . Among the DNA lesions caused by cisplatin the most commonly reported is the 1,2-intrastrand crosslink, with the platinum covalently bound to the N7 positions of adjacent purine bases. Other platinum – DNA adducts include 1,3-intrastrand, interstrand and protein–DNA crosslinks[17]. Such crosslinks disrupt DNA replication and transcription and trigger various signaling pathways which could cause cell death [11] [18].

Being highly electrophilic cisplatin can also interact with other nucleophilic targets in the cytoplasm accounting for additional antineoplastic effects of the drug [15]. Researchers have proposed other mechanisms of cisplatin's toxicity including its effect on membrane transporters, the ability to modulate calcium signaling, induction of oxidative stress to name a few [5]. Studies have shown that like DNA, cisplatin can also bind to rRNA, tRNA, and other small RNA molecules. Numerous studies have demonstrated that cis-Pt toxicity can also originate from modification of proteins, small peptides, lipids and RNA and is not limited solely to modification of DNA[19]. Given the chemical similarity of the nucleobases it is no surprise that cisplatin can interact with RNA in a comparable manner. In fact, it has been shown that cis-Pt derived RNA adducts are more prevalent than DNA adducts [20] [21]. The cytotoxic effects of cis-Pt although attributed mainly to its ability to bind to DNA, it has been seen that less than 10% of intracellular cisplatin accumulates on DNA, indicating the possibility of involvement of other targets [22]. Various studies suggest that cisplatin could exert its effect through other mechanisms and more variable cellular targets beyond nuclear DNA [23] (more refs). In fact Hostetter et al (2012) demonstrated that the when comparing the in-cell Pt concentrations and Pt accumulation on poly(A)-mRNA, rRNA, total RNA, and DNA

quantified using ICP-MS showed a ~4–20 fold more Pt accumulation in total cellular RNA than in DNA[20]. Jordan and Carmo-Fonseca showed that cis-Pt inhibits rRNA synthesis and this is involved in the cytotoxicity of cis-Pt [17]. Melnikov et al showed that cisplatin intercalates to between the ribosome and mRNA in the mRNA channel impairing mRNA translocation which could be the reason for its cytotoxicity [19]. Cis-Pt binding within rRNA, tRNA, siRNA and miRNA has been demonstrated in vitro [22]. RNA molecules are important regulators affecting various levels of gene expression. Damage to the RNA or RNA-drug interactions can disrupt the RNA regulatory pathways and in turn impact fate of the cell [20]. Such studies demonstrate the potential ribotoxic roles of platinum which likely contributes to the cytotoxicity of the drug.

Even decades after its introduction cis-Pt still remains a cornerstone drug for treating neoplasms and is widely used as a first-in-line treatment in many solid cancers [15]. Despite its efficacy its use is largely hindered by severe toxic side effects. Approximately 40 specific toxicities of cisplatin are known including ototoxicity, neurotoxicity, gastrointestinal toxicity etc with nephrotoxicity being the most common [24]. Such adverse side effects reduce the quality of life patients and eventually requires lowering or even stopping the drug administration.
Another and important limitation to the usefulness of cis-Pt is the very high inherent and acquired resistance to the drug. Treatment with cis-Pt is often associated with initial therapeutic success but many patients are intrinsically resistant to cisplatin-based therapies. Moreover, a significant fraction of originally sensitive tumors eventually develops chemoresistance. A high incidence of chemoresistance forms the major challenge in the clinical use of cisplatin [10 12 21 25].

Intrinsic resistance to the drug has been observed commonly in colorectal, lung and prostate cancers whereas acquired resistance is seen more in ovarian cancer [10]. Ovarian cancer is a very good example of limitation of cisplatin as an anticancer drug wherein the patients initially respond well to therapy with an initial response rate of ~70% but unfortunately the tumors become resistant to the drug and the 5year survival rate drops to ~15-20% [10 18].

This resistance can be mediated by a number of cellular processes [14]. Various studies have attempted to define what causes resistance to the drug and described various factors that could be involved. The most often studied mechanisms of resistance to platinum therapy is increased DNA repair [26]. Increased excision of adducts by enhanced repair pathways or increased lesion bypass commonly leads to resistance. The reduction of drug accumulation in the cancer cells, decreased drug uptake, increased reflux or reaction with sulfhydryl molecules such as

glutathione and metallothioneins leading to drug inactivation are some other reported causes. Besides these factors, altered expression of proteins involved in signal transduction pathways which regulate the apoptotic pathway can also affect sensitivity to the drug [27] [28]. Galluzi et al (2012) have systematically classified alterations that account for cis-Pt resistant phenotype in tumor cells into broad categories - 1) Pre-target resistance, that involve steps preceding the binding of cisplatin to DNA, 2) On-target resistance, that directly relate to DNA– cisplatin adducts, 3) those concerning the lethal signaling pathway(s) elicited by cisplatin-mediated DNA damage (post-target resistance) and (4) Off-target resistance, affecting molecular circuitries that do not present obvious links with cisplatin-elicited signals [10]. Epitranscriptomic modifications of the RNA such as the m^6A are also shown to be associated with resistance to cis-Pt [29].

1.3 Ovarian cancer

Ovarian cancers are a heterogenous group of malignancies originating from or involving the ovaries or fallopian tube [30]. Being one of the most common cancers affecting females, ovarian cancer (OC) accounts for 1.6% of the newly diagnosed cases and 2.1% of the cancer deaths [1]. In early stages ovarian cancer is generally asymptomatic and more than 70% of the cases are not diagnosed until it has progressed to advanced stages [31] [32]. In spite of being less prevalent compared to other cancers such as breast cancer, it is known to have a worse prognosis and a higher mortality rate. The high mortality rates have been attributed, in most cases, to slow and asymptomatic growth, delayed onset of symptoms and lack of proper screening/ diagnostic tools [3]. Amongst gynecological malignancies that pose a serious threat ovarian cancer is the most fatal cancers affecting the female reproductive system [31].

Ovarian cancer can be subdivided into 3 main types: epithelial, germ line and sex-cord-stromal; epithelial carcinomas accounting for majority of the cases whereas the latter 2 comprise just 5% of all ovarian cancer. [31]. Epithelial ovarian carcinomas (EOC) are further classified into several categories based on the cell type: serous carcinomas (SC), mucinous carcinomas (MC), endometrioid carcinomas (EC), and clear-cell carcinomas (CCC), transitional-cell Brenner tumors, mixed, and undifferentiated type. Despite the heterogeneity they are all treated as a single disease and fall under the umbrella term ovarian cancer [33]. Although classification into various subtypes is clearly defined, understanding of the disease is far from simple. Comprised of multiple histological subtypes, with numerous genotypes and phenotypes within each

histotype, ovarian cancer is a complex malignancy, tumor heterogeneity being very high both across subtypes and within a single tumor. This impacts the response to chemotherapy and could represent a major cause of treatment failure [33] [34].

The primary routes of spread of ovarian cancer involve: (i) direct extension, where the tumor invades the ovarian capsule and the exfoliated cells directly invade adjoining organs such as the bladder, rectum, uterus or peritoneum. (ii) lymphatic dissemination to pelvic and/or para aortic lymph nodes. (iii) dissemination of exfoliated tumor cells by movement of ascetic fluid whereby the tumor spreads to the entire upper abdomen [35]. This debilitating disease is often diagnosed only at advanced stages with wide spread metastasis leading to 5-year survival rate of less than 30% [30].

Treatment paradigms for the first line management of newly diagnosed ovarian cancer employ a combination of cytoreductive surgery to excise the tumor followed by cytotoxic chemotherapy using platinum-based agents and taxane [36] [37]. Even with optimal front line treatment, EOC is characterized by high recurrence rates and the disease is usually incurable from the time of recurrence [38]. Most patients respond well with an initial response rate of 80-90%, but majority of the cases relapse and develop recurrent disease with low 5-year survival rates[33] [39]. Patients who relapse within 6 months of completing first line treatment are classified as 'platinum resistant'. Recurrence is observed in up to 75% of cases and such patients develop resistance to the drug and ultimately succumb to the disease [8]. Advances in technology have led to improving the 5 year survival rates for most solid tumors, but ovarian cancer still remains an exception and is considered five times deadlier than breast cancer [30]. As platinum forms the backbone of the currently available treatment in ovarian cancer cases with cisplatin being a frontline chemotherapeutic agent, the development of resistance to platinum based drugs is a major barrier for successful treatment and is associated with poor survival [38] [40]. Tumor heterogeneity and its ability to develop resistance over time pose major challenge in detection of the resistance mechanism.

Resistance mechanisms can be either intrinsic or acquired, multifactorial and with the ability to evolve over time [38]. Various studies have attempted explaining the mechanism causing treatment resistance [18] [28] [41] and many factors have been linked to the resistant phenotypes. [36,38,42]. Resistance of ovarian cancer cells to chemotherapeutic mechanisms appears to be complex and multifactorial including DNA damage response, cell metabolism, oxidative stress,

cell cycle regulation, abnormal signaling pathways to name a few. Therefore, one single mechanism cannot fully explain the resistance of ovarian cancer cells to treatment [43]. Besides that, modification of RNA have also been also been shown to cause resistance in ovarian cancer. Developing more effective therapeutic strategies and improving outcomes in EOC requires a thorough understanding of the biological processes involved and mechanisms driving treatment resistance.

1.4 Translation

The central dogma explains how information stored in DNA flows from nucleic acid sequences to proteins within a biological system. Translation or protein synthesis is the final step in this sequence of events whereby the nucleotide sequence transcribed into the mRNAs is read by the ribosome, a macromolecular machine present in the cytoplasm, and converted into a covalently linked chain of amino acids. Beginning with a start codon read by $tRNA^{Met}$ (CUA) the ribosome adds amino acids to a growing peptide chain and terminates this process when it encounters a stop codon. Due to the universality of the genetic code the fundamental mechanism of protein synthesis remains highly conserved between eukaryotes, bacteria, and archaea[44] though there are some differences in how these steps are regulated in each species. Protein synthesis accounts for a large proportion of the cells' energy (~20% of cellular energy) and requires tight regulation[45]. A complex but highly coordinated interplay of various factors ensures accuracy of translation.

Translation is subdivided into four subsequent stages: i) initiation ii) elongation iii) termination and iv) ribosome recycling.

1.4.1 Translation in eukaryotes

Translation begins by assembling together the mRNA, an initiator tRNA(Met-tRNAi) and the individual 40S and 60S ribosomal subunits into a translationally competent 80S ribosome wherein the Met-tRNAi is positioned in the ribosomal P site at the initiation codon [46]. Eukaryotes have evolved a very complex translation initiation pathway involving atleast 12 proteins known as the eukaryotic initiation factors (eIFs), each playing an essential role in the process [47]. The process starts with the formation of a ternary complex of Met-tRNAi, eIF2 and GTP followed by binding to the 40S ribosomal subunit with eIF5, eIF3, eIF1, and eIF1A

leading to formation of 43S pre-initiation complex (PIC) [48]. Aided by various factors including eIF3, the poly(A) binding protein (PABP), eIF4B and the eIF4F complex (comprising the cap-binding protein eIF4E, eIF4A and eIF4G), the PIC is then recruited to the capped 5′ end of mRNA [48 49]. This complex with associated factors scans the 5' untranslated region (UTR) to locate an initiating codon, typically an AUG in eukaryotes. When it encounters the start codon the PIC ejects eIF1, assisted by eIF5 eIF2 is converted to its GDP bound state. This stabilizes the interaction with mRNA and arrests the scanning process. EIF5 and eIF2GDP are then dissociated. EIF5B then collaborates with eIF1A and mediates the joining of 60S subunit [50]. eIF5B and eIF1A are subsequently released allowing the ribosome to move on to the elongation phase [48]. The initiation phase culminates with formation of an 80S initiation complex in which the initiator tRNA, base-paired with the start codon of the messenger RNA (mRNA) is bound in the P-site (peptidyl site) of the ribosome and the second codon of the open reading frame (ORF) is in the A-site (aminoacyl site) of the ribosome. In the next phase i.e. translation elongation, the 80S complex aided by various elongation factors (EFs, eukaryotic elongation factors (eEFs)), moves along the mRNA, three nucleotides at a time, extending the protein chain [51 52]. Elongation commences with delivery of a cognate aminoacyl-tRNA to the A site of the ribosome[51]. The eukaryotic elongation factor eEF1A in concert with GTP directs tRNAs to the A site of the ribosome. Recognition of the cognate tRNA stimulates GTP hydrolysis which aids release of the factor and accommodation of the amino acylated tRNA in the A site of the ribosome. After an aminoacyl-tRNA is accommodated into the A site, the ribosomal peptidyl transferase center (PTC) catalyzes rapid peptide bond formation [53,54]. The ribosome then undergoes a rearrangement whereby the ribosomal subunits rotate relative to each other [55 56] This leads to movement of the A and P site tRNAs from a 'classic' to 'hybrid' state with the anticodon ends remaining in their original A and P sites but the acceptor ends moving to the P and E sites respectively[57]. eEF2 then binds and stabilizes this rotated ribosome. Conformational changes in eEF2, GTP hydrolysis and Pi release then allow the movement of tRNA and mRNA and then lock the ribosomal subunits in the post translocation state [57]. Following such a translocation, a deacylated tRNA occupies the E site, peptidyl-tRNA is positioned in the P site and the A site is vacant and ready for the next incoming tRNA[51]. Once the ribosome is assembled around a messenger RNA (mRNA), it carries out many rounds of the peptide elongation cycle and remains engaged with the mRNA throughout the process until it encounters a stop codon [58]. When a stop codon (UAA, UAG or UGA) enters the A site of elongating ribosomes protein synthesis is terminated, a process mediated by release factors (RFs) eRF1 and eRF3 [59]. Unlike the sense codons, there are no cognate tRNAs corresponding

to the stop codons and in the absence of a tRNA to decode the codon, the release factors (eRFs) bind to the ribosome instead [60] [59]. The interaction between the ribosome and the release factors leads to hydrolysis of the ester bond that links the nascent polypeptide chain to P- site tRNA thereby releasing the peptide [61] [60]. Subsequently the ribosome releases the mRNA and dissociates into its two subunits, which can then reassemble on another molecule and start a new round of protein synthesis.

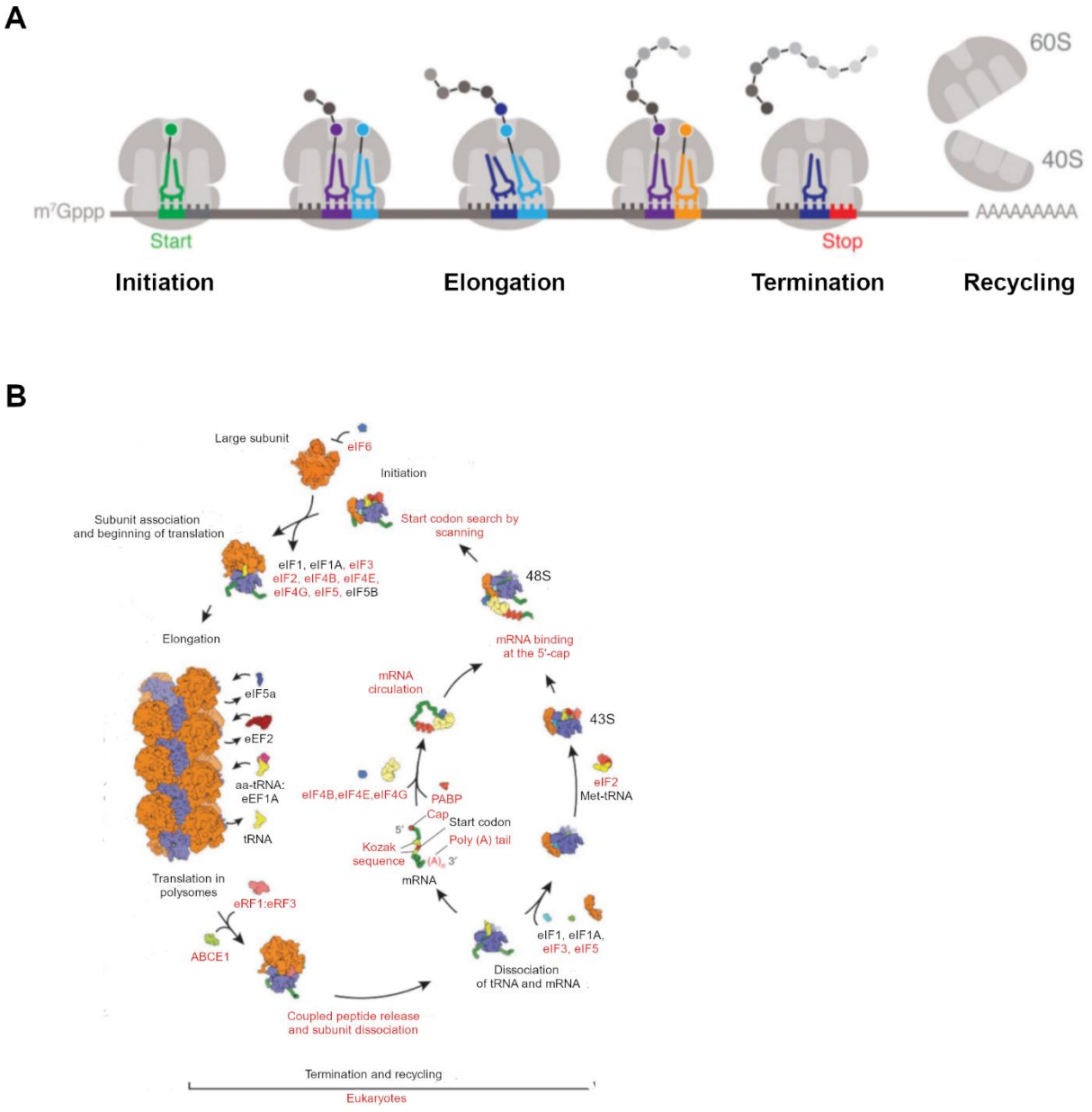

Figure 1.2 ***Translation****. [A] Translation can be primarily divided into four stages, namely initiation, elongation, termination and recycling, adapted from* [44] *[A]. Each of the four stages of translation involves various factors [B] as depicted in the detailed in the schematic, adapted from* [62] *de scheme of translation in eukaryotes showing the different factors involved at each stage.*

1.5 The multifaceted ribosome: protein synthesis and beyond

At the core of protein synthesis machinery is the ribosome, a universally conserved multicomponent ribonucleoprotein assembly, often and rightly referred to as a macromolecular machine. Structurally they are made up of two independent subunits of unequal sizes, each comprised of RNA and proteins, that come together to create a functioning ribosome. 'Within an active ribosome, the small subunit (SSU) binds the mRNA and provides the decoding site. The large subunit (LSU) contains the ribosomal catalytic site, namely the peptidyl transferase center (PTC), in which peptide bonds are formed, and the exit tunnel through which the nascent proteins emerge out of the ribosome' [63 64 65,66]. The human ribosome has a molecular weight of 4.3 MDa and is made up of a large subunit (60S) and a small subunit (40S). The large subunit consists of 28S, 5S and 5.8S rRNAs and 47 proteins, while the small subunit comprises a single 18S rRNA chain and 33 proteins [67 68]. Each subunit has three binding sites for tRNA, designated the A (aminoacyl) site, which accepts the incoming aminoacylated tRNA; P (peptidyl) site, which hold the tRNA with the nascent peptide chain; and E (exit) site, which holds the deacylated tRNA before it leaves the ribosome [65]. The ribosome reads messages three nucleotides at a time and its translocation on the mRNA codon by codon determines the fidelity of translation.

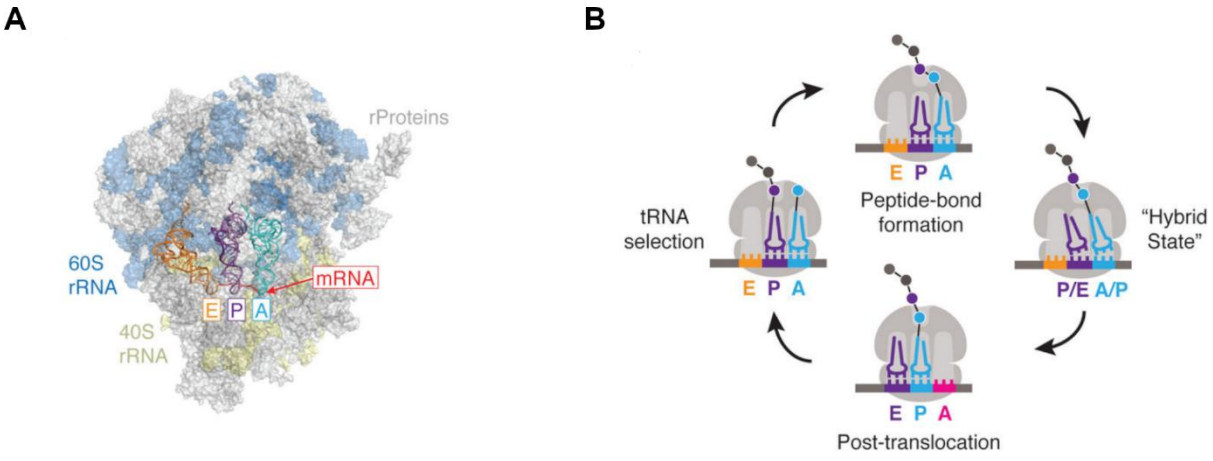

Figure 1.3 ***The Ribosome*** *[A] Structural model of a eukaryotic ribosome, highlighting its components i.e. the large (60S) and small (40S) ribosomal subunit, ribosomal proteins and the tRNA binding sites E (exit), P (peptidyl) and A (aminoacyl), adopted from [44] [B] Translation elongation cycle depicting movement of tRNA in the ribosome through the A, P and E-site.*

Ribosome biogenesis is the process by which the ribosomal RNAs are transcribed, processed, and assembled with the ribosomal proteins (RPs) to form the small (40S) and large (60S) ribosomal subunits. After their export to the cytoplasm, the two subunits join in the presence of an initiator tRNA and mRNA and form the pre-initiation complex (PIC). Further processing

results in a mature ribosome. Ribosome biogenesis is a complex, multi-stepped and the most energetically expensive process that a cell has to carry-out and hence is very tightly regulated and controlled. Starting in the nucleoli the process follows sequential rounds of assembly and modification of the ribonucleoprotein (RNP) complexes as they migrate from the nucleoli to the nucleoplasm and eventually to the cytoplasm, where the final assembly and maturation occurs. In eukaryotes, this process entails coordinated efforts of all three RNA polymerases (RNA pol I, RNA pol II, and RNA pol III), 79 ribosomal proteins (33 in the 40S subunit and 46 in the 60S subunit), and more than 200 proteins (including helicases, splicing factors, and chaperone proteins) and non-coding RNA (ncRNA) species (miRNAs, scaRNAs, and snoRNAs). Alterations at any steps can cause severe consequences to the organism [69].

A single human cell contains millions of ribosomes producing thousands of unique proteins that contribute to a cell's identity and function. Although the core features of the ribosome including the RNA and protein components as well as the catalytic mechanism of peptide bond formation are conserved, there is scientific evidence showing that ribosomes composition can be varying and dynamic [70]. Initially thought of as a molecular factory with a rather passive role in translation, the ribosome is now considered as a complex machinery with multifaceted roles in the regulation of gene expression [71]. Although the primary role of ribosome is protein synthesis, they are also involved in quality control [72], cellular signaling, tissue patterning [73]

As the availability of functional ribosomes determines the status of protein synthesis maintaining a healthy pool of these protein synthesizing machines is an important feat for cells. Generally, cells use a dynamic process called ribosome homeostasis to balance the availability and demand of functional ribosomes for mRNA translation. Translation of an mRNA draws ribosomes from the available pool in the cytoplasm disrupting this homeostasis and a cell coordinates events to reestablish this homeostasis [74]. At the end of every normal translation round, the eukaryotic release factors and the adenosine triphosphate-binding cassette family E member (ABCE1) split the ribosome into the 40S and 60S ribosomes and recycle them back into the cytoplasm. Dysfunctional translation due to ribosome stalling, complex mRNA structure, truncated mRNAs, or the lack of tRNAs distorts the ribosome homeostasis and results in stress. Cells use surveillance mechanisms to detect and retrieve these stalled ribosomes and coordinate with the ribosome recycling machinery in order to restore the ribosome homeostasis [74 75]. How stress is sensed by abnormal ribosome states and how those can cross talk with the other cellular check points and connect with cell cycle proliferation is interesting. Researchers

are now starting to look in this direction and at the interplay between different pathways to uncover new aspects of how ribosomes can affect various signaling pathways.

1.5.1 Ribosome Stalling

Proteins synthesis occurs at an average speed of 5.6 amino acids per second [76 77]. But translation elongation does not always proceed at a uniform rate and the dwell times or the elongation rates of ribosomes along the length of mRNAs vary. Ribosomes can have different dwell times based on factors such as availability of the elongation factors, codon optimality, properties of the nascent chain or peptide-bond formation efficiency. Similarly, impediments to translation such as unfavorable codons, problematic amino acid sequences, secondary structures or damaged mRNAs, could interrupt the movement of the ribosome [78] and cause the ribosome to pause at such positions. Cells generally utilize ribosomal pausing during elongation for regulatory purposes, to fine-tuning or halt protein production until needed[76]. Although elongation normally resumes following such pauses, sometimes influenced by one or more factors, the dwell time of the ribosome could be prolonged to an extent that the ribosomes stop during the elongation phase. This is known as ribosome stalling. In some cases ribosome stalling aids correct folding of proteins, complex assembly, protein targeting or protein interactions [79]. Given the high energy costs of protein synthesis, ribosomes that stall aberrantly during translation need to be rescued in order to prevent proteotoxicity [80]. If such a stall is not resolved in time, the trailing translating ribosome collides with this leading/stalled ribosome [52]. Though collisions are a general consequence of ribosome stalling, different kinds of stalling have been shown to trigger different consequences[80]. What exactly determines the assignment of appropriate responses still remains to be characterized. Researchers are now starting to uncover the causes and fates of stalled ribosomes. Studies are beginning to show that such stalls/collisions could act as signals that indicate the presence of defective mRNAs or altered physiological states [52] in turn calling for the activation of various pathways to deal with this and rescue the ribosomes.

Impairment of ribosomal biogenesis or impediments to its smooth translocation can be detrimental to cell function as it disrupts protein synthesis, increases inflammatory signals and, if left unresolved, can lead to cell death [81]. To ensure proper functioning, cells have adapted various pathways serving as check points to keep everything under control.

1.5.2 Surveillance mechanisms

Maintaining optimal ribosomal function is crucial and hence various control mechanisms have evolved to sustain proteostasis. The ribosome-associated quality control (RQC) pathway which detects and resolves collisions between arrested and/or slowly translating ribosomes is the best studied amongst such pathways. Characterized by ZNF598 this pathway mediates ubiquitination of the ribosomal small subunit proteins and subsequent splitting of the stalled ribosomes. The dissociation of such stalled ribosomes is followed by sequential action of various factors that target aberrant translation intermediates for degradation and rescue the stalled ribosomal subunits for recycling [82 83]. This co-translational quality control of individual translation events is essential for sustaining proteostasis. Though this pathway can efficiently manage occasional problems during translation, large-scale perturbations can overwhelm the RQC and other mechanisms are needed to overcome the stress. Some stressors such as UV irradiation, translation inhibitors, ribotoxins etc. are known to induce more global ribosome stalling. In such cases, specific ribosome associated factors activate stress signaling pathways to regulate translation and maintain homeostasis or determine the fate of the cell [78,80,81]. Integrated stress response (ISR) is one such signaling pathways activated by ribosomal collisions. More specifically the GCN2 arm of the ISR has been shown to be activated in response to ribosome collisions [78 84–87]. The pathway suppresses translation initiation by phosphorylating the translation initiation factor eIF2α. Ribotoxic stress response (RSR), is another such ribosomal surveillance pathway, which in response to ribosomal insults, manifests as the activation of the mitogen-activated protein (MAP) kinases p38 and JNK [81].

a. Ribosome-associated protein quality control (RQC)

The RQC pathway is triggered as a result of ribosome stalling and causes proteasomal degradation while the newly synthesized proteins are still on the ribosomal 60S subunit. The process can be split into two sequential steps, first step recognizes stalled ribosomes and mediates splitting of the 80S into subunits and the second step promotes proteolysis of the nascent chain and recycling of the 60S subunit [76]. When a trailing ribosome collides with a blocked or slowed-down ribosome (leading ribosome) it forms a ‘disome’ which acts a molecular signal for initiation of the RQC pathway. Such a ‘disome’ formed has an extensive 40S – 40S interface which can be identified by different quality control factors. The protein EDF1 has been shown to be the first to engage with the disomes [81]. If collisions persist, EDF1

stabilizes the recruitment of 2 different factors, the GIGYF2–4EHP complex and the E3 ubiquitin ligase ZNF598 (Hel2 in yeast). These two factors work in different ways to reduce collisions: GIGYF2–4EHP prevents re-initiation on problematic transcripts, and ZNF598 triggers downstream RQC events to resolve the internally stalled ribosomes [81]. Molecular details of ribosomes in a collision captured through structural studies reveal that the leading ribosome is in an ‘‘unrotated state’’ with an empty A site and a peptidyl tRNA in the P site, and the colliding ribosome is in a ‘‘rotated’’ state, where a peptidyl-tRNA is present in the A-P state and an uncharged tRNA in the P-E state [88]. In mammals the E3 ubiquitin ligase ZNF598 (Hel2 in yeast) recognizes this collision interface in internally stalled ribosomes, binds to the 40S-40S interface of collided ribosomes and monoubiquitinates the 40S subunit proteins eS10 an uS10 [89 90]. Subsequently an RQC trigger (RQT) complex, comprising components of the activating signal co-integrator complex (ASCC) ASCC2 & ASCC3, binds to the ubiquitinated ribosome and enables ribosomal splitting [83].

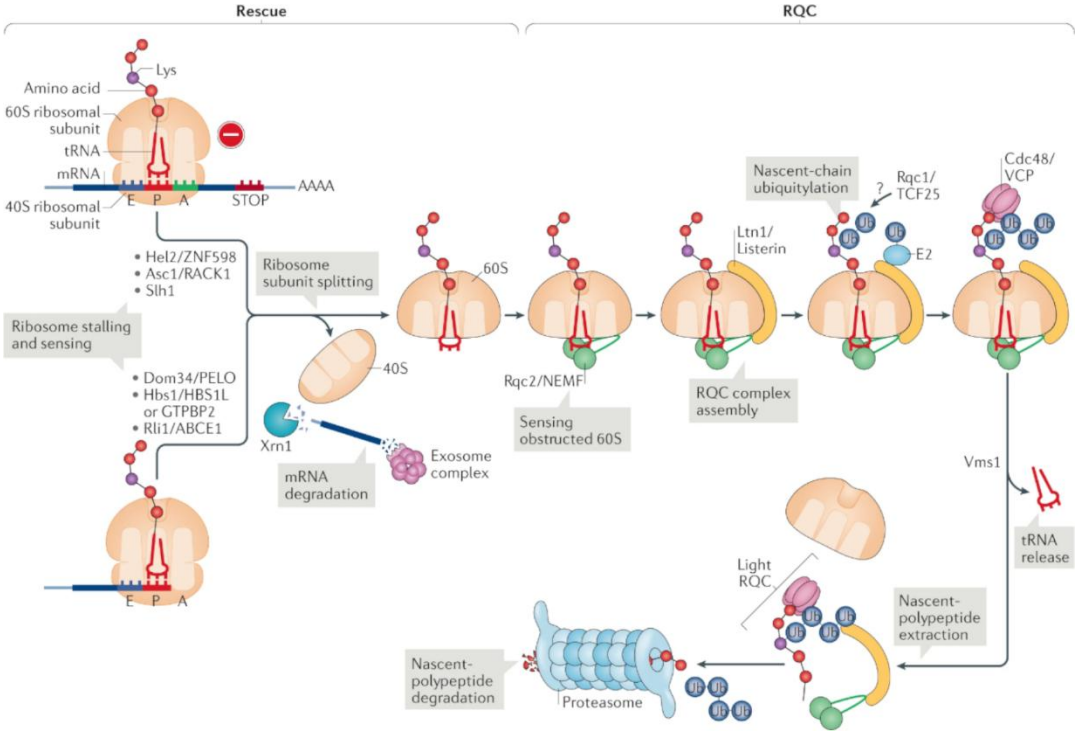

Figure 1.4 ***Eukaryotic ribosome associated quality control pathway.*** *Schematic representation of different steps of the RQC including the factors that regulate each stage, adapted from* [76]

After the 40S dissociates from the 60S, nuclear export mediator factor (NEMF), which recognizes exposed peptidyl-tRNA, binds to 60S ribosome-nascent chain complexes. NEMF occupies the 40S binding interphase and thus prevents re-association of the ribosomal subunits [81] and additionally recruits the E3 ubiquitin ligase Listerin which ubiquitinates the nascent chain.. The nascent chain is thereafter released from the 60S targeted for degradation [81 91].

b. Integrated Stress Response (ISR)

To overcome imbalances, cells have various defense/ protective mechanisms, the evolutionarily conserved signaling network, ISR is one such cellular response. When a cell is subjected to stress, the ISR tries to restore homeostasis [81]. Under stress conditions, the correct regulation of translation is an important requirement for maintaining cellular homeostasis. Such translation regulation as a response to stress, involves phosphorylation of serine 51 of the eukaryotic translation initiation factor 2α (eIF2α). This phosphorylation in turn leads to a general downregulation of translation and is accompanied by enhanced translation of specific stress-response mRNAs [92]. The ISR is activated in response to various intrinsic and extrinsic stresses by four distinct kinases namely PKR-like ER kinase (PERK), general control non-derepressible 2 (GCN2), double-stranded RNA-dependent protein kinase (PKR) and heme-regulated eIF2α kinase (HRI) each responding to a specific stressor [93] [94] but all converging at the phosphorylation of the eIF2α. Shown to exhibit both pro-survival and pro-death activities, the ISR is a double-edged sword which may influence tumor progression as well as response to therapy [95]. Of the 4 kinases, the GCN2, has been associated with ribosome associated surveillance mechanisms.

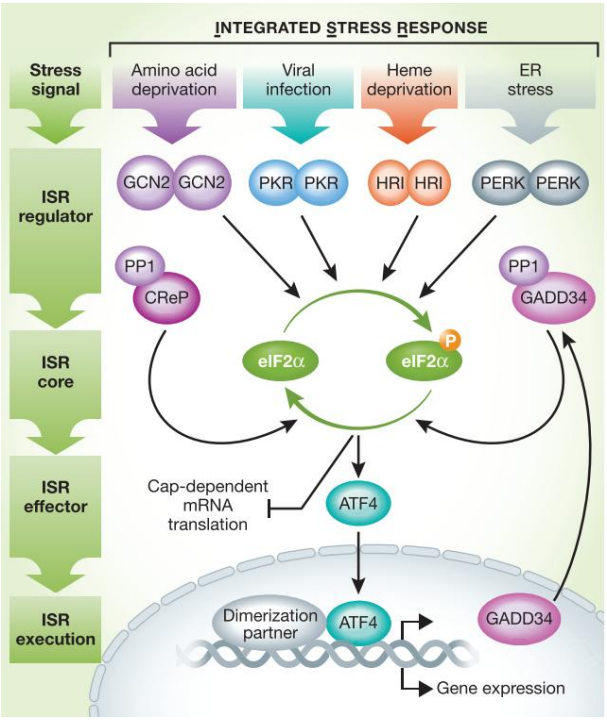

Figure 1.5 ***Integrated stress response.*** *Amino acid deficiency, ds-RNA virus infection, heme depletion or ER stress activate the GCN2, PKR, HRI and PERK sensor kinases leading to phosphorylation of eIF2α. eIF2α phosphorylation leads to global inhibition of protein synthesis but allows selective translation of ATF4 mRNA. Adopted from* [94]

General control non-derepressible 2 (GCN2)

GCN2, one of the master regulators of the ISR in vertebrates, primarily senses amino acid availability and regulates changes in gene expression as a response to amino acid deficiency. As an arm of the ISR, GCN2 exerts its role by phosphorylating the eIF2α leading to global reduction of protein synthesis [93] [96]. Mechanistically, eIF2α is required for the formation of translation preinitiation complex (PIC) and for initiator Met-tRNAi ribosome interaction. Phosphorylation of eIF2α by GCN2 limits the availability of GTP-bound eIF2, interrupts the formation of PIC formation and suppresses global cap-dependent protein synthesis [97] [98]. The reduced protein synthesis helps conserve resources and allows cells enough time to reprogram its transcriptome to combat the stress experienced and aid cell survival [99].

In mammals, the GCN2 is also known as eukaryotic translation initiation factor 2 alpha kinase 4 (EIF2AK4) [96]. Although initially discovered and predominantly studied in S. cerevisiae, this pathway is present and highly conserved in nearly all eukaryotes [96]. Human GCN2 is 1649 amino acids long, with a molecular mass of ~190 kDa (380 kDa as a dimer). The protein has five conserved folded domains namely an N-terminal RWD (RING-finger proteins, WD repeat-containing proteins and the yeast DEAD-like helicases) domain, a pseudokinase domain, a catalytically active kinase domain, a 'HisRS-like' domain (similar to histidyl-tRNA synthetase) and a C-terminal domain (or CTD). Additionally, it also contains a 'charged linker' region, a stretch of arginine, lysine, glutamate, and aspartate residues, between the RWD and pseudo kinase domains [100]. The domain organization is shown below in Fig 1.6. It was shown that the GCN2 KD exists as an antiparallel inactive dimer until uncharged tRNA binds to it and triggers conformational changes that shift the equilibrium to the active parallel dimer [101].

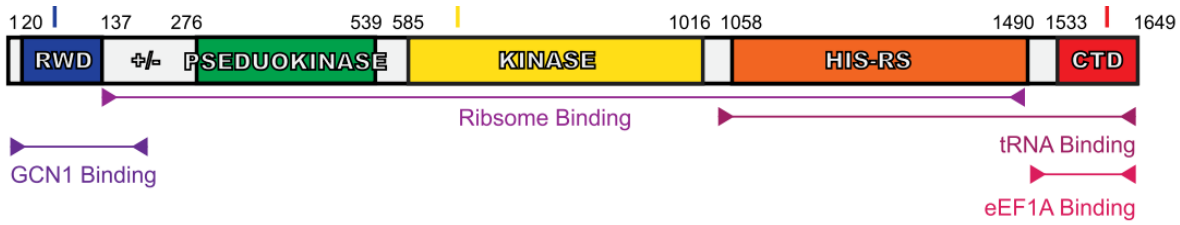

Figure 1.6 ***Domain organization of GCN2****. adapted from Masson, 2019* [100]

Activation of GCN2:

For decades it has been believed that lack of amino acids is the key activator, under nutrient starvation uncharged tRNAs accumulate and bind to the HisRS domain in GCN2. This binding leads to a conformational change and activates the kinase [102–104]. Dimerization is the key to its activation while autophosphorylation in its kinase loop at Thr882 & Thr887 are also essential for kinase activity [93]. Studies have shown that in addition to amino acid starvation stress various other kinds of stresses can also activate GCN2. These include ultraviolet violet (UV) irradiation, MMS (methyl methanesulfonate) treatment, oxidative stress (H_2O_2) and ER (endoplasmic reticulum) stress, osmotic stress, purine starvation [105]. But exactly how GCN2 is activated under such circumstances was unclear. Anda et al demonstrated that not only in response to starvation but also after UV irradiation and oxidative stress GCN2 activation requires the binding of tRNA [92]. With the wealth of literature supporting the theory that deacylated tRNAs activate GCN2, it is certain that deacylated tRNA plays a key role in activating GCN2. But researchers are now questioning whether that is the only means of activation of GCN2 or whether there are multiple and/or parallel pathways involved. Recent evidence points towards alternate, tRNA independent methods of activation, especially in higher eukaryotes [100]. Other mechanisms leading to activation of GCN2 are now coming to the limelight and showing that binary interaction between GCN2 and uncharged tRNAs may not be the sole activator [106]. In 2019, Inglis et al. reported that the human ribosome is a potent activator of GCN2, with the P-stalk of the ribosome playing a key role in this interaction [86]. Other studies showed that ribosome stalling was responsible for activating the GCN2 [86,87,106,107]. Yan and Zaher (2021) also showed that ribosome collisions not only trigger activation of RQC but also activates the GCN2, infact the activation of RQC antagonizes activation of ISR and vice versa. They show that GCN2 is activated by ribosome collisions and prefers the A site of the stalling ribosome to be empty unlike the activation of RQC which has no specific preference [108]. Thus unlike previously thought of, GCN2 can be activated by tRNA dependent or tRNA independent means (reviewed in [100])

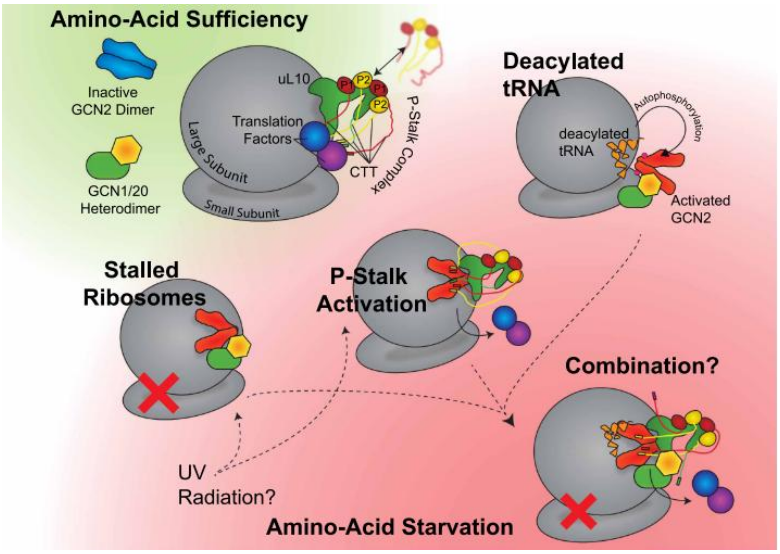

Figure 1.6 ***GCN2 activation****. Schematic illustration depicting the different possible routes of activation of GCN2 including the detection of deficiency of amino acids or stalled ribosomes, adopted from* [100]

Activation of GCN2 requires a coactivator GCN1 conserved from yeasts to humans, the N terminal region being required for ribosome binding [109]. Studies in yeast have shown that activation of GCN2 is regulated by 2 other proteins namely GCN1 and GCN20 [84 110 111]. GCN1-GCN20 form a complex and binding of this complex to polyribosomes is essential for activating GCN2. GCN1 and GCN2 form a trimeric complex with the ribosome. GCN20 associates with GCN1 and possibly forms an integral part of this complex [112]. Though GCN20 has been associated with the function of GCN2 in yeast, a functional homologue has not yet been characterized in humans. The mammalian ABC-containing protein ABC50, has some shown similarity with GCN20 (20% identity and 30% similarity between their N-terminal region) [112]. In mammalian cells, GCN1 complexes with GCN2 and both proteins interact with translating ribosomes[112] . GCN1 binds to both the ribosomes in a colliding disome and has important implications for the GCN2 activation as well as the ribosome-associated quality control pathways [109].

c. Ribotoxic stress response (RSR)

The RSR is a mitogen-activated protein (MAP) kinase signaling cascade mounted in response to defective ribosomes or impaired ribosomal function. It is one of the ribosome surveillance pathways, a cellular response which is conserved in both prokaryotes and eukaryotes [113 114]. RSR is a pathway that responds to ribosomal insults or impaired translation by activating the stress-activated protein kinases (SAPKs) signaling through p38 and JNK which mediate cell

cycle arrest, production of inflammatory cytokines and activate apoptotic signaling [107 115]. The term 'ribotoxic stress response' was originally coined by Iordanov et al. (1997) who demonstrated that drugs which interfered with 28S rRNA triggered activation of p38 and JNK [81]. Several kinases have been implicated in the activation of this response. Three protein kinases, the HCK (haematopoietic cell kinase), PKR (double-stranded RNA-dependent protein kinase) and ZAKα (zipper sterile alpha motif kinase) are known to recognize ribosomal damage, amongst which the ZAKα is the best characterized mediator of RSR [114].

ZAKα

ZAK, the sterile-alpha motif and leucine zipper-containing kinase AZK, is a serine-threonine kinase belonging to the family of mitogen-activated protein kinase kinase kinases (MAPKKK or MAP3K) [116] . ZAK is one of 7 known mixed lineage kinases (MLKs) whose actions have been shown to mediate the activation of JNK and p38 MAPK. Found both in the cytoplasm and in the nucleus, ZAK mRNAs are ubiquitously expressed, higher levels having been reported in heart and skeletal muscle. The ZAK gene encodes two splice variants ZAKα (91.7kDa) and ZAKβ (51.3 kDa) [83 117]. Activated by a variety of stressors the ZAK proteins contribute to cell's adaptation to stress or cell death based on the degree of damage. Activation of ZAK requires autophosphorylation. The long isoform of ZAK i.e. ZAKα has in recent years gained recognition as a ribosome binding and ribotoxic stress sensing kinase [81,107,118]. Activated by translational inhibitors (anisomycin, cycloheximide), amino acid deprivation, ribotoxins (ricin, Shiga toxin type 2) and UV radiation [83 114], ZAKα undergoes autophosphorylation [119]. ZAK binds to normally elongating, transiently colliding, ribosomes, but under conditions of heavy cellular stress with more abundant collisions it is acutely auto phosphorylated which then activates downstream signaling pathways. Vind et al., demonstrated that ZAKα is a direct sensor of ribotoxic stress. They highlighted that ZAKα interacts with the ribosome and this interaction is through two partly redundant sensing domains in its C terminus [118]. Activated ZAKα undergoes extensive self- phosphorylation and phosphorylates downstream SAPKs[119]. Wu et al. (2020) showed that collision mediated stress response in human cells involved the activity of ZAKα [107]. They presented evidence that activation of both ISR and RSR as a response to ribosome collisions depend on this MAPKKK[107]. They demonstrated that when cells are subjected to UV or amino acid starvation stress, the collisions that occur are not very severe and ZAKα activates the ISR, inducing phosphorylation of eIF2α and blocking translation initiation. On the other hand, treatment with

translation inhibitors causes collisions that are more severe, and in such cases ZAKα activates the RSR pathway by inducing phosphorylation of p38/JNK leading to cell cycle arrest or apoptosis [107] [78]. The activation of ZAKα signals pathways to promote survival or death, the outcome being based on the severity of ribosome collisions [120]. Many other studies have also identified ZAKα as the responsible upstream MAP3K responsible for RSR activation [107,121,122].

JNK pathway

The c-Jun N-terminal kinase (JNK) pathway, originally described as a stress activated protein kinase (SAPK), is a multifunctional kinase involved in different physiological and pathological processes, shown to be activated in response to various environmental stresses [123] [124]. It is among the three well-characterized subfamilies of the conserved MAPK signaling cascades involved in the regulation of cellular activities [124]. JNK regulates many physiological processes such as inflammatory responses, cell proliferation, differentiation, survival, and cell death [125] and has been linked to various pathological conditions including neurodegenerative diseases, inflammation, and cancer progression[126] [127]. Activation of JNK occurs through sequential protein phosphorylation mediated by the typical three-tier MAP kinase module i.e., MAP3K→MAP2K→MAPK [128] [129] and requires dual phosphorylation of threonine and tyrosine residues within a threonine/proline/tyrosine motif located in kinase domain [130]. The JNK pathway is activated by two upstream mitogen activated protein kinase kinases (MAP2Ks) (MKK4 and MKK7) which directly phosphorylate the JNKs on the threonine (Thr183) and tyrosine (Tyr185) residues of the conserved ThrProTyr (TPY) [131] [132]. In mammals, 3 JNK genes have been identified: Jnk1, Jnk2, and Jnk3 on 3 different chromosomes, each gene having alternative splice variants resulting in at least 10 different JNK isoforms (46–55 kDa) [124]. JNK1 and JNK2 are ubiquitously expressed, but the expression of JNK3 is mainly restricted to central nervous system (CNS) neurons (high level), cardiac smooth muscle, and testis (low levels) [124] [130] [131] [128]. JNK1 and JNK2 are often considered to have overlapping or redundant functions, JNK3 on the other hand due to its tissue specificity is thought to have distinct functions compared to JNK1 & JNK2 [130]. The transcription factor c-Jun, a component of the adaptor protein-1 (AP-1) complex is known to be the primary target of JNK [127]. The JNKs are shown to be activated by diverse stimuli leading to a multitude of cellular responses [133].

The JNK signaling pathway is involved in physiological and pathological processes; it regulates diverse cellular behaviors such as proliferation, differentiation, morphogenesis, and

apoptosis, DNA repair, metabolism , it is implicated in various human diseases such as immunological conditions, neurological disorder, diabetes, respiratory and cardiac diseases [124] [134] . The activation and response of JNK has been widely studied in cancer too with some studies supporting the onco-suppressive role of JNK while other provide evidence that JNKs contribute to tumor growth as well, thus showing JNK conflicting roles [127] [135] [136]. Bode et al rightly called JNK an "archetype of contrariety of intracellular signaling" [130]. Owing to such conflicting roles JNK is said to have a Janus face exhibiting a 'Yin and Yang' function of regulating both cell apoptosis and survival [126] [127] [137] [138]. Contrary to the notion that JNK1 & JNK2 have redundant functions, distinct isoform specific roles have been reported [139]. Evidence shows that JNK1 plays a role in malignant transformation of cells and in tumorigenesis [140]. Pan et al (2016) demonstrated that in bladder cancer JNK2 acts as a tumor suppressor, and decreased JNK2 expression promotes bladder cancer tumorigenesis [141]. Recently, JNK1 and JNK2 have been shown to exert different functions in pancreatic cancer and even act as counter players in tumor invasion [142]. In the JNK-regulated pathways which play a crucial role in both cell proliferation and cell death, the cellular context determines whether the cells will be committed to proliferation or to programmed death [143]. The cell/ tissue specificity and more importantly the upstream and downstream molecules involved in the cascade are important factors and will eventually affect the fate of the cell.

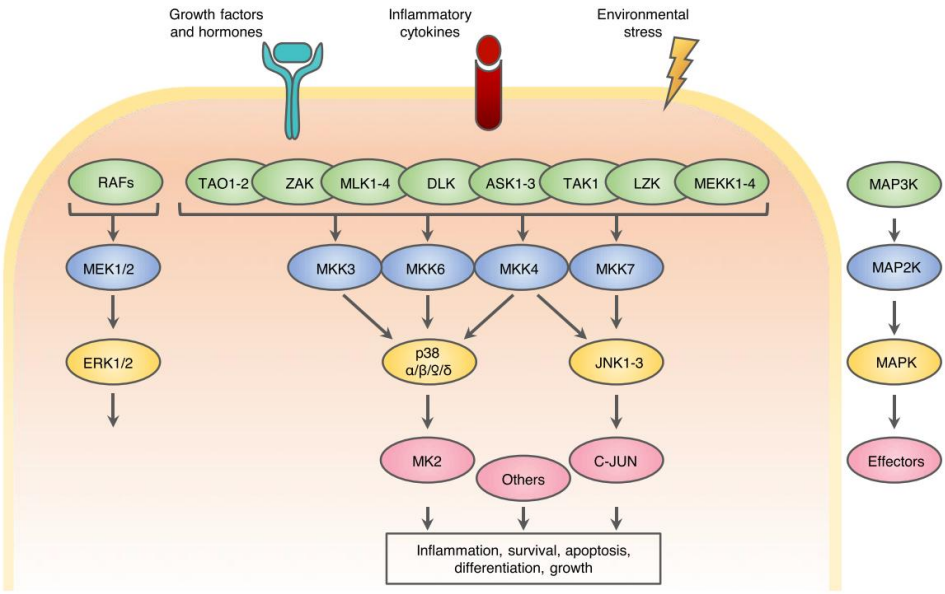

Figure 1.7 ***The MAP kinase network****. The MAP kinase signaling cascade is activated by a variety of stimuli and its cellular effect is mainly mediated through the phosphorylation of various effector proteins. The canonical activation pattern is triggered by the stimulus dependent activation of a MAP kinase kinase kinase (MAP3K, in green) which then activates MAP kinase kinases (MAP2K, in blue) which further activates MAP kinases (MAPK, in yellow). Adapted from Vind et al (2020)* [81]

Stoneley et al (2022) revealed that although the ribosome splitting activity of ASCC resolves many stalled ribosomes during translation, ribosomes stalled due to bulkynucleobase mRNA modifications are resistant to ASCC splitting, they are long lived in cells and activate the ZAK/p38 pathways downstream [120] Studies such as these indicate that these pathways are not completely independent of one another but rather work in coordination [107 78 81]. How the different ribosome rescue pathways operate under diverse cellular contexts, how they deviate or collaborate with one another and eventually how they function in context of diseases is an interesting field with a lot more still to be uncovered [80].

1.6 Translation in cancer

Translation involves the orchestrated interaction of mRNA, tRNAs, ribosomes, and various supporting factors. The process is tightly controlled and has a major role in regulation of gene expression [144]. The rapid and continuous proliferation of cancers cells necessitates continuous protein synthesis and increased ribosome content [145 146]. Cancers exploit the mechanisms by which translation is controlled so as to create a proteome conducive to proliferation, invasion and migration. While healthy cells diligently control translation to maintain homeostasis, malignant cells in contrast, seize the canonical translation machinery and distort various factors leading to aberrant protein synthesis providing the cells the ability of unregulated cellular divisions or dysregulated metabolism [147]. In other words, cancer cells hijack the regulatory mechanisms that govern translation and rewire the translational programs which lead to the phenotypic hallmarks of cancer. Researches have demonstrated that oncogenic signaling pathways most commonly found to be altered in human cancers — including RAS–MAPK, PI3K–AKT–mTOR, MYC and WNT–β-catenin — ultimately lead to reprogramming of the genome at the translation level [148]. Various parameters such as ribosome biogenesis, factors involved in translation (eg eIF4F or eIF2), tRNAs, post transcriptional modifications, cis-regulatory elements have all been shown to be deregulated in cancers (reviewed [146 149 148,150]). A key feature that enables cancer cells to survive and proliferate is their ability to adapt to different kind of stresses (replicative, oxidative, genotoxic, metabolic and proteotoxic stress) encountered during tumorigenesis. Translational dysregulation grants cancer cells this ability to promptly adapt to a diverse array of stresses associated with a hostile microenvironment and promote cancer onset, its progression and also resistance to anticancer therapies. “Translation is a critical nexus in neoplastic transformation. Multiple oncogenes and signaling pathways that are activated, upregulated, or mutated in cancer converge on translation and their

transformative impact “bottlenecks” at the level of translation” [151]. Every element involved in translation, the transcriptional template, the components of the translational apparatus, the proteins that interact with the transcriptome etc. have been found to be qualitatively and/or quantitatively perturbed in cancer[151]. Such translational control in cancer is multifaceted, can result from alterations in the levels of one or many translation factors, can be unique to different types of cancers or the disease stages and vary according to each tumour microenvironment [146]. In addition to process of translation itself, stress response pathways and also individual factors have been studied and implicated in various cancers. The factors we discussed in the previous sections namely the GCN2 (reviewed in [97]) [152] [153] [154], ZAK [155] [156] [157] and JNK [136] [158] have all been associated with various cancers and shown to have pro oncogenic roles in certain cases but tumor suppressive roles in others. The interplay between different factors and more than one pathway adds to the complexity. Furthermore, translation deregulation is emerging as a mediator of resistance to several clinical therapies [150,159] [160]. Understanding the alterations to translational control in the different contexts will provide opportunities for improving therapeutic intervention in human cancer. Our study serves as a step in this direction as we unveil factors involved in resistance and likely targetable to improve chemo sensitization in ovarian cancer.

2 Aim of the thesis

Cancer, one of the leading causes of mortality and morbidity, represents a major health problem. Constant efforts are being made to tackle this devastating disease. Although advanced technologies have improved treatment options, conventional chemotherapeutic drugs such as platinum-based agents remain a cornerstone of cancer management. Unfortunately, resistance to chemotherapy is a common problem limiting the efficacy of the drugs. Circumventing resistance to maximize the benefits of drugs is therefore a critical goal for anticancer therapy. Cis-Pt, the first approved chemotherapeutic drug is an effective anti-cancer agent that constitutes one of the key therapeutic options for many solid cancers, but the associated resistance affects its efficiency. It is thus crucial to decipher the cause of cis-Pt resistance in cancer cells. Understanding the mechanisms that drive cis-Pt resistance can help identify potential targets and define chemo-sensitization strategies. This study aimed at seeking insights into the underlying molecular mechanisms of cis-Pt resistance in ovarian cancers.

Using SKOV3, a cell line resistant to cis-Pt we looked for molecular changes triggered by cis-Pt treatment. Aiming to elucidate how the cells acquire resistance, we narrowed on the stress response signals elicited by cis-Pt treatment and how they affected cells. With this we sought to identify the molecular mechanisms that caused the resistance phenotype (Chapter 2). Having identified the role of GCN2 in resistance to cis-Pt, we next addressed whether this or similar effects were also seen in other cells. Our next objective was to determine the effects of cis-Pt in another ovarian cancer cell line A2780, a cell line considered sensitive to cis-Pt. Furthermore, aiming to understand of how cis-Pt affects ovarian cancer cells, we looked for parameters that we previously identified in the resistant cells as well as other parameters such the internal m^6A modification and its regulators (Chapter 3).

In the final section of this thesis we sought to establish a method to sequence tRNA molecules, the key players in the process of protein synthesis. Growing evidence from literature and our results in the previous chapters show the involvement of tRNAs and their modifications in various biological processes necessitating a comprehensive analysis of the tRNAs. The small size, complex structure and numerous modifications make tRNAs difficult to sequence with the commonly used methods. To address this issue, we aimed to develop a method to sequence

tRNAs. Acknowledging the potential of direct RNA sequencing on the nanopore platform we set to adapt the method to sequence tRNAs and detect modifications on them (Chapter 4).

3 GCN2 activation by ribosome collisions confers cisplatin resistance

The data presented here are results from collaborative efforts of various research groups in the attempt to understand the mechanisms involved in resistance to cis-Pt. This chapter has been submitted for publication and is currently under revision "GCN2 activation by ribosome collisions confers cisplatin resistance in ovarian cancer. Priyanka Nair, Leonardo Santos, Ryder F. Whittaker Hawkins, Dörte Jechorek, Virginie Marchand, Megan C. DeWeerd, Nikhil Bharti1, Moritz Freyberg, Yuri Motorin, Atanas Ignatov, Robert Rottapel, and Zoya Ignatova" The experiments presented here were carried out as follows: Ribosome profiling, tRNA microarrays, immunoblot analysis by myself; analysis of the deep sequencing data was done by Leonardo Santos, a fellow PhD student under the supervision of Prof. Dr. Zoya Ignatova (University of Hamburg, Germany); silencing of the GCN2 and the paired end RNA sequencing experiments were performed by Prof. Dr. Rottapel's Lab (Princess Margaret Cancer Centre, University Health Network, Toronto, Ontario, Canada/ Departments of Medicine, Immunology and Medical Biophysics, University of Toronto, Toronto, Ontario, Canada; Figure 3.1 A, 3.11 A&C); the tRNA sequencing experiments were performed by Prof Dr. Yuri Motorin's lab (Université de Lorraine, Nancy, France; Figure 3.7) and the patient analysis was carried out by Dr. Dörte Jeschorek and Dr. Atanas Ignatov's lab (Clinics Gynecology and Obstetrics, University Clinics Magdeburg, Germany; Figure 3.15 and 3.16, Table 3.1), who also hold ethics approval.

3.1 Introduction

Platinum-containing drugs, e.g. cisplatin (cis-Pt), oxaloplatin or carboplatin, are commonly used chemotherapy agents to treat solid tumors, including ovarian, lung, bladder and testicular cancers [8]. However, approximately 70% of patients will relapse with chemoresistant disease following initial therapy [36]. Innate and acquired resistance to Pt-based agents limits the clinical efficacy of these chemotherapies contributing to the poor survival outcome in patients [38]. Cis-Pt is a potent DNA damaging agent creating both intra- and interstrand DNA crosslinks [42,161]. The cis-Pt associated genotoxic stress induces activation of ATM and ATR kinases, two components central to the DNA damage response signaling pathway, and multiple downstream

signal transduction pathways, including mitogen-activated protein kinase (MAP3) pathways, p38 mitogen-activated protein kinase (p38 MAPKs) and/or c-Jun N-terminal kinase (JNK), which all affect DNA replication, mediate cell cycle arrest, and programmed cell death [162] [11,154,163]. Cis-Pt treatment causes also prolonged induction of extracellular signal-regulated kinases 1 and 2 (ERK1/2) [164]. Suppression of translation with cycloheximide decreases the cis-Pt induced ERK1/2 activation, suggesting that the cytotoxic drug effect is coupled to de novo protein synthesis [164]. Yet, the mechanisms underlying the cis-Pt resistance remain elusive.

Tumor cells undergo metabolic adaptation to ensure survival and proliferative capacity under conditions of limited nutrient supply [165,166]. The general control nondepressible protein 2 (GCN2, also called eIF2AK4) is commonly activated by deacylated tRNAs accumulating by amino-acid deprivation [103]. A persistent nutrient scarcity is an universal hallmark of early cancers and as a critical node in managing this starvation stress GCN2 appears as an attractive oncotarget [97]. In particularly for tumors that depend on certain amino acids for proliferation, GCN2 inhibition appears attractive strategy, however the GCN2 role in the clinical outcome of such amino acid depletion strategies undergoing clinical evaluation is not clear [167]. GCN2 activates transcription factor ATF4 which controls two opposing pathways pro-survival to support cancer cell progression and pro-apoptotic pathways promote cell death during conditions of persistent nutrient scarcity [100,154,168–170], with yet elusive mechanism of what drives the expression programs to survival or cell death. Although uncharged tRNAs that accumulate during nutrient deficiency are the most potent activator of GCN2 [103], other studies suggest an activation mechanism independent of uncharged tRNAs [87,171,172] or by interactions with the ribosomal P-stalk [86,106]. A recent work showed that GCN2 is a component of the kinase signaling complex including ZAKα and p38/JNK which monitors ribotoxic stress arising from ribosome collisions [107].

Here, we identify that GCN2 is required for acquired cis-Pt resistance in the ovarian carcinoma cell line, SKOV3. Selective Ribo-seq (ribosome profiling), RNA-seq, AlcAnilineSeq and biochemical analysis demonstrate that cis-Pt treatment alters ribosome synthesis and cause tRNA damage leading to ribosome stalling and collisions. GCN2 acts as a main communicator linking ZAKα-mediated sensing of ribotoxic stress and the innate cellular signaling pathways processing ribosome stalling and collisions to confer cis-Pt resistance. Retrospective study with patients with stage III epithelial ovarian cancer corroborate the central role of GCN2 in the acquisition of cis-Pt resistance.

3.2 Results

3.2.1 Cis-Pt treatment induces ribotoxic stress and activates GCN2 kinase

To assess the effect of cis-Pt on gene expression, we first considered an ovarian cancer cell line, SKOV3, that is derived from the ascitic fluid of a patient with advanced stage disease [173,174] and using RNA-seq compared the gene expression profiles of treated (with 10 μM cis-Pt) and untreated control cells (Fig. 3.1 A). Global transcript expression analysis revealed marked changes in gene expression (Fig. 3.1 A, B); among the upregulated transcripts (i.e. log2 ≥ 1) gene ontology (GO) terms related to RNA transcription and regulation of transcription, and inflammatory processes were enriched (Fig. 3.1 C). Considering the strong preclinical evidence supporting the notion that alterations of the ability of cells to repair cis-Pt-induced DNA damage contribute to drug resistance in ovarian cancers (reviewed in [42,161]), we specifically analyzed the gene expression changes of the genes from the DNA-repair pathways. Following cis-Pt treatment, we detected mild perturbation in expression (i.e. less than two-fold or - 1 < log2 > 1) of the genes constituting the five major DNA-damage response pathways, however, with several genes reduced and others increased (Fig. 3.1 D), suggesting that these rather subtle expression alterations alone do not explain the adaptive response of SKOV3 to cis-Pt.

Among the downregulated transcripts were many translation factors and the majority of the ribosomal proteins, albeit to much lower extent than transcription-related GO terms (Fig. 3.1 E). This overall decrease was mirrored by an overall lower translation as evidenced by a decreased fraction of polysomes in the polysome profiling analysis (Fig. 3.1 F).

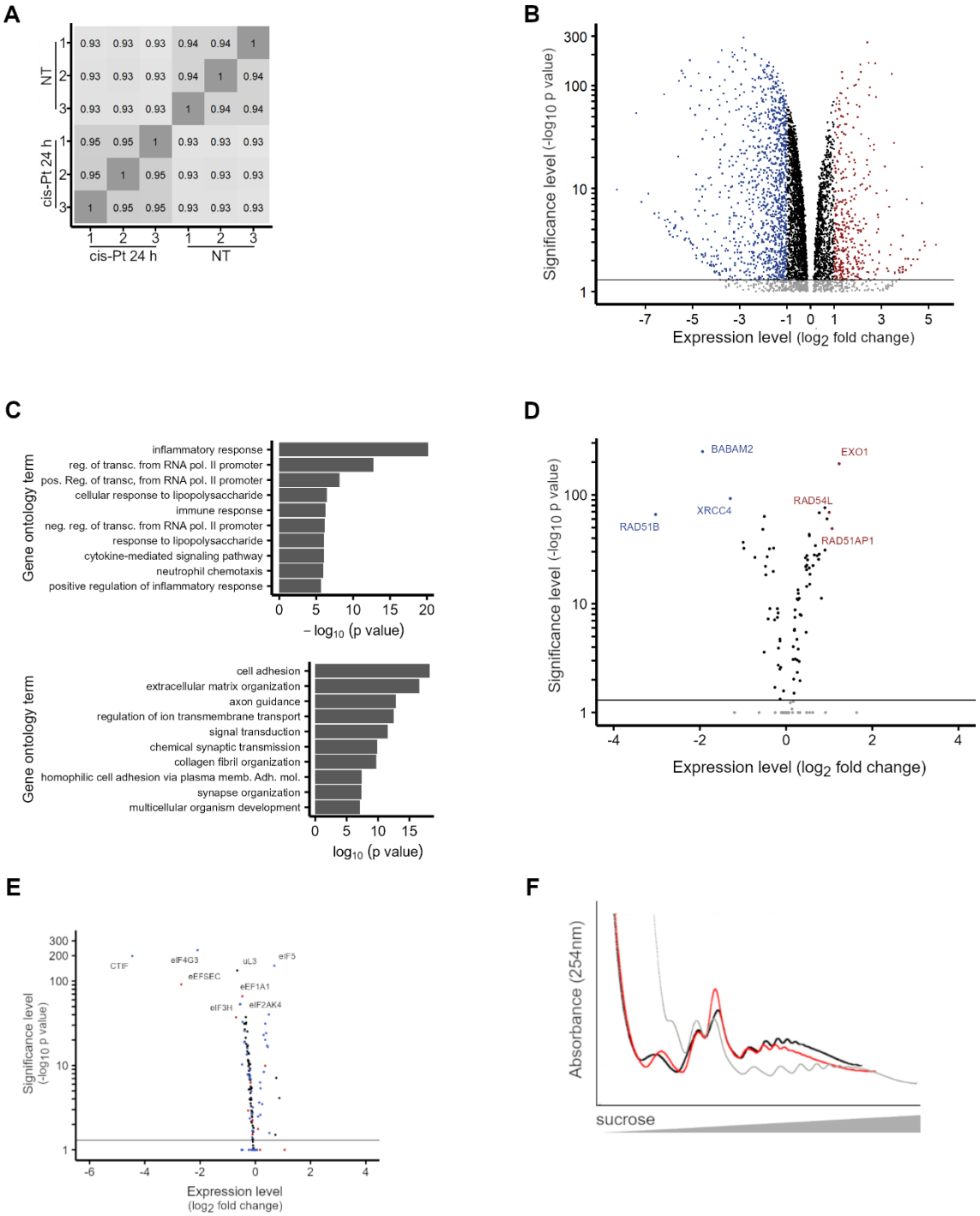

Figure 3.1 ***Differential gene analysis.*** *[A] RNA-seq replicates show very good pairwise correlation. Spearman correlation coefficient between individual biological replicates of RNA-seq. NT, untreated SKOV3 cells; cis-Pt 24h, SKOV3 treated with 10 μM cis-Pt for 24h. [B] Volcano plot of differentially expressed genes in SKOV3 treated with 10 μM cis-Pt for 24h compared to untreated cells as determined by RNA-Seq. Upregulated transcripts (log2≥1) are color coded red, and downregulated (log2 ≤ 1) blue. [C] Top 10 most significant GO terms within the group of upregulated (up) and downregulated (down) genes following 24h cis-Pt treatment. GO terms are ordered according to the p value. [D] Volcano plot of differentially expressed genes from the DNA damage pathways in SKOV3 treated with 10 μM cis-Pt for 24h compared to untreated cells as determined by RNA-Seq. Upregulated transcripts (log2 ≥ 1) are color coded red, and downregulated (log2 ≤ -1) blue. Genes RAD51AP1, RAD54L, RAD51B, and BABAM2 belong to the homologous recombination pathway, XRCC4 to non-homologous end-joining pathway and EXO1 to the mismatch repair pathway. [E]Differential expression of ribosomal proteins (black), initiation factors (blue) and elongation factor (red) in SKOV3 cells treated with 10 μM cis-Pt for 24h compared with untreated cells as determined by RNA-seq. [F] Polysome profiles of untreated (black), cis-Pt-treated (10 μM) for 4h (gray) and 24h (red) SKOV3 cells. Polysome fraction decreased at 4h posttreatment and recovered at 24h, remaining, however, slightly lower than the polysomal fraction of untreated SKOV3 cells.*

Ribosome biogenesis is a tightly coordinated process [175–178] and any imbalance in synthesis or damage of ribosomal proteins or rRNA triggers the ribotoxic stress response (RSR), a state sensed by ZAKα and transduced downstream by p38 and JNK. At 4h and 24h following treatment with cis-Pt, we detected ZAKα phosphorylation as monitored by Phos-Tag immunoblot analysis (Fig. 3.2 A) and a modest activation of JNK at 24h with no additional induction of p38 phosphorylation over the basal levels of phosphorylated p38 present in untreated cells (Fig. 3.2 B). Since activation of RSR induces GCN2 phosphorylation downstream of ZAKα [107], we interrogated GCN2 phosphorylation level following cis-Pt treatment, and found that GCN2 was robustly activated at 24h but not at shorter 4h-treatment times (Fig. 3.2 B). We noted the basal activation of JNK and GCN2 in untreated cells (Fig. 3.2 B). Together, these analyses demonstrate that cis-Pt treatment of SKOV3 triggered RSR and induced the phosphorylation of the RSR-sensing kinases ZAKα and GCN2.

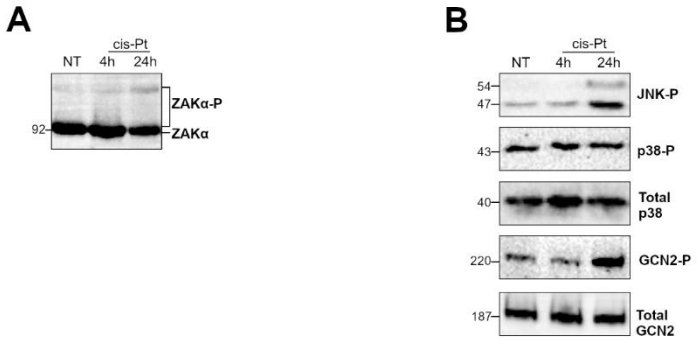

*Figure 3.2 C**is-Pt triggers RSR and activates GCN2.** [A] Representative Phos-tag immunoblot (n=3 biologically independent replicates) of phosphorylation of the endogenous ZAKα following cis-Pt treatment. [B] Representative immunoblots (n=2-3 biologically independent replicates) of cis-Pt treatment-induced phosphorylation of JNK and GCN2 but not of p38. NT, no treatment. Molecular weight of the corresponding bands shown on the left.*

3.2.2 Cis-Pt treatment damages tRNA^{Leu}(UAA) and induce ribosome stalling at Leu TTA codons

To explore the effect of GCN2 activation on translational dynamics, we performed Ribo-seq of SKOV3 cells treated with cis-Pt for 4h and 24h. We computed the ribosome dwelling frequency (or codon occupancy) for all 61 sense codons in the A site (that is, the ribosomal site accepting the charged aminoacyl-tRNAs) and compared to untreated cells (Fig. 3.3 A, B). While the A-site ribosome frequencies at the early time point of treatment were undistinguishable from the control (Fig. 3.3 A), we detected a marked increase at the Leu TTA codon at the later time point (Fig. 3.3 B). The A-site ribosomal occupancy at Asp and Glu

codons also increased, but by an order of magnitude lower than at the Leu TTA codon. For all other codons, we detected slightly diminished ribosome frequency post treatment (Fig. 3.3 B).

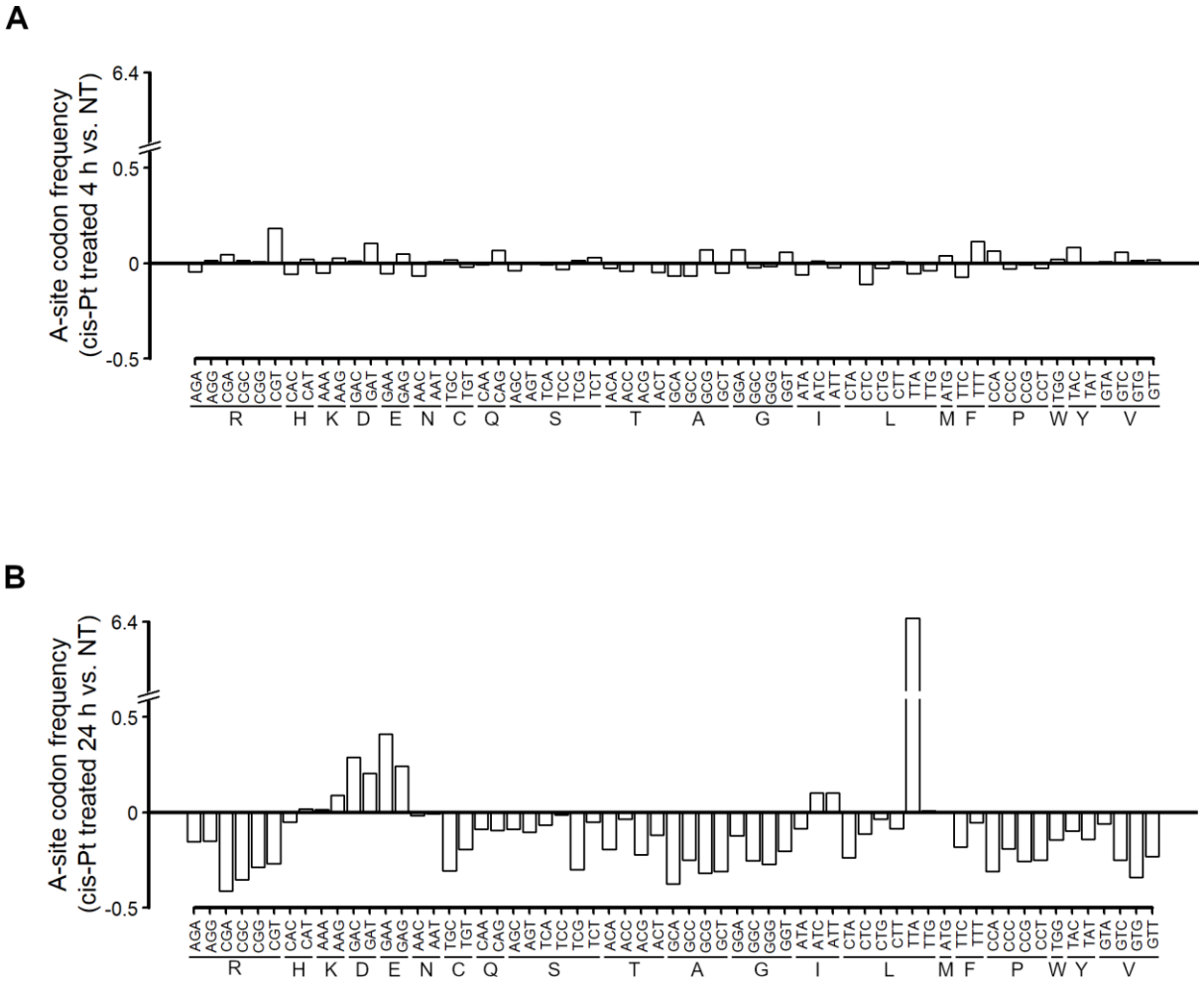

Figure 3.3 ***Ribosomal stalling at TTA (Leu) codon following cis-Pt treatment in SKOV3*** *as determined by Ribo-seq. Normalized codon occupancy of the A site is presented as a ratio of cis-Pt treated vs. untreated (NT) cells, 4h [A] or 24h [B] cis-Pt treated cells.*

Cis-Pt treatment did not decrease the levels of the aminoacyl-tRNAs as determined by tRNA tailored microarrays (Fig. 3.4 A). In contrast, at 24h following cis-Pt treatment, the overall aminoacyl-tRNA levels increased (Fig. 3.4A) and such accumulation of charged tRNAs is indicative of decreased translation as corroborated by a decreased overall fraction of polysomes (Fig. 3.1 F). The total tRNA levels were unaffected by cis-Pt treatment (Fig. 3.4 B), thus excluding the possibility that increased aminoacyl-tRNAs appear to result from decreased levels of total tRNA. Specifically, $tRNA^{Leu}$(UAA) isodecoders (that are tRNAs with the same anticodon but differ in their body sequence) reading both TTA and TTG Leu codons did individually change (i.e. the fraction of isodecoder 1 decreased post treatment from 0.013 to 0.007, but that of isodecoder 2 increased from 0.003 to 0.008); however, collectively their

concentration remained the same (i.e. 0.016 vs 0.015). It should be noted, that the TTG codon that wobble pairs to tRNA^{Leu}(UAA) is read by another isoacceptor in Watson-Crick geometry. Enhanced expression of aminoacyl-tRNA synthetases have been found to promote tumor growth in a variety of cancers [179], however we did not detect any significant alterations in their expression following cis-Pt treatment. Together, the tRNA microarray data suggest GCN2 activation and ribosome stalling at the TTA codon is not linked to leucyl-tRNA^{Leu}(UAA) paucity.

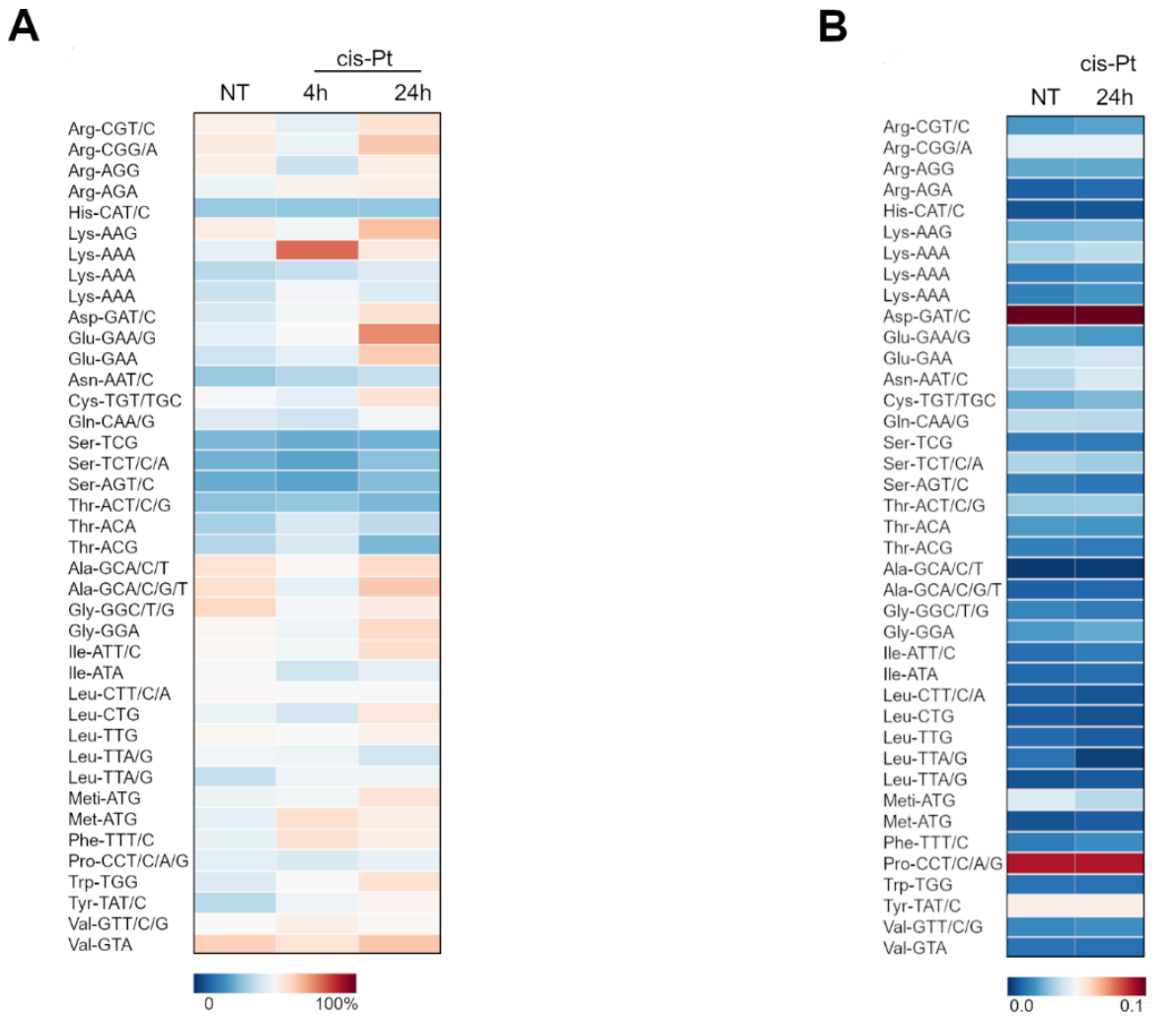

Figure 3.4 ***Cis-Pt treatment causes increase in aminoacylated tRNAs.*** *[A] Microarrays of aminoacyl-tRNA of untreated (NT) or SKOV3 cells treated with 10 µM cis-Pt for 4h and 24h. The color key indicates the percentage of charged tRNAs over the total amount of each isoacceptor. The microarrays were performed in triplicates (for control and 24 treatment) and are represented as mean values. Confidence intervals between replicates 1 and 2, 1 and 3, and 2 and 3 were 98%, 97%, and 98% for untreated, and 97%, 98% and 96% for SKOV3 treated for 24h with cis-Pt, respectively. [B] tRNA microarrays to measure the absolute concentration of the tRNA isoacceptors in untreated (NT) SKOV3 cells or treated with 10 µM cis-Pt for 24h. The microarray was performed as a single experiment and the abundance was compared to that of HEK293T cells, whose absolute tRNA abundance was determined earlier [170]. Color code denotes concentration represented as fraction. tRNA probes are depicted with their cognate codon and the corresponding amino acid. Two or three different probes recognizing two tRNA^{Leu} or tRNA^{Lys} that pair to the same TTA/G Leu codon or AAA Lys codons, respectively, represent tRNA isodecoders that bear the same anticodon but differ in their sequence outside the anticodon.*

Two adjacent pyrimidines in single-stranded RNAs are highly susceptible to form dimers following exposure to UV and oxidative reagents [113,180]. To address whether cis-Pt treatment-induced mRNA damage at di-pyrimidines and thus, contributes to the alterations in A-site ribosome dwelling frequency, we compared the A-site ribosome occupancy for cis-Pt treated and untreated cells. However, we observed a good correlation for all codons, except for the Leu TTA codon (Fig. 3.5) suggesting no perturbations at other codons containing two adjacent pyrimidines.

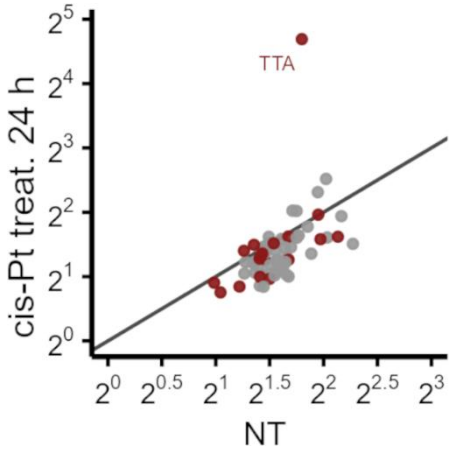

Figure 3.5 ***Ribosomal occupancy is strikingly different only at the TTA codon****. Scatterplots of codon-specific A-site ribosomal occupancy (log2 scale) comparing untreated (NT) vs. cis-Pt-treated SKOV3 cells for 24h. Codons with two adjacent pyrimidines are highlighted in red.*

Cis-Pt-induced ribosome stalling at the Leu TTA codon was not purely a feature of transformed SKOV3 cells as we observed similar effect in non-transformed immortalized fallopian tube-derived secretory cell line FT194. Following cis-Pt treatment for 24h, we again observed ribosome stalling only at the Leu TTA codon (Fig. 3.6 A), which was independent of the levels of aminoacylated or total $tRNA^{Leu}$(UAA) (Fig. 3.6 B, C). Although in FT194 cells, the effect on other codons with two adjacent pyrimidines was slightly more pronounced than in SKOV3 cells (Fig. 3.6 D). Together our results suggest that the robust ribosome stalling at TTA Leu codons is unlikely to be a result of a selective cis-Pt-induced di-pyrimidine damage of mRNA solely at TTA codons; codons containing two consecutive pyrimidines are equally susceptible to di-pyrimidine formation [107].

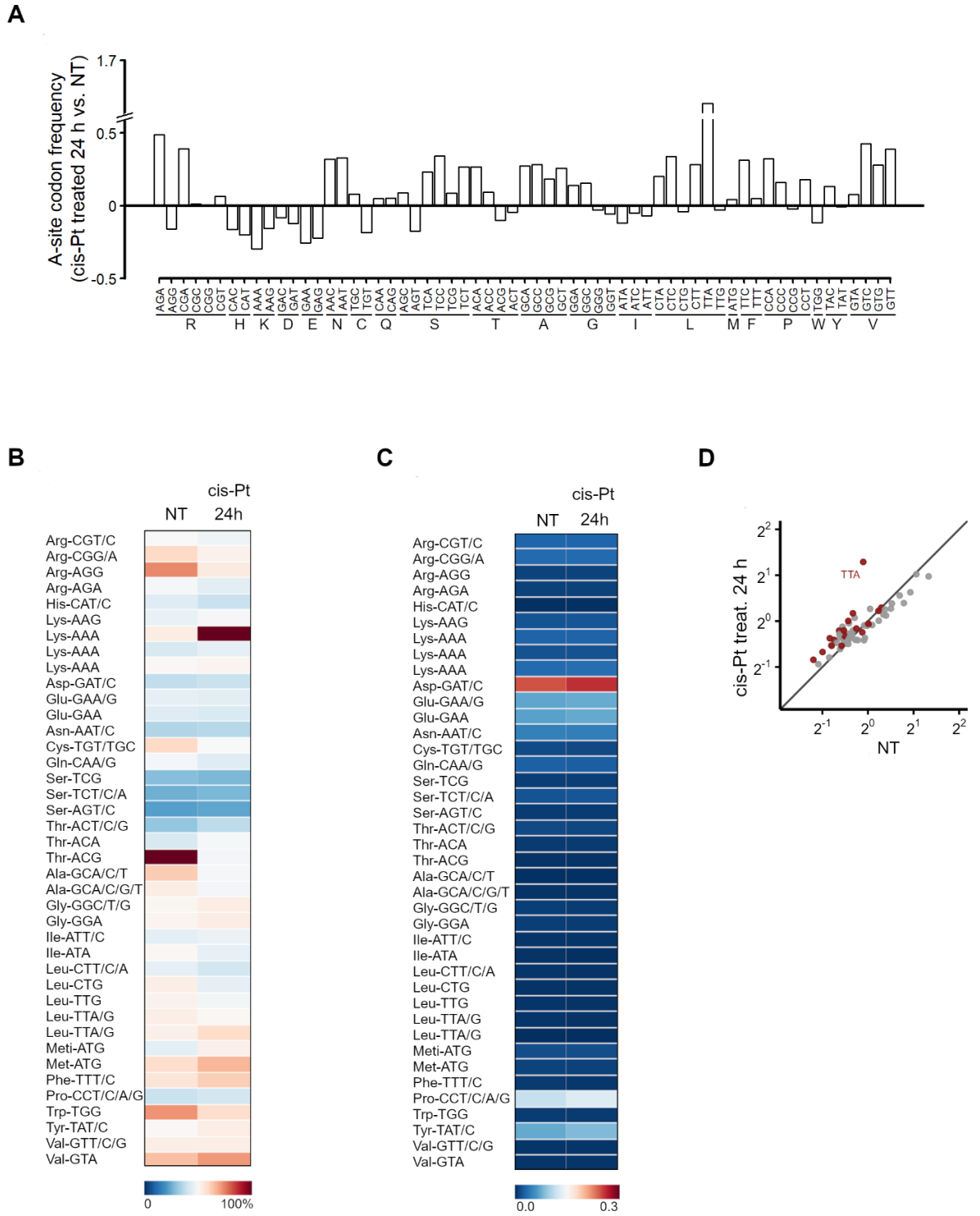

Figure 3.6 ***Cis-Pt affects FT194 cells also in a manner similar to SKOV3*** *[A], Relative changes in ribosome dwelling frequency at A-site codons FT194 treated with 5 μM cis-Pt for 24h versus untreated (NT) cells, as determined by ribosome profiling. The normalized codon occupancy of the A site is presented as a ratio of cis-Pt treated vs untreated. Leu TTA codon exhibits the highest occupancy. In general, the ribosome dwelling frequency at many codons is modestly increased posttreatment compared to untreated cells. [B] Microarrays of aminoacyl-tRNA of untreated (NT) or FT194 cells treated with 5 μM cis-Pt for 24 h. The color key indicates the percentage of charged tRNAs over the total amount of each isoacceptor. The microarrays were performed in duplicates and represented as mean values. Confidence intervals between replicates 1 and 2 were 97.3 and 97.8 for the untreated and cis-Pt treated cells, respectively. [C] tRNA microarrays to measure the absolute concentration of the tRNA isoacceptors in untreated (NT) FT194 cells or treated with 5 μM cis-Pt for 24h. The microarray was performed as a single experiment and the abundance was compared to that of HEK293T cells. [D] Scatterplots of codon-specific A-site ribosomal occupancy (log2 scale) comparing untreated (NT) vs cis-Pt treated FT194 cells for 24h. Codons with two adjacent pyrimidines are highlighted in red.*

We next investigated whether cis-Pt alters post-transcriptional tRNA modification that could contribute to diminished translation. We performed AlkAnilineSeq which specifically detects oxidized and methylated RNA bases and putative abasic sites resulting from fragile N-glycoside bond [181], and inspected the reverse transcription signatures for tRNA^{Leu}(UAA). By comparing tRNA profiles from untreated and treated SKOV3 cells, we did not detect any cis-Pt induced alterations of the natural modifications or any new signals in the tRNA isoacceptors, except for tRNA^{Leu}(UAA). Detailed analysis of AlkAnilineSeq profiles revealed a reproducible signal (n=5 biological replicates) at the G27-U27 pair in tRNA^{Leu}(UAA) following cis-Pt treatment (Fig. 3.7A), indicating an altered reactivity towards OH-cleavage and aniline, used as reagents in AlkAnilineSeq protocol.

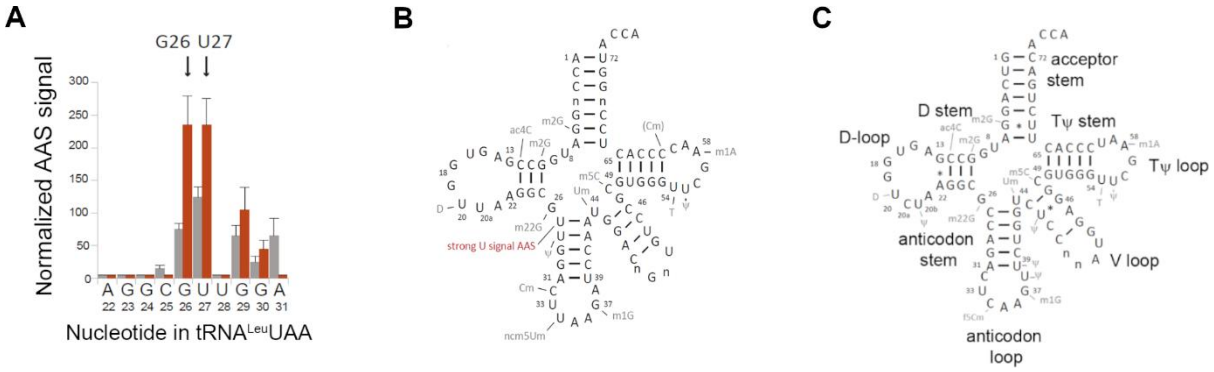

Figure 3.7 ***Cis-Pt affects tRNA modification.*** *[A]AlkAnilineSeq (AAS) in the vicinity of G26-U27 of tRNA^{Leu}UAA from untreated (gray) and cis-Pt treated (red) cells. The signal is a mean cumulative intensity of the normalized AAS signal ± SEM (n = 5 biological replicates). [B] Modification pattern of tRNA^{Leu}UAA shown on a generic sequence representing all tRNA^{Leu}UAA isodecoders. n, sequence differences among isodecoders; gray, natural post-transcriptional modifications; Cm not confirmed by RiboMetSeq; red, cis-Pt induced modification detected in AlkAnilineSeq (AAS). [C] Modification pattern of tRNA^{Leu}CAA shown on the generic sequence for all tRNA^{Leu}CAA isodecoders.*

The very low coverage of tRNA^{Leu}(UAA) should be noted; it is one of the least abundant tRNAs in SKOV3 and human tissues in general (Fig. 3.4 B, 3.6 C and ref.[182]).

These data demonstrate that cis-Pt caused robust ribosome stalling at TTA-Leu codons in a manner that was independent of the levels of aminoacylated or total tRNA^{Leu}UAA. It is consistent with cis-Pt induced chemical modification of tRNA^{Leu}UAA, which likely renders tRNA^{Leu}UAA translationally incompetent.

3.2.3 Cis-Pt treatment induces ribosome collisions in SKOV3 cells

Having observed that cis-Pt triggered RSR and subsequent ZAKα and GCN2 activation (Fig. 3.2) – both activated in response to ribosome collisions [107,183], we next focused on the A-site ribosome occupancy surrounding the TTA codons. At 24h following cis-Pt treatment, we observed a secondary peak approximately 30 nucleotides (nt) upstream of the marked stalling at TTA codon (Fig. 3.8). An A-to-A sites distance of 30 nt is indicative of two adjoining or colliding ribosomes [107,184]. Notably, this upstream peak, likely representing a queued trailing ribosome, was detectable only at the 24h time point and not at 4h (Fig. 3.8), suggesting that RSR arises from the accumulation of tRNA^{Leu}UAA damage over time. Importantly, there was no evidence of ribosome stalling and collisions in the proximity of the other Leu codon (CTT).

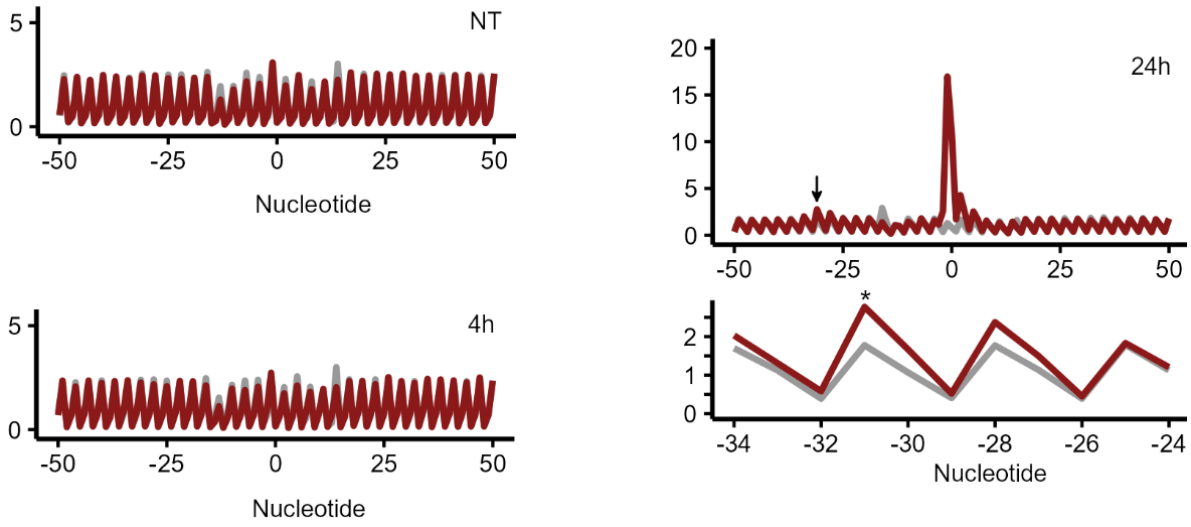

Figure 3.8 ***Ribosome dwelling frequency*** *surrounding the Leu TTA codon (red) compared to Leu CTT codon (gray) in untreated (NT) and treated SKOV3 with 10 μM cis-Pt for 4h or 24h. Cumulative plots of transcript fragments coverage surrounding TTA or CTT codons, centered at the middle T of the TTA or CTT codons, respectively, which is designated as zero. Trailing ribosome at 31 nt upstream of the TTA-Leu codon stalling site is designated by an arrow. Inset, zoom in into the trailing or queued ribosome upstream of the TTA (red) and CTT (gray) Leu codon of cells treated for 24h. *, p = 4.84x10-40, Mann-Whitney test.*

Consistent with the idea of ribosome collisions, GCN1 an important effector for GCN2 that binds to both colliding ribosomes [109], was enriched in the disome fraction (Fig. 3.9).

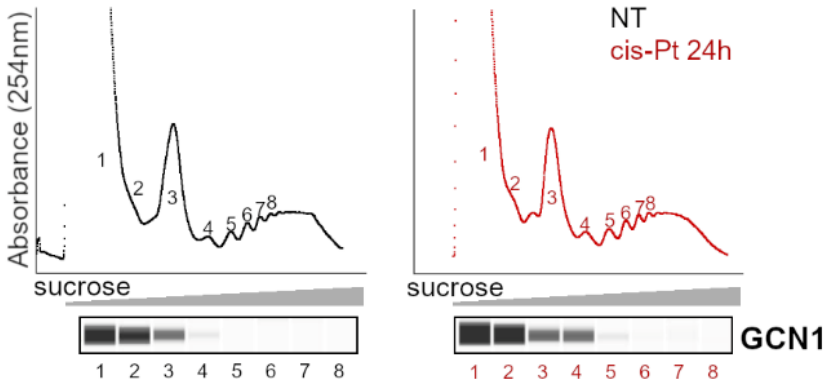

Figure 3.9 ***GCN1 is enriched in the disome fraction following cis-Pt treatment.*** *Polysome profiles of untreated (black) and cis-Pt treated (10μM) for 24h (red) SKOV3 cells. Polysomal fractions analyzed by automated western blot (Jess, Protein Simple)*

In distinction to SKOV3 tumor cells, we did not detect any upstream peak of the stalled ribosomes at the TTA codon in FT194 cells (Fig. 3.10 A), suggesting that the lower level stalling observed in FT194 cells (Fig. 3.6 A) was insufficient to cause detectable ribosome collisions. Consistent with this observation, GCN2 was not phosphorylated in FT194 cells in response to cis-Pt treatment (Fig. 3.10 B). Together, these data demonstrate that cis-Pt induced marked stalling at Leu TTA codon in SKOV3 cells and triggered subsequent ribosome collisions which is sensed by GCN2 in a GCN1-dependnet manner.

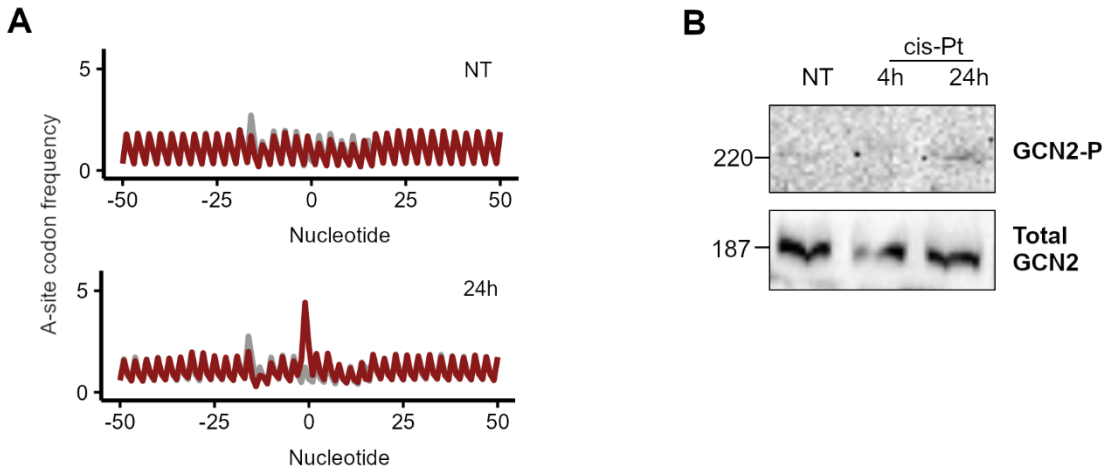

Figure 3.10 ***Cis-Pt does not cause ribosome collisions and GCN2 activation in FT194 cells.*** *[A]Ribosome dwelling frequency surrounding the Leu TTA codon (red) compared to Leu CTT codon (gray) in untreated (NT) and treated FT194 with 5 μM cis-Pt for 24h. Cumulative plots of transcript fragments coverage surrounding TTA or CTT codons, centered at the second T nucleotide of the TTA or CTT codons, respectively, which is designated as zero. Differences were insignificant, Mann-Whitney test. [B] Cis-Pt treatment does not induce phosphorylation of GCN2 in FT cells. Representative immunoblots (n=2 biologically independent replicates).*

3.2.4 GCN2 depletion abolishes cis-Pt-dependent ribosome collisions and triggers apoptosis

To elucidate the role of GCN2 in SKOV3 cis-Pt resistance, we knocked down GCN2 using shRNA and produced the shGCN2-SKOV3 cell line, in which GCN2 level was reduced to ~15% (Fig. 3.11 A). GCN2 knockdown impaired cell growth and morphology (Fig. 3.11 B) and increased the cytotoxic effect of cis-Pt resulting in a lower EC50 dose (Fig. 3.11 C).

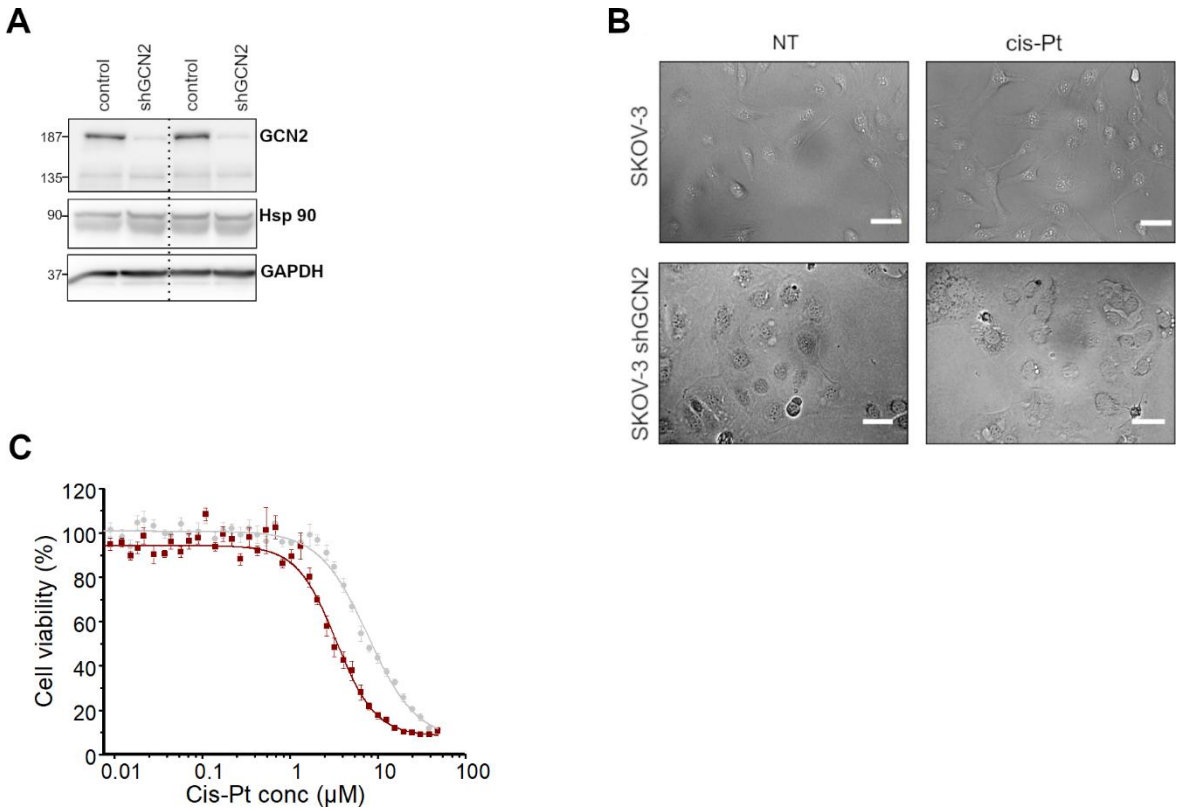

Figure 3.11 ***GCN2 knock-down sensitizes SKOV3 to cis-Pt treatment*** *[A] Efficiency of the GCN2 knockdown estimated by immunoblot using anti-GCN2 antibodies. The GCN2 level in shGCN2-SKOV3 cells (designated shGCN2) was reduced to ~15%. Note the high basal expression of GCN2 in SKOV3 even without treatment (control). Thin vertical lanes denote excised samples unrelated to this experiment. [B] Cell morphology of cis-Pt treated shGCN2-SKOV3 changes. Bright-field microscopy images of cells grown for 24h in absence (NT) or presence of 10 µM cis-Pt for SKOV3 and 3.5 µM for shGCN-SKOV3. [C] Cell viability of SKOV3 (gray) and shGCN2 (red) cells upon treatment with different cis-Pt concentrations for 5 days. EC50 is 3.5 µM and thus, we established 3.5 µM for the cis-Pt treatment. Data are means ± SEM (n=8 biological replicates).*

Moreover, in the absence of GCN2, global translation was markedly impaired as evidenced by the decreased polysomal fraction observed following cis-Pt treatment (Fig. 3.12 E). In support of diminished translation in response to cis-Pt treatment, we observed the accumulation of charged tRNAs in shGCN2-SKOV3 cells (Fig. 3.12 D), likely a result of diminished consumption of tRNAs.

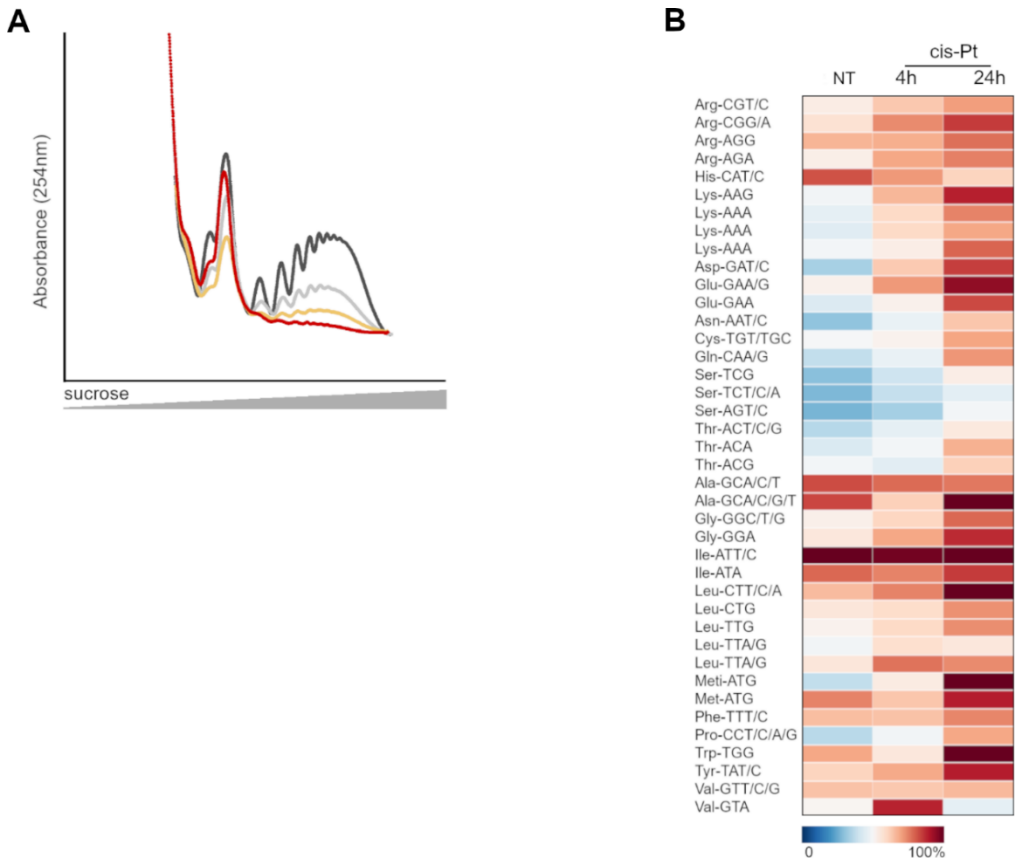

Figure 3.12 ***Cis-Pt treatment affects translation in GCN2 knock-down SKOV3 cells****. [A] Polysome profiles of untreated (black), or treated for 24h with cis-Pt 3 µM (gray), 4 µM (yellow) or 5 µM (red) shGCN2-SKOV3 cells. [B] Microarrays of aminoacyl-tRNA of untreated (NT) or shGCN2-SKOV3 cells treated with cis-Pt for 4h and 24h. The color key indicates the percentage of charged tRNAs over the total amount of each isoacceptor. The microarrays were performed in duplicates and represented as mean values. Confidence intervals between both replicates is 98% for the untreated cells and 93% for treated with cis-Pt for 24h, respectively.*

Notably, at 24 h post treatment we also detected stalling at the Leu TTA codon in the shGCN2-SKOV3 cells (Fig. 3.13A), which was not due to leucyl- $tRNA^{Leu}$(UAA) paucity (Fig. 3.12 B) or cis-Pt-induced mRNA damage on adjacent pyrimidines (Fig. 3.13.B). Although ribosome stalling at the TTA codon was of the same magnitude as in SKOV3 cells (compare Fig. 3.3 B and 3.13 A), we did not detect any peak upstream of the peak at the TTA codon, suggesting an absence of ribosome collisions in shGCN2-SKOV3 cells (Fig. 3.13 C). ZAKα was phosphorylated in shGCN2-SKOV3 cells, at 24 h post treatment, along with markedly activated JNK (Fig. 3.13 D). We noted increased basal levels of p-JNK in untreated shGCN2-SKOV3, suggesting a chronic basal activation of the JNK/p38 pathways in the absence of GCN2. GCN2 knockdown cells were susceptible to cis-Pt induced cell death as detected by cleaved PARP1 (Fig. 3.13 E). By contrast, cis-Pt treatment in the parental SKOV3 cell line did not activate apoptotic pathways (Fig. 3.13 E). These data support the notion that GCN2 absence

sensitized cells to cis-Pt treatment and decreased their ability to resolve ribosome stalling, leading to unresolved RSR and subsequent apoptosis.

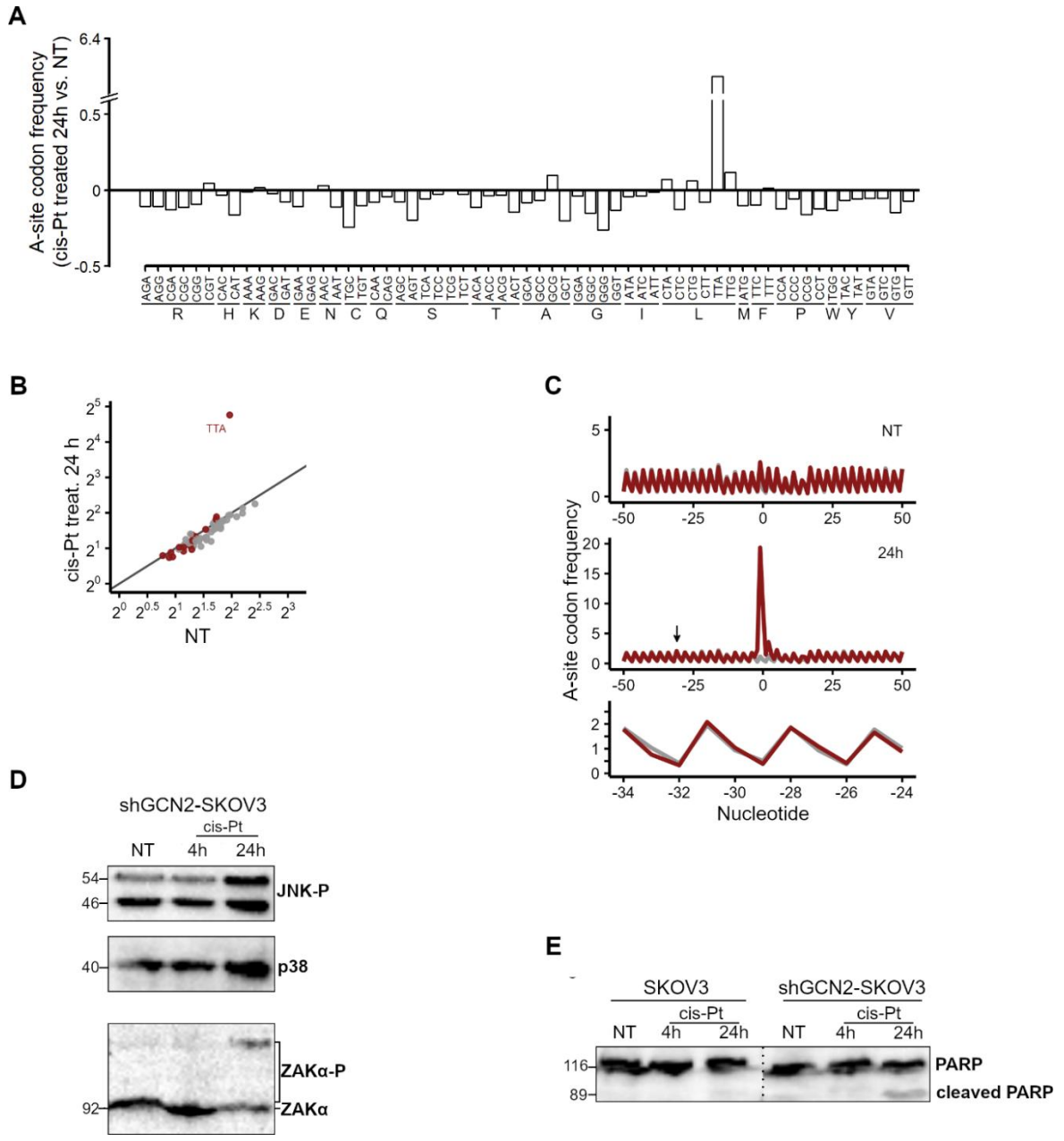

Figure 3.13 ***GCN2 knockdown induces apoptotic cascade.*** *[A] Relative changes in ribosome frequency at A-site codons in shGCN2-SKOV3 treated with 3.5 µM cis-Pt for 24h versus untreated (NT) cells, as determined by Ribo-seq. The normalized codon occupancy is presented as a ratio of cis-Pt treated vs. untreated. [B] Scatterplots of codon-specific A-site ribosomal occupancy (log2 scale) comparing untreated (un) vs cis-Pt-treated shGCN2-SKOV3 cells for 24h. Codons with two adjacent pyrimidines are highlighted in red. [C] Ribosome frequency at A-site codons in untreated shGCN2-SKOV3 (NT) or treated with 3.5 µM cis-Pt for 24h centered at Leu TTA (red) or CTT (gray) codons. Cumulative plots of transcript fragments coverage surrounding TTA or CTT codons, centered at the second T nucleotide of the TTA or CTT codons, respectively, which is designated as zero. Trailing ribosome at 30 nt upstream of the TTA-Leu codon stalling site is designated by an arrow. Inset, a zoom-in at appr. 30 nt upstream of the TTA (red) and CTT (gray) Leu codons of cells treated for 24h. Differences were insignificant, Mann-Whitney test. [D] ZAKα phosphorylation and JNK activation in shGCN2-SKOV3 following treatment with 3.5 µM cis-Pt for 24h. NT, no treatment. p38 serves as loading control. [E] Cis-Pt treatment induces cleavage of the apoptotic marker PARP1. shGCN2-SKOV3 were treated with 3.5 µM cis-Pt and SKOV3 with 10 µM for 24h. Representative immunoblots (d, e; n=2, biologically independent replicates). Thin vertical lanes denote excised lanes with samples unrelated to this experiment. Molecular weight of the corresponding bands (D, E) shown on the left.*

3.2.5 GCN2 resolves ribosome collisions at Leu-TTA codons

Cis-Pt treatment caused a similar degree of stalling at Leu-TTA codons in both SKOV3 and shGCN2-SKOV3, with no detectable collisions in shGCN2-SKOV3 cells (Fig. 3.6 A, 3.8, 3.13 A and C). The stalling sites of the top 100 transcripts in SKOV3 and shGCN2-SKOV3 cells showed a very little overlap (Fig. 3.14 A), overall suggesting a stochastic nature of the stalling at TTA codons. When comparing the ribosome-protected fragments (RPFs) coverage surrounding the TTA-codon stall sites, we detected a significant decrease of RPFs downstream of the TTA codon in shGCN2-SKOV3 post treatment (Fig. 3.14 B), suggesting a spontaneous ribosome drop-off at TTA codons. In addition, lack of GCN2 led to a detectable decrease in translation of TTA-codon containing transcripts (Fig. 3.14 C). By contrast, despite the same marked stalling in SKOV3 cells, the RPFs were nearly equally distribution up-and downstream of the TTA-stall sites (Fig. 3.14 B), which we attribute to GCN2-dependent resolution of collisions to maintain unperturbed elongation downstream of the TTA-stall sites.

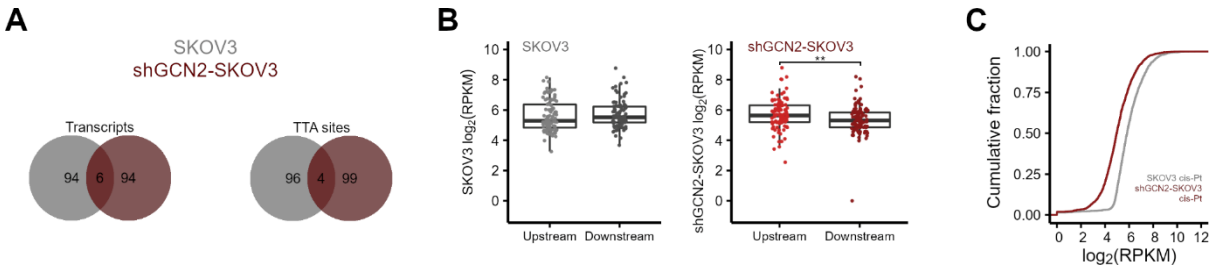

Figure 3.14 ***GCN2 resolves stalling at Leu-TTA codons and restores translation.*** *[A] Venn diagram of the overlap between the top 100 transcripts and the TTA-stalling sites for SKOV3 and shGCN2-SKOV3 treated with cis-Pt for 24h. [B] Boxplot of the RPFs in the upstream (light color) and downstream (dark color) vicinity of the Leu-TTA codons in SKOV3 (left panel) and shGCN2-SKOV3 (right panel) treated with cis-Pt for 24h. **, p = 0.0038, Mann-Whitney test. [C] Cumulative RPF fraction of transcripts containing TTA codons of cis-Pt treated SKOV3 and shGCN2-SKOV3 cells.*

Two tumor suppressor genes, EMP3 (encoding epithelial membrane protein 3) and GGT5 (encoding g-glutamyltransferase 5) have recently been described as poorly translated in some cancer types due to low expression of leucyl-tRNA synthetase and consequently poor translation of Leu codon [185]. GGT5 transcript was not expressed in SKOV3 and we did not detect any change in EMP3 expression following cis-Pt treatment. Both genes are enriched in Leu codons, but mainly CUC and CUG (e.g. GGT5 has one TTA and EMP3 none), suggesting that the marked stalling at TTA did not contribute to their expression and it is unlikely they contribute to cis-Pt resistance.

3.2.6 GCN2 is markedly activated in patients with recurring Pt-resistant ovarian cancer

In a retrospective study, we considered ten patients with advanced stage III epithelial ovarian cancer, with a median age of 61 years (range 52-73 years). The patients were divided into two groups (i) Pt-treatment resistant group – with a disease relapse during or within six months of completion of the Pt therapy, and (ii) Pt-treatment sensitive group with a disease recurrence longer than six months of completion of the therapy. Compared to the sensitive group, the primary tumors of the resistant group exhibited significantly higher immunoreactive score (IRS) of activated GCN2 (GCN2-P) and GCN2 (Fig. 3.15 A, B and Fig. 3.15 D). In addition, the JNK-P IRS was also higher in the resistant group compared to its nearly basal expression in the tumors from patients from the sensitive group (Fig. 3.15 C).

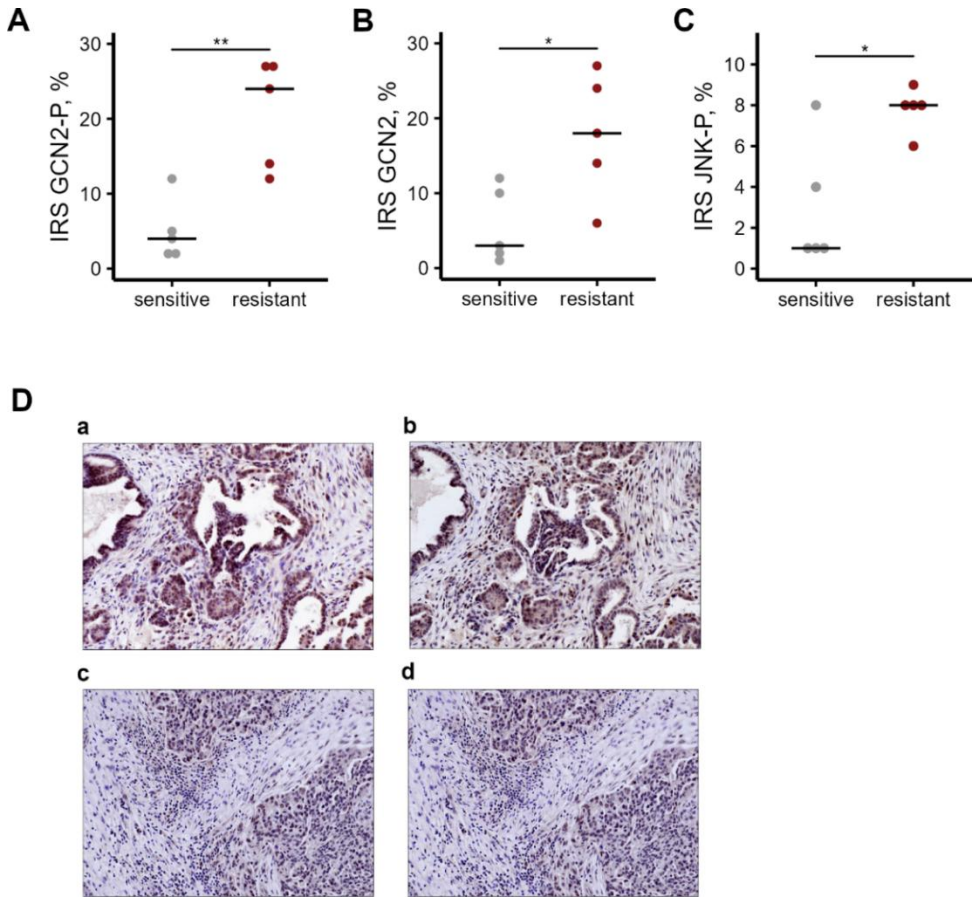

Figure 3.15 ***GCN2 is activated in tumors of patients with chemoresistant ovarian cancer.*** *A-C, Expression of GCN2-P [A], GCN2 [B] and JNK-P [C] of five patients sensitive to cis-Pt treatment (gray) and five patients resistant to treatment (red) as quantified by the IRS score (that is built from the intensity of immunohistochemical protein expression and the percentage of positive cells) from the histochemical immunostaining. p = 0.001 (A); p = 0.023 (B); p = 0.011 (C) (ANOVA test). [D] represents GCN2 and GCN2-P immunohistochemical analysis of primary tumor material from patients. a-d Representative examples of immunohistochemical staining of primary tumors with high expression of GCN2 (a) and GCN-P (b) and low expression of GCN2 (c) and GCN2-P (d). a, b, primary tumors of patient from the cis-Pt-treatment resistant group. c, d, primary tumors of patient from the cis-Pt-treatment sensitive group. Magnification, x200.*

For three patients (one from the resistant group and two from the sensitive group), a metachronous recurring tumor was accessible for analysis (Table 3-1). In the metachronous metastatic tissues we detected much higher GCN2 activation (i.e. higher GCN2-P ISR score, Fig. 3.16 A) and enhanced GCN2 levels (Fig. 3.16 B). The progression-free survival correlated with the GCN2 activation and patients in the resistant group (i.e. with high GCN2-P IRS) exhibited much shorter median survival time (Fig. 3.16 C). The analysis convinces that GCN2 activation is a hallmark of cis-Pt-resistant tumors.

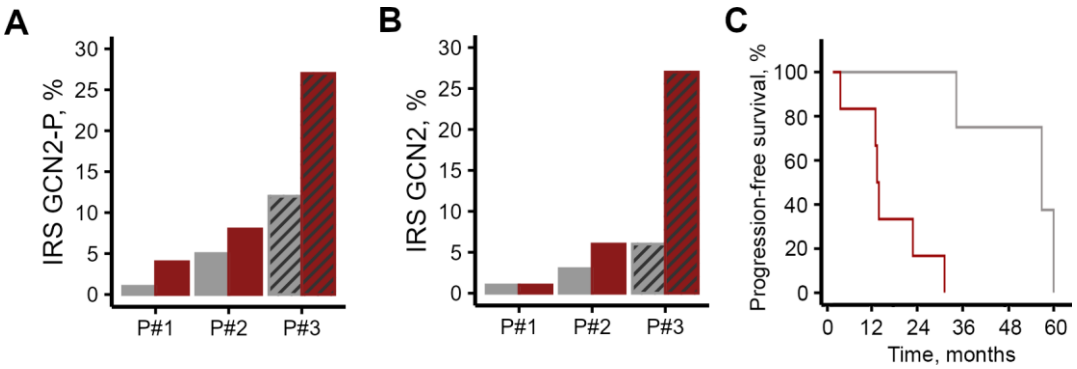

Figure 3.16 ***GCN2 activation in cis-Pt resistant tumors.*** *[A, B] Comparison of GCN2-P (A) and GCN2 (B) expression in primary (gray) and secondary (red) tumors of two patients from the sensitive group (plain bars) and one patient with Pt-resistant disease (dashed bars). [C] Progression-free survival of patients sensitive (gray) and resistant (red) to cis-Pt treatment. Median of the GCN2-P IRS for all patients in the cohort is 12 and is used a cut-off value. The sensitive group had GCN2-P IRS < 12; the resistant group - GCN2-P IRS > 12. p = 0.004 (Chi-squared test).*

Table 3-1 Patients with secondary recurring tumor.

Patient	Type of metastasis	Time (in months) between primary tumor surgery and appearance of metastasis	Time (in months) between cis-Pt treatment and appearance of metastasis
P#1	peritoneal	56	47
P#2	retroperitoneal	60	54
P#3	mesenteric	12	5

3.3 Discussion

Here, we show that prolonged cis-Pt treatment activates RSR and causes ribosome collisions. Cis-Pt induced damage of the $tRNA^{Leu}$(UAA) leads to ribosome stalling at TTA and ribosome collisions which unleash an adaptive signaling response to activate GCN2 to sustain gene expression, culminating in survival benefit and resistance against chronic cis-Pt treatment (Fig. 3.17 A). In contrast, GCN2 depletion sensitizes cells to cis-Pt; cells lacking GCN2 are unable

to process ribosome stalling causing an increased and sustained activation of JNK/p38 which triggers apoptosis (Fig. 3.17 B). In presence or absence of GCN2, JNK signaling is activated; however, the levels of activation are very different and resulted in different outcomes, thus, corroborating earlier observation that sustained activation of JNK leads to apoptosis, while transient, milder activation leads to cell survival [138]. We did not find evidence for significantly activated DNA-repair pathways. Poly(ADP-ribose) polymerase (PARP) inhibitors were approved for maintenance therapy for patients with Pt-sensitive ovarian cancer with a partial or complete response to Pt-based chemotherapy, but not for such with a relapse of Pt-resistant disease [186] which supports the notion that DNA-damage response might not be central to the acquisition of resistance to chronic Pt treatment.

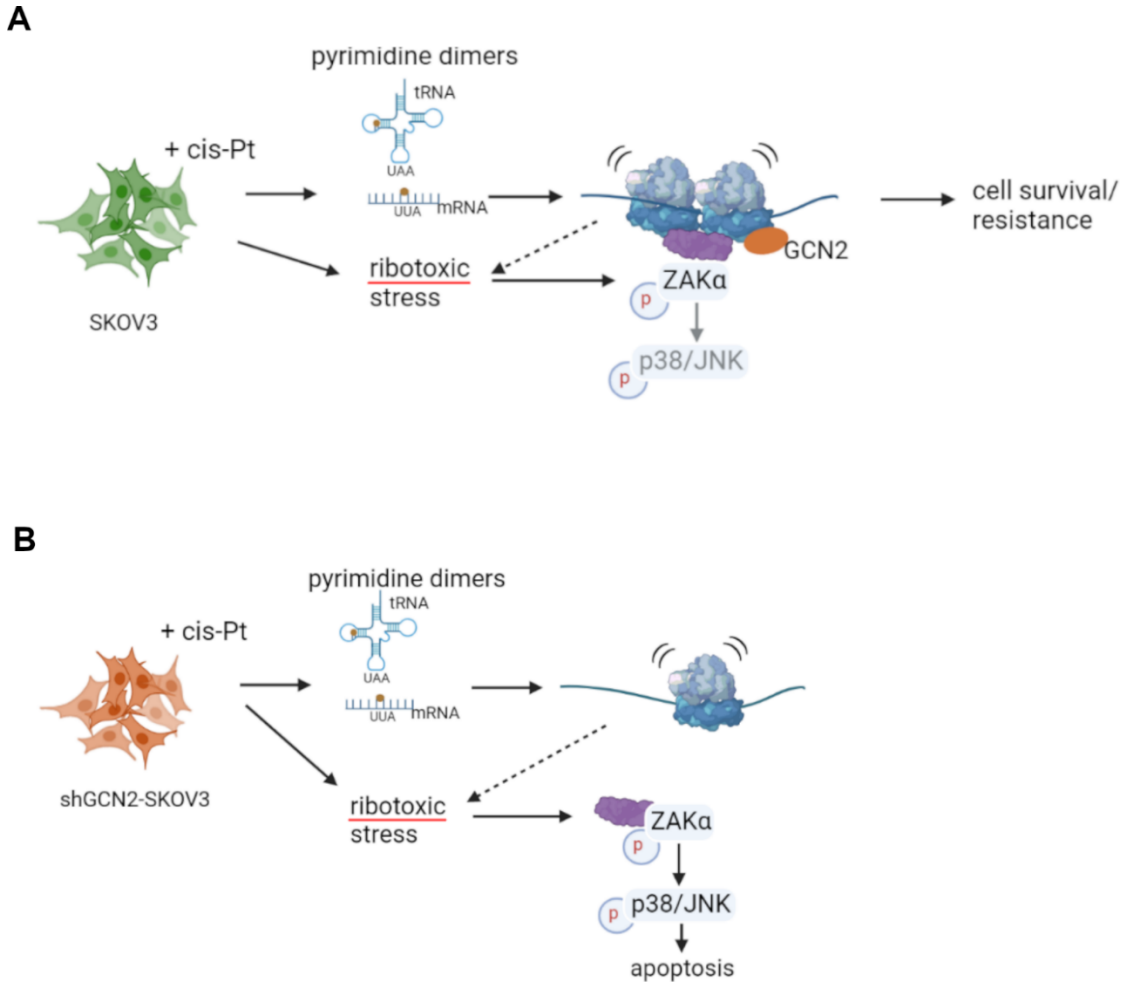

Figure 3.17 ***Model of enhanced cell survival following cis-Pt treatment by sensing and resolving ribosome collisions****. [A] Cis-Pt-induced ribosome stalling at TTA codons and ribotoxic stress induce ZAKα autophosphorylation and GCN2 to GCN2-P to resolve collisions and confer cell survival following cis-Pt treatment (i.e. acquisition of resistance). JNK signaling is marginally activated, likely through ZAKα autophosphorylation. [B] In absence of GCN2 autophosphorylated ZAKα triggers apoptosis through severe activation of p38/JNK. Damage of tRNA^{Leu}(UAA) (and di-pyrimidine dimers mRNA) can also induce ribotoxic stress through ribosome stalling (dashed arrow). We cannot exclude di-pyrimidine formation within the codon itself, but it is less likely to be the major factor driving ribosome stalling; codons containing two consecutive pyrimidines are equally susceptible to di-pyrimidine formation but we did not observe any detectable stalling at any codons (Fig. 3.6 D and 3.13 B). Overall, our results are consistent with a model where ZAKα-senses the cis-Pt-induced ribotoxic stress and the activation of GCN2 fine tunes cellular response.*

An obvious question is why ribosome stalling occurs only at TTA codons. The ribosome stalling is driven by cis-Pt induced chemical modification within the cognate $tRNA^{Leu}$(UAA). Experimental work with E. coli tRNAs selects cytidine or uracil adjacent to naturally modified ψ as hotspots sensitive to pyrimidine crosslinking agents and susceptible of forming di-pyrimidines [187], and tRNAs containing such crosslink are translationally incompetent [188]. Thus, U27 adjacent to ψ28 $tRNA^{Leu}$(UAA), which we detected as the target of cis-Pt, likely form di-pyrimidine dimers, which alter the U27-A43 and ψ28-A42 pairs (Fig. 3.7 B) and consequently the flexibility of the anticodon stem. The flexibility of the anticodon stem is crucial for decoding [189,190], hence the cis-Pt induced chemical change at U27 affect $tRNA^{Leu}$(UAA) functions in translation. $tRNA^{Leu}$(UAA) is low-abundance tRNA (i.e. within the lower 10%ile of abundance [182]) and even small alterations in such low-abundance tRNA would have profound effect on the ribosome dwelling.

Transcriptome-wide analysis of HEK293 cells treated with DNA-damaging chemotherapeutic drugs, provides evidence of enhanced expression of human Schlafen 11 (SLFN11) that sensitizes tumor cells to the chemotherapeutics [163]. SLFN11-dependent cleavage of type II tRNAs (e.g. $tRNAs^{Ser}$ and $tRNAs^{Leu}$, and specifically $tRNA^{Leu}$(UAA) that pairs to TTA codon), downregulates expression of genes essential in maintaining the DNA damage response and repair [163]. Consistent with this study, we detected an increase in SLFN11 mRNA expression in the cis-Pt-sensitive shGCN2-SKOV3 cells post treatment (Table 3.2), however with no changes in the $tRNA^{Leu}$ and $tRNA^{Ser}$ levels (Fig. 3.12 B), suggesting that SFN11 is not required for cis-Pt-sensitivity of shGCN2-SKOV3.

Table 3-2. Changes in mRNA expression of SLFN11 following cis-Pt treatment. Expression changes are represented as fold-changes changes of the SPFN11 transcript expression (RNA-seq set) of treated vs untreated cells.

Sample	Fold-change mRNA expression (log_2 FPKM)
SKOV3 24h cis-Pt	0.66
shGCN2-SKOV3 24h cis-Pt	1.50

Cells have evolved dedicated quality control pathways to process basal levels of ribosome collisions and resolve gene expression, thus, providing a fitness benefit to survive under moderate chronic stress [120,183]. Combined with the observations in the patient cohort, our data select GCN2 as the central molecular node in providing a survival benefit and acquisition of resistance to cis-Pt. Thus, GCN2 inhibitors may prove useful as adjuvants to Pt-based

chemotherapies, diminishing the intrinsic adaptive ability of cells to resolve chronic stress and thus, preventing the acquisition of chemoresistance. However, GCN2 is a vital stress-activated kinase [100], thus, combination therapies to sensitize cells to Pt-based therapeutics may work in a narrow concentration window of GCN2 inhibitors.

3.4 Methods

3.4.1 Cell lines

SKOV3 cells (ATCC culture collection) were cultured in RPMI 1640 (Panbiotech) medium supplemented with 10% fetal bovine serum and 2 mM glutamine at 37°C under a humidified environment with 5% CO2.

To generate GCN2 knockdown cell lines, shRNA sequences targeting exon 2 of human GCN2 (5'-GCCTAACTGGTGAAGAAGTAT-3') or irrelevant target luciferase (5'-CGCTGAGTACTTCGAAATGTC-3') were designed and cloned into the pLKO.1-puro vector. pLKO.1 plasmid was transfected into HEK293T cells alongside the packaging vectors psPAX2 and pMD2.G. The following day, medium was replaced with 2.5mL virus production medium containing 30% fetal bovine serum. After two days, the virus-containing supernatant was sterile filtered and used to infect SKOV3 cells in the presence of 4µg/mL polybrene. SKOV3 cells bearing the shRNA transgene were selected using 3 µg/mL puromycin to generate shGCN2-SKOV3 and shLuc-SKOV3, respectively.

FT cells were grown in DMEM (Panbiotech) supplemented with 10% fetal bovine serum at 37°C under a humidified environment with 5% CO2 were used as a control cell line. All cells were regularly tested for mycoplasma and were determined mycoplasma-free.

3.4.2 Cis-Pt treatment

To determine the EC_{50} of cis-Pt in the SKOV3 and shGCN2-SKOV3 cell lines, the viability of cells was determined using the Vi-CELL Cell Viability Analyzer. A suspension of 20 x 10^3 cells/mL in media was generated. Using the Multidrop Combi reagent dispenser, 50 µL of the cell suspension was added into each well of a 384-well View plate (Perkin Elmer) for a total of 1000 cells/well and incubated overnight at 37°C. The next day, using the HP D300 Digital Dispenser DMSO (control) or cis-Pt were sprayed in concentration ranging from 8 nM to 50 µM in a scrambled pattern. Plates were further incubated for 5 days at 37°C. The total

luminescence was read after adding 40 µL of ATPlite (Perkin Elmer) on Envision plate reader equipped with a US-Luminescence detector. Data was analyzed using XLFit.
In all experiments, SKOV3, shGCN2-SKOV3 and FT174 cells were treated with 10, 3.5 or 5 µM cis-Pt, respectively.

3.4.3 Immunoblotting

0.5-1.0x106 SKOV3, shGCN2-SKOV3 or FT194 cells were grown with and without cis-Pt and lysed in lysis buffer (0,625 M Tris-HCl pH 6,8; 10% glycerol; 3% SDS; 0.5 mM EDTA, 5% (v/v) 2-mercaptoetanol, 0,1% (w/v) bromophenol blue [191]. Cell lysates were separated on SDS-PAGE, transferred onto a PDVF membrane (Merck Millipore) and probed with a primary antibody overnight at 4°C. The following antibodies were used: anti phospho-SAPK/JNK (Thr183/Tyr185) (1:1000 dilution, Cell Signaling Technology, cat# 81E11), anti phospho-p38 MAPK (Thr180/Tyr182) (1:1000 dilution, Cell Signaling Technology Cat# 9211), anti p38 MAPK (1:1000 dilution, Cell Signaling Technology, cat# 9212), anti PARP (1:1000 dilution, Cell Signaling Technology, cat# 9542) anti beta actin (1:1000 dilution, Cell Signaling Technology, cat# 8457), recombinant anti-GCN2 antibody (1:1000 dilution, Abcam, cat# ab134053), rabbit anti-GCN1L1 antibody (1:50 dilution, Bethyl Laboratories, cat# A301-843A), anti phospho-GCN2 (1:1000 dilution, Cell Signaling Technology, cat# 94668). HRP-conjugated goat anti-rabbit IgG antibody (1:3000 dilution, Biorad, cat# 172-1019) was used as secondary antibody and detection was performed by ECL (Bio-Rad Gel Doc XRS+). Immunoblot analysis of GCN1 utilized the capillary electrophoresis system (Jess, ProteinSimple) and the GCN1 positive band was normalized to the total protein with the Jess quantification module.
For Phos-tag gel immunoblotting, the cell lysates were resolved by 7% SDS-PAGE containing 10.7 mM Phos-tag (Wako, AAL-107) and 21.3 mM MnCl225. The gels we blotted onto PDVF membrane and immunostained with anti ZAKα antibody (dilution 1:2000, Bethyl Laboratories Inc lab, cat# A301-993A) overnight at 4°C.

3.4.4 Polysome profiling

Approximately 2 million SKOV3 or shGCN2-SKOV3 cells were used for each experiment. Untreated cells or cells treated with cis-Pt for 4h or 24h were harvested in polysome lysis buffer (10 mM Tris.HCl (pH 7.4), 5 mM MgCl2, 100 mM KCL, 1% Triton X-100) supplemented

with 100 µg/ml cycloheximide and 2mM DTT. Samples were layered onto a 5 ml sucrose gradient and then centrifuged for 1.5 h at 148,900xg (Beckman Coulter, SW 55Ti rotor) at 4°C. The gradients were fractionated on a piston gradient fractionator (Biocomp) and the absorbance at 254nm was recorded.

For analysis of the GCN1, fractions from the sucrose gradients were collected and subjected to immunoblotting using the rabbit anti-GCN1L1 antibody. Analysis utilized the capillary electrophoresis system (Jess, ProteinSimple). For normalization, the peak area corresponding to the GCN1 band was normalized to the total protein with the Jess quantification module.

3.4.5 tRNA microarrays

Comparative microarray analysis was performed to quantify the absolute tRNA amount and the fraction of aminoacyl-tRNAs using protocols described earlier[170] [192]. To determine the fraction of aminoacyl-tRNAs, total RNA was extracted from cells using acidic phenol (Roth, pH 4.5), which preserves the aminoacyl group at the 3'tRNA end. Extracted total RNA was split into 2 aliquots, one aliquot was treated with periodate to oxidize non-aminoacylated tRNAs leaving the aminoacyl-tRNAs intact. Thereafter, both aliquots were deacylated by incubating with 125 mM Tris-HCl, pH = 9.0 containing 0.1 M EDTA and 0.5% (w/v) SDS at room temperature for 45 minutes, followed by a treatment with an equal volume of 1M NaOAc, pH = 5.5. The single stranded 3' NCCA ends of the deacylated tRNAs were then ligated to a fluorescently labelled RNA/DNA stem loop oligonucleotide; the oxidized sample with a Cy3-labelled oligo and the non-oxidized control sample with an Atto647-labelled oligonucleotide respectively.

For tRNA abundance, total RNA was isolated with TriReagent (Sigma Aldrich), which simultaneously deacylates all tRNAs. tRNAs were ligated to a Cy3-labelled RNA/DNA hybrid oligonucleotide. For comparison, total RNA from HEK cells was isolated and labeled with Atto647-labeled oligonucleotide.

Labeled tRNA samples were then loaded onto a microarray consisting of 40 full-length tDNA probes recognizing all nuclear encoded human isoacceptor tRNAs and hybridized for 16 h at 60°C. Fluorescence signals of microarrays were recorded with a GenePix 4200A scanner (Molecular Devices) and statistically analyzed with in-house scripts in Python (version 3.7.0) [182]. A detailed protocol is available at dx.doi.org/10.17504/protocols.io.hfcb3iw.

3.4.6 Ribo-seq and analysis

Approximately 5 million SKOV3, SKOV3-shGCN2 or FT194 cells were used to extract ribosome-bound complexes. Untreated cells or cells treated with cis-Pt for 4h or 24h were washed once with PBS and lysed in polysome lysis buffer (10 mM Tris HCl (pH 7.4), 5 mM MgCl2, 100 mM KCL, 1% Triton X-100) supplemented with 2 mM DTT and 100 µg/ml cycloheximide). Lysates were centrifuged at 14,000xg for 10 min at 4°C. Cleared lysates were digested with RNase I (15 U; Lucigen) and layered onto sucrose gradients to collect the monosomes. RPFs were extracted and libraries were prepared as described previously [192] [193]. Samples were sequenced on Hi-Seq3000/4000 (Illumina).

Sequenced reads were trimmed (fastx-toolkit v0.0.13.2; quality threshold=20) and depleted from the adapter sequences (cutadapt v1.8.3; minimal overlap=1 nt). The remaining reads were mapped to the human genome (GRCh38.p13) using STAR v2.5.4b 52 (--outFilterMultimapNmax 1 --outFilterMismatchNmax 1). Uniquely mapped reads were normalized to reads per million mapped reads (RPM), or reads per kilobase per million mapped reads (RPKM). Independent biological replicates of SKOV3 untreated show high reproducibility (R2=0.783, Pearson correlation coefficient), thus, the replicates were merged into one metagene set using samtools v1.7. To identify the ribosomal A site within the RPFs, the RPFs were binned into groups of identical read length and then each bin aligned individually to the start codon thus identifying the P-site 22,53,54, using the calibration tool https://github.com/AlexanderBartholomaeus/MiMB_ribosome_profiling). Briefly, bins with RPFs of the same size were plotted individually covering the start codon region including 50 nt upstream and downstream of it, which is used to determine the individual offset distance between the 5' end of the RPF and the start codon in the ribosomal P site, and by adding 3 nt to the A site. We considered six bins for calibration (29-34 nt length).

For each transcript, all A-site codon occupancies are summed up and normalized on the transcript background as described [171]. The comparison between A-site codon occupancy (frequency) between untreated and cis-Pt treated cells, the A-site codon occupancy across all transcripts for treated cells were divided by the those for untreated cells and presented as the differential A-site codon frequency [172].

Transcripts with stalled ribosomes at Leu-TTA codon were ranked by the number of reads (RPM) detected at the TTA codon. The top 100 Leu-TTA positions with stalled ribosomes were used to calculate ribosomal coverage (RPKM) of 30 nt up- or downstream of those Leu-TTA codons and to generate boxplots. Ribosomal stalling at TTA codons within one transcript

was mostly prevalent at one TTA codon despite the much larger number of Leu-TTA codons within each CDS. However, there was also significant stalling at other Leu-TTA codons albeit to much lower extent. To rule out the influence of other TTA codons, we selected a window of 30 nt up- and downstream of the TTA codon with the highest ribosomal accumulation. This window represents the footprint of a single ribosome, though the results were not affected by increasing the window up to 60 nt by a step of 10 nt.

3.4.7 Profiling of tRNA^{Leu} (UAA) modifications by AlkAnilineSeq

Analysis of potential alterations of tRNA modifications upon cis-Pt treatment was performed by AlkAnilineSeq protocol, as described previously [181,194]. This method displays high sensitivity for detection of sub-stoichiometric amounts of natural modifications (e.g. m7G, m3C, D and ho5C), as well as RNA abasic sites resulting from spontaneous loss of bases in vivo or following chemical treatment. In brief, total tRNA was isolated by low-scale column chromatography[195], and subjected to mild alkaline hydrolysis, followed by cleavage of RNA abasic sites by aniline. Specific adapter was ligated to the 2'-end of tRNAs, and the 5'-phosphate released from the tRNA fragment upon aniline treatment was used for direct adapter ligation in library preparation protocol (NEBNext Small RNA Library Prep set for Illumina). Sequencing was performed on NextSeq2000 in single read 50 nt (SR50) mode, to collect ~ 20 million reads per sample. Data analysis included trimming step, alignment to the reduced tRNA reference sequence [196], counting of 5'-reads extremities and calculation of AlkAnilineSeq scores [194] AlkAnilineSeq signals are calculated as a number of read mapped to the 5'-reads' extremities mapped to a given position divided by median value of reads mapped to a neighboring 10 nt window.

Comprehensive profile of natural RNA modifications was not firmly established for human tRNA^{Leu}(UUA), because of its low expression level in human cell lines [182]. However, analysis of FTSJ1-dependent tRNA modifications by LC-MS allowed for mapping Cm32, ncm5Um34 and m1G37; both 2'-O-methylations at Cm32 and Um34 are FTSJ1-dependent [197]. To complete the modification profile of tRNALeuUAA, we further analyzed high-throughput tRNA mapping obtained for human tRNAs using RiboMethSeq (for detecting 2'-OMe (Nm) residues) [198], AlkAnilineSeq (for m3C, m7G, D and ho5C) (this work), Bisulfite-Seq (for m5C and some other non-deaminated C) and HydraPsiSeq (for pseudouridine (ψ), m^{5}U and some other hydrazine-insensitive modifications at U*34) [199]. Our analyses validated the majority of previously mapped natural modifications for human tRNA^{Leu}(UAA) (Fig. 3.7 B) and other

isoacceptors (Fig. 3.7 C), except the recently reported Cm61 in $tRNA^{Leu}(UAA)$ [200], which was not confirmed by RiboMethSeq analysis.

3.4.8 Patients and tissue samples

The study was approved by the Research and Ethics Committee of the Otto-von-Guericke University, Magdeburg, Germany (Nr.57/17). Patients gave written informed consent before surgery. Additional individual consent for this analysis post surgery was not needed.
For the study, ten patients with primary invasive epithelial ovarian cancer, who had been admitted to the Department of Obstetrics and Gynecology, University Clinics, Magdeburg, Germany were retrospectively selected.
All patients underwent a primary debulking surgery and these samples from the primary tumor stored at the Department of Patology (Otto-von-Guericke University, Magdeburg, Germany) were used to determine the status of GCN2, GCN2-P, and JNK-P.
All patients had advanced (stage III) high-grade serous epithelial ovarian cancer. The median age at the time of primary diagnosis was 61 years (range 52-73 years). Following a primary debulking surgery, the patients received six cycles of carboplatin AUC5 treatment and paclitaxel 175 mg/m² every three weeks. In all cases, a complete resection was achieved. The follow-up was performed to the time of first recurrence/ progression. The progression-free survival (PFS) was estimated as a time between the date of the first diagnosis and the date of relapse and/or progression. Pt-resistant ovarian cancer was defined as disease recurrence during or within six months of completion of Pt-based therapy. Patients with recurrence longer than six months of completion of Pt-based therapy were defined as Pt-sensitive.

3.4.9 Immunohistochemistry of patients' tissues

The samples from the primary or metastatic tumor tissue were stored at the Department of Pathology (University Clinics, Magdeburg, Germany) and used to determine the status of GCN2, GCN2-P, and JNK-P. The formalin-fixed, paraffin-embedded tissue sections (3 µm) were dewaxed in xylol and rehydrated by descending concentrations of ethanol, followed by antigen retrieval with CC1mild (for GCN2, phGCN2 analysis) or CC2mild (for JNK-P, caspase-3 analysis). For antigen detection, we used the automated immunohistochemistry slide staining system VENTANA BenchMark ULTRA (Roche Diagnostics GmbH, Mannheim, Germany), the VENTANA iVIEW DAB Detection Kit (Roche Diagnostics GmbH) and the

indirect biotin-streptavidin method before counterstaining with Haemalaun solution. Incubation at 36°C for 32 min, dilution 1:100, was carried out for specific primary antibodies recognizing GCN2 (polyclonal rabbit antibody; ThermoFischer: #PA5-17523), GCN2-P (polyclonal rabbit antibody; ThermoFischer: #PA5-105886), or of caspase-3 (clone D2RGY, monoclonal mouse antibody; CellSignaling: #14220). The primary antibody for JNK-P (clone Thr183/Tyr185, monoclonal rabbit antibody; CellSignaling: #4668) was applied at room temperature for 30 minutes, dilution 1:50.

For assessment of immunohistochemical protein expression of GCN2, GCN2-P und JNK-P, staining intensity ([SI], 1=weak, 2=moderate, 3=strong) and the percentage of positive cells ([PC], divided into 10%iles, i.e. 1=1-10%, 2=11-20%, 3=21-30% etc. up to 10=91-100%) were scored and merged into a final immune-reactive score [IRS= SI x PC], which ranged from 0 to 30. The degree of apoptosis was evaluated by the percentage of caspase 3-positive cells.

In three patients, the expression of GCN2, GCN2-P, and JNK-P in the primary tumor was compared with their expression in the corresponding recurrent tissue (Table 3-2).

3.4.10 Statistics

The Mann-Whitney U test (confidence level = 0.95) was used to statistically assess differences in the sequences surrounding the A-site codon frequency in RStudio. Reproducibility between replicates in the RNA-seq and Ribo-seq were assessed by Pearson correlation analysis, and Spearman coefficient was used in the DESeq2 analysis [201]. Differences were considered significant when $p < 0.05$. The method of Kaplan-Meier was used to estimate PFS and was conducted by using software package SPSS 26 (Chicago, IL, USA). The equality of the survival curves was tested by the log-rank test. The mean IRS value for GCN2-P analysis was estimated 12, which was used as cut-off value for survival analysis. Pearson's chi-squared test was applied for testing the independence of categorical variables in order to compare expression in ovarian cancer tissue.

3.4.11 Data availability

RNA-Seq and Ribo-Seq data are deposited in Gene Expression Omnibus (GEO) database under accession number GSE197476. tRNA microarray data are deposited in GEO under the accession number GSE197648. AlkAnilineSeq is deposited in European Nucleotide Archive under the accession number PRJEB56781.

4 Effects of cis-Pt on a sensitive ovarian cancer cell line

Outlined in chapter 2 we determined the mechanism of resistance to cis-Pt in SKOV3 cells. Intrigued by the results, we set to determine the effects of cis-Pt in other ovarian cancer cells. To explore this, we chose the A2780 cell line, a human ovarian cancer cell line derived from the tumor tissue of an untreated patient [202]. Since the cell line has not been exposed to any anticancer drugs or chemicals, it was interesting to see the effects of cis-Pt on these cells. Cis-Pt led to a reduction of tRNAs in these cells but did not elicit the classical GCN2 activation or affect the ribosomal occupancy at the sense codons. We further explored the effects of cis-Pt on the internal mRNA modification m^6A and its regulator proteins. We compared the observations to SKOV3 cells to identify commonalities and disparities. Exactly which pathways or which molecules are responsible for the effects seen in A2780 still remains elusive and needs to be explored further.

All experimental data such as the RNA seq and ribo-seq and tRNA microarrays were obtained by myself while the bioinformatic analysis of the deep sequencing data (Fig 4.3 and 4.4) was performed by Leonardo Santos, a colleague and fellow PhD student in our lab.

4.1 Introduction

Cisplatin (cis-Pt) is widely used as a broad-spectrum anti-cancer agent effective against various solid tumors. Genomic DNA is generally considered the primary pharmacological target causing alterations such as DNA mono adducts, intrastrand and interstrand DNA cross-links and DNA-protein cross-links [18,203]. And the ability to bind to DNA in turn affects various downstream processes rendering cancer cells susceptible to its toxic effects. However, there is evidence suggesting that DNA is not the exclusive target of cis-Pt and that other biomolecules such as RNAs, phospholipids, peptides and proteins are likely involved in the anticancer activity, drug toxicity and resistance of cancer cells [19,203–205]. Besides the key biomolecules or the translation machinery itself, chemical modifications on the biomolecules also affect their molecular function. Such modifications on the DNA, RNA or proteins are also known to play a regulatory role and affect various signaling pathways. DNA modifications are widely known and have been extensively studied; RNA modifications however are relatively new in this arena

but there is increasing interest in the field. Post transcriptional modification on RNA molecules have important ramifications on the fate of the proteins. Researchers are now focusing attention on RNA modifications and their regulatory roles in various biological processes [206] [207], and have implicated RNA modifications to play an important role in regulation of various cellular processes and in diseases including cancer [208] [209] [210] [211]. Among the well characterized modifications is the m^6A modifications on RNA which is the most prevalent internal mRNA modification in mammals, occurring at a frequency of 0.15–0.6% of all adenosines [212]. m^6A has been a focus of research in epigenetics and has been shown to be a widespread modification on both protein coding and noncoding RNAs such as mRNA, miRNA, lncRNA, circRNA, tRNA [213]. This highly abundant m^6A modifications has been associated with cancer [214] [215].

The N^6 – Methyladenosine (m^6A) is a chemical derivative of adenosine in RNA that has wide-ranging roles in regulating gene expression. m^6A modification mostly occurs at RRACH motif (R denotes A or G, H denotes A, C, or U). In recent years m^6A has gathered tremendous scientific interest as an important modification. As the most abundant epitranscriptomic modification in eukaryotes, m^6A has been associated with almost all aspects of RNA-related biological processes including transcription, precursor mRNA (pre-mRNA) splicing, RNA translation, stability, structure, nuclear export and decay [203,216,217] [218]. m^6A RNA methylation is dynamic and reversible in mammalian cells regulated by 3 kinds of proteins namely the writers (methylases) which install the modification, the erasers (demethylases) which reverse the modification and readers which recognize the m^6A modified sites. A multicomponent methyltransferase complex m^6A catalyzes the m^6A modification, and the complexes they form jointly pro- mote. Methyltransferase 3 (METTL3), methyltransferase 14 (METTL14) and Wilms tumor 1-associating protein (WTAP) were the earliest discovered writers, which came together to form a complex jointly promoting the incorporation of m^6A onto RNA[219]. METTL16, a more recently discovered paralog of METTL3 has been shown to control cellular SAM levels and methylates U6 snRNA. With recent discoveries, the writer family has been extended to include more proteins KIAA1429, RNA-binding motif protein 15 (RBM15) and Zinc finger CCC domain protein 13 (ZC3H13) which have also been found to exhibit methyltransferase activity [219]. The demethylases FTO and ALKBH5 are the two known erasers. And the modification is recognized by reader proteins including YTHDF1/2/3, YTHDC1/2, and additionally some RNA-binding proteins, such as insulin-like growth factor 2 binding protein 1/2/3 (IGF2BP1/2/3), RNA-bound ELAV protein 1 (ELAVL1, also known as HuR), heterogeneous ribonucleoproteins (HNRNPs), FMR1 (Fragile X mental retardation 1) [149].

m^{6}A in cancer

As the most prevalent modification of RNA, m^{6}A has been widely studied and linked to various cancers [220] (reviewed in [221]). Studies have reported both oncogenic as well as onco-suppressive roles of m^{6}A [222]. m^{6}A methylation is thus referred to as a double-edged sword for cancer - excess m^{6}A modification in some genes lead to alterations of mRNA behavior and expression, in turn accelerating tumor development, while lack of m^{6}A modification on other genes may also lead to tumor progression [223]. The three types of regulatory proteins (writers, erasers and readers) are also often dysregulated in cancer. Through regulation of different downstream molecules and pathways, they play roles in promoting and/or suppressing cancer [213]. m^{6}A and is regulators have also been linked to various aspects of ovarian cancer [224] (reviewed in [225]). Downregulation of m^{6}A demethylases FTO and ALKBH5 is associated with reduced PARPi sensitivity in ovarian cancer [226]. The role of m^{6}A modification and m^{6}A-associated proteins is context dependent. Context- specific orchestrated interactions among m^{6}A-associated proteins govern the cellular consequences of the m^{6}A modification [218]. The molecular intricacies underlying the interplay between m^{6}A and the m^{6}A-associated proteins in and how this crosstalk impacts drug responses are worth investigating.

4.2 Results

4.2.1 Cis-Pt treatment decreases the levels of aminoacylated tRNAs

To assess the changes cis-Pt caused in A2780 cells, we performed RNA sequencing, ribosome profiling and tailored tRNA microarrays. RNA sequencing data from untreated and cis-Pt treated A2780 cells were used to compare the expression levels of the transcripts. Global expression analysis showed changes in various genes. Consistent with the fact that DNA damage was the main effect of cis-Pt, gene ontology (GO) analysis of the genes that were upregulated after treatment with cis-Pt (i.e. $\log_2 \geq 1$) showed enrichment in GO terms related to DNA damage response, transcription and regulation of transcription. The downregulated genes did not show any particular pattern or clustering.

We performed tRNA microarrays to elucidate if cis-Pt treatment alters the total and aminoacyl-tRNA levels. Cells were treated with 2µM cis-Pt and compared to untreated cells. Comparison of the tRNA levels before and after treatment showed that the total amount of tRNAs does not

change subject to treatment (Fig 4.1 B) but the levels of aminoacyl-tRNAs were greatly reduced after 24h of cis-Pt treatment (Fig 4.1 A). This effect was not specific to any particular tRNA or any tRNA family (i.e. tRNA isoacceptors charged with the same amino acid) but a general decrease in all tRNAs with the exception of few tRNAs such as $tRNA^{Arg}$(CGG), $tRNA^{Lys}$(AAG) which remained unaltered by treatment.

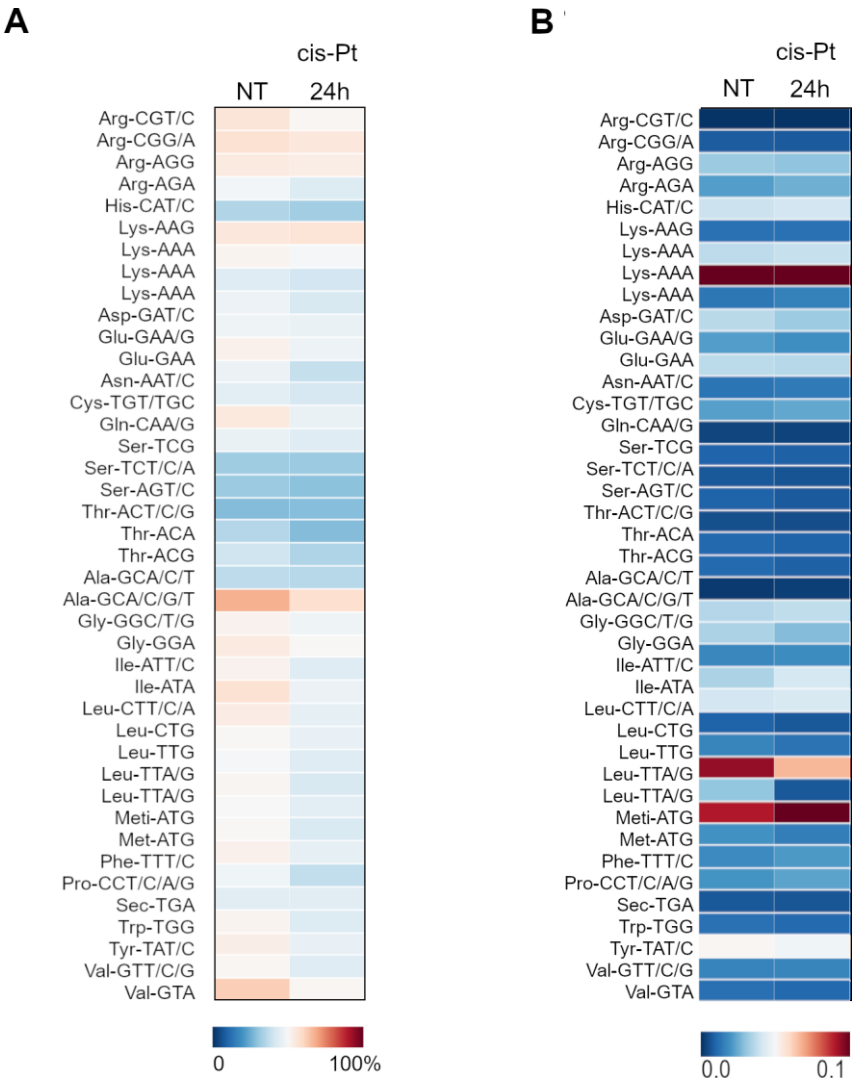

Figure 4.1 ***Cis-Pt treatment leads to reduction of aminoacylated tRNAs.*** *A) Heatmap representing microarray analysis of aminoacyl-tRNAs of untreated (NT) or A2780 cells treated with cis-Pt for 24h. The colour key indicates the percentage of charged tRNAs over the total amount of each isoacceptor. The arrays were performed in triplicates and are represented here as mean values. Confidence intervals between the replicates 1&2, 2&3 and 1&3 were 98%, 98% and 99% for the untreated cells and 96%, 98% and 98% for cells treated with cis-Pt for 24h, respectively. B) Heatmap representing the total amount of tRNA (abundance) in the cells under the mentioned conditions.*

4.2.2 Cis-Pt treatment in A2780 does not lead to ribosome stalling

Reduced levels of aminoacylated tRNAs could affect translation. Scarcity of amino acids could hinder the movement of the ribosomes on transcripts as the ribosome has to wait longer at the codons if it does not receive the corresponding amino acids as it traverses along the mRNA. We next performed ribosome profiling and computed the dwell times of the ribosomes on each of the sense codons (A-site ribosome occupancy). Fig 4.2 A represents the difference between cis-Pt treated vs untreated cells. Though treatment with cis-Pt led to a considerable decrease in charged tRNAs (Fig 4.1 A), this did not appear to largely affect the movement of the ribosomes along the transcripts. The A-site frequencies of the ribosomes of treated and untreated cells were comparable with only a marginal difference seen at a few codons (Fig 4.2 A). The codons where the ribosome stayed slightly longer after exposure to cis-Pt corresponded to isoacceptors of alanine, glycine, arginine (Fig 4.2 A). The highest difference was observed on the codons comprising only G & C namely GCG (alanine) and GGC (glycine) as seen in Fig 4.2 A. The codons with adjacent Gs and/or Cs appeared to be the ones with slightly increased ribosomal occupancy (Figure 4.2 B). Importantly, we did not detect an increased ribosomal occupancy at the leucine TTA codon at which we detected the marked stalling in SKOV3 cells (Chapter 2). Polysome profiles of these cells treated with or without cis-Pt showed no noticeable effect on translation upon cis-Pt treatment (Fig 4.2 C).

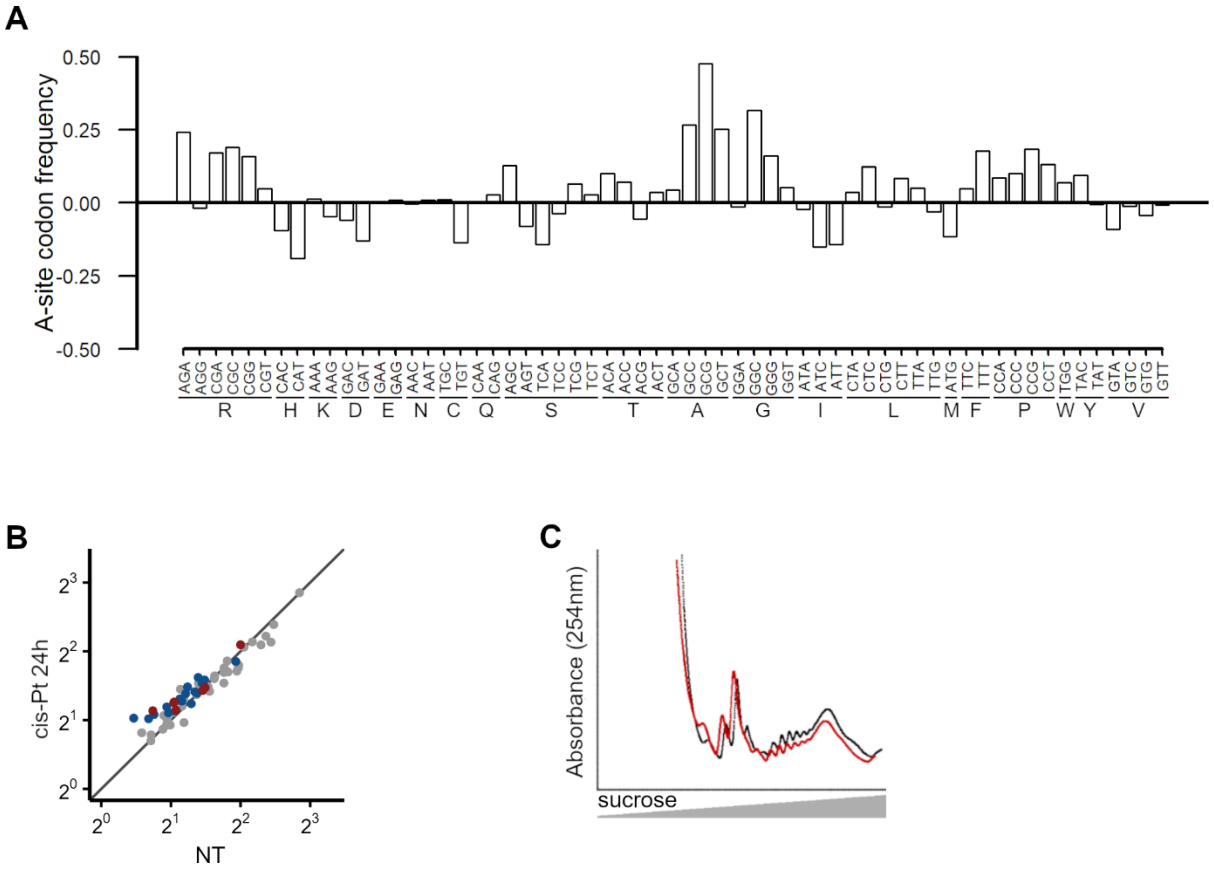

Figure 4.2 ***Cis-Pt treatment does not cause ribosome stalling in A2780 cells.*** *[A] Relative changes in ribosome dwelling occupancy (frequency) at A-site codons in A2780 treated with 2μM cis-Pt for 24h as determined by Ribo-seq. Normalized codon occupancy of the A site is presented as a ratio of cis-Pt treated vs. untreated cells. [B] Scatterplot of codon-specific A-site ribosomal occupancy (log2 scale) comparing untreated (NT) vs. cis-Pt-treated A2780 cells for 24h. Codons with two adjacent guanines or guanines and cytosines are colour coded; GG containing codons - red, CC/GC/CG containing codons - blue, and all other codons – grey. [C] Polysome fractions of untreated (black) and cells treated with 2μM cis-Pt for 24h (red).*

4.2.3 Cis-Pt treatment causes a decrease of charged tRNA levels but does not activate GCN2

Nutrient deprivation or starvation stress classically elicits the activation of ISR through the GCN2. The observed decrease in charged tRNA levels after cis-Pt treatment raised the question as to whether the aminoacyl-tRNA paucity activated the GCN2 branch of the ISR. To assess this, we performed immunoblot assays to detect the phosphorylation status of the GCN2. Although we detected very high amounts of GCN2, even without treatment, we detected no phosphorylation of GCN2 in these cells (Fig 4.5).

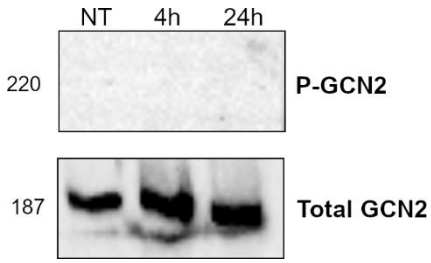

Figure 4.3 ***Cis-Pt treatment does not activate GCN2 in A2780 cells.*** *Untreated (NT) and A2780 cells treated with cis-Pt for 4h and 24h were subjected to immunoblot analysis to detect total and phosphorylated GCN levels. A high level of GCN2 was detected in these cells but the treatment did not alter the levels and no phosphorylation was detected under these conditions.*

Thus, 24h of cis-Pt treatment albeit leading to noticeably reduced levels of amino-acyl tRNAs in these cells it does not activate the classical GCN2 pathway. This is contrary to our observed phosphorylation of GCN2 in SKOV3 cells with no significant changes of aminoacyl- tRNAs (Chapter 2). A2780 uses other mechanisms to regulate the effect of the drug.

Besides the key biomolecules or the translation machinery itself, chemical modifications of the biomolecules play a role in various biological processes. And such modifications on the DNA, RNA or protein are also known to play a regulatory role and affect various signaling pathways. RNA modifications are relatively new in this arena but there is increasing interest in the field. Post transcriptional modification on RNA molecules also have important ramifications on the fate of the proteins. Researchers are now focusing attention RNA modifications and their regulatory roles in various biological processes. In the past few years RNA modifications and the field of epitranscriptomics has gained increasing interest and rightly so as the growing body of literature shows that these modifications have diverse functions including regulating gene expression and RNA metabolism [206] [207]. There is evidence showing the importance of RNA modifications and their role in diseases including cancer [208] [209]. Various kinds of modifications have been reported. Among the well characterized modifications is the m^6A modifications on RNA which is the most prevalent internal mRNA modification in mammals, occurring at a frequency of 0.15–0.6% of all adenosines [212]. This highly abundant m^6A modifications has been implicated in cancer [214] [215].

4.2.4 Cis-Pt treatments leads to reduction in total m^6A levels in sensitive cells

The m^6A modification of mRNA is the most prevalent internal modification in eukaryotic messenger RNAs exhibiting diverse and important roles in biological processes. Aberrant dysregulation of m^6A and its regulators have been identified in numerous tumors [218] [227]. To

assess the m^{6}A levels on the RNA we performed dot blot assays using total RNA extracted from cells grown with and without cis-Pt. Treatment with cis-Pt reduced the m^{6}A levels in A2780 cells. Intrigued by this observation, we next assessed the m^{6}A levels in the other ovarian cancer cells SKOV3 and undifferentiated FT cells as well and compared the levels before and after treatment. SKOV3 cells did not show a similar result. Interestingly, upon treatment with cis-Pt the m^{6}A levels reduced in the undifferentiated FT cells (~64%) and A2780 (~15%) cells but remained unaltered in the resistant SKOV3 cells (Fig 4.6). As we noticed different patterns in the 2 ovarian cancer cells, for the rest of the experiments we continued to use all 3 cell lines and compared all the parameters between cell lines.

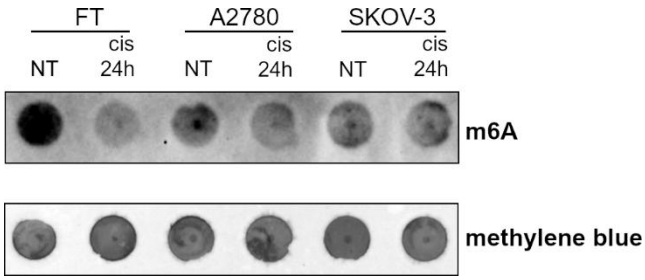

Figure 4.4 ***Cis-Pt alters the m^{6}A levels in A2780 and FT cells but not in SKOV-3 cells****. Equal amounts (2µg) of total RNA isolated from FT194, A2780 and SKOV-3 cells grown with and without cis-Pt were loaded onto the membrane and probed with m^{6}A antibody (top) and methylene blue (bottom). Figure is a representative image of 3 replicates of the dot blot analysis.*

Immunofluorescence experiments detected m^{6}A signal both in the nucleus and cytoplasm in all three cell lines and treatment with cis-Pt did not affect this distribution (Fig 4.7)

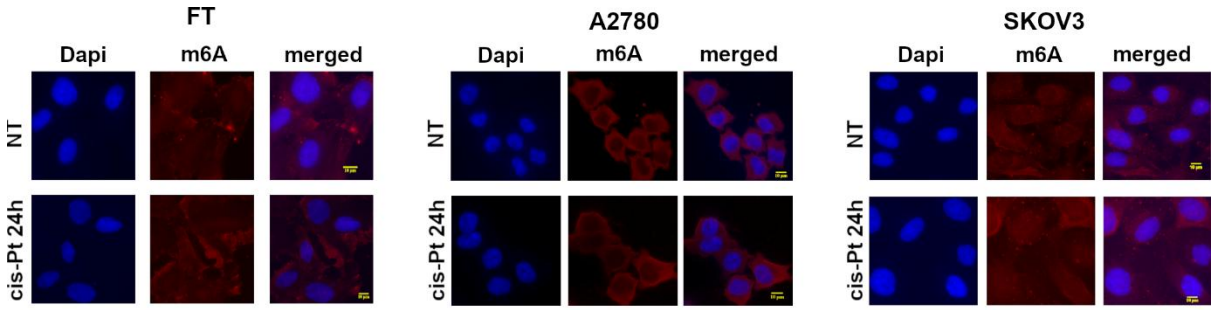

Figure 4.5 ***m^{6}A levels are not much affected upon cis-Pt treatment.*** *Untreated (NT) or cells treated with cis-Pt for 24h were fixed on slides and subjected to immunofluorescence to detect m6A levels; m^{6}A antibody (red), nuclei were counterstained with DAPI (blue). Scalebar, 10µM*

We determined m^{6}A levels in the pool of total RNA, it would be interesting to know which transcripts were specifically affected and if that influenced the effect of the drug on the cells.

m^{6}A is a dynamic reversible modification of mRNA regulated by proteins which act as writers and erasers. Hence, we looked at the effect of cis-Pt on these individual proteins. Immunoblot analysis was carried out to assess the levels of m^{6}A writers METTL3, METTL14 and WTAP and erasers ALKBH5 and FTO in cells grown with and without cis-Pt. Fig 4.8 shows the gel results comparing these protein levels between the cell lines.

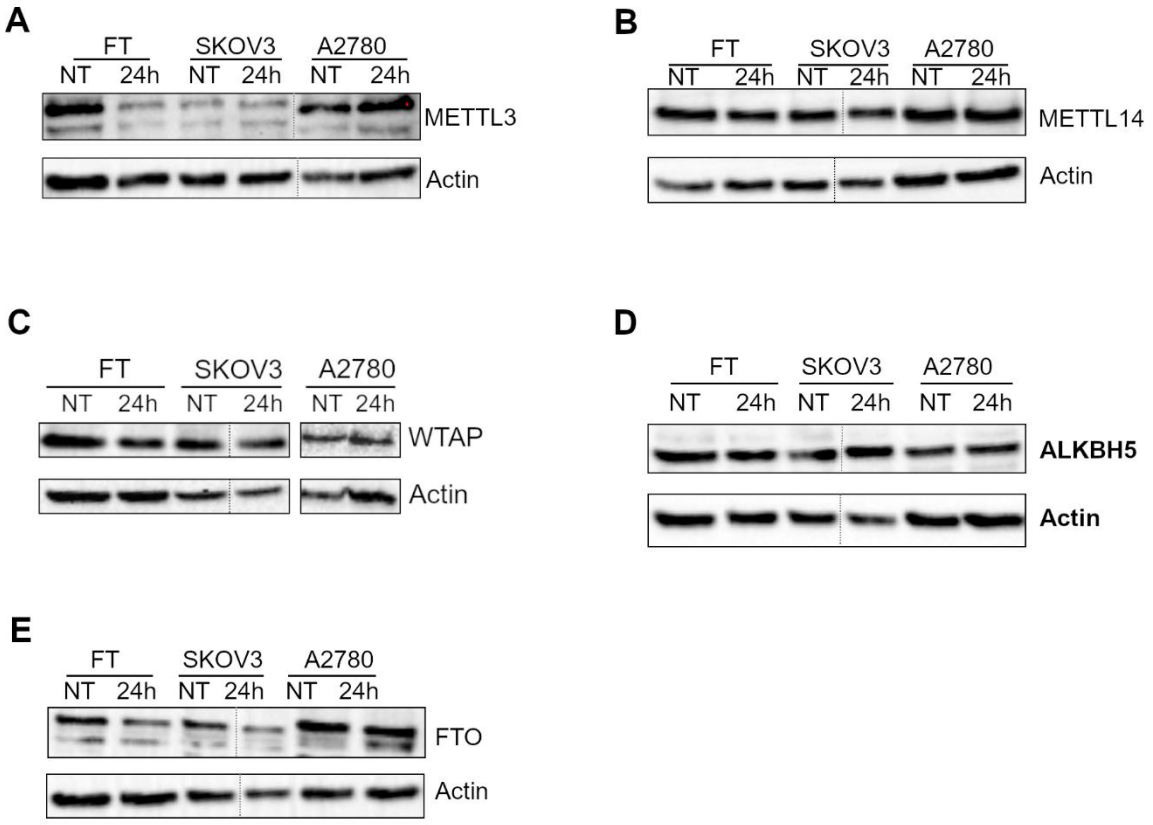

Figure 4.6 ***FTO levels decrease in SKOV cells upon treatment with cis-Pt.*** *Immunoblot analysis of m^{6}A writers [A]METTL3, [B] METTL14, [C] WTAP and erasers [D]ALKBH5 and [E] FTO in cells grown with and without cis-Pt. The dotted line indicates excised lanes, containing samples not relevant in this context.*

In the FT cells, we noticed that amounts of the m^{6}A writer, METTL3, was drastically reduced upon cis-Pt treatment. The other members of the writer complex as well as the two erasers (ALKBH5 and FTO) remained unaffected. This could possibly explain the reduced m^{6}A levels observed. In A2780 cells, neither the writers nor the erasers were affected upon cisplatin treatment.

An interesting observation here is that in SKOV3 cells, unlike in the other cell lines, we observed a distinct reduction in the FTO levels after cis-Pt treatment (Fig 4.8 E). Not only the protein expression but a reduction was also detected in the mRNA expression using RNA seq

data as shown in Table 4.1. The other eraser ALKBH5 and the three writers of m^6A remained unaltered upon cis-Pt treatment in these cells (Fig. 4.8 A-D). These findings however could not explain the constant m^6A levels observed. We also noted that, the expression of m^6A writer METTL3, was very low in SKOV3 cells as compared to the other two cell lines but remained unaltered by cis-Pt treatment.

Table 4-1 ***Changes in mRNA expression of m^6A writers and erasers following cis-Pt treatment.*** *Expression changes are represented as fold-changes changes of the respective transcript expression (obtained from the RNA-seq data) of treated vs untreated cells. FTO expression is noticeably reduced in SKOV3 cells (highlighted with a red circle).*

	FT	**A2780**	**SKOV**
Genes	Differential RNA expression log_2FC	Differential RNA expression log_2FC	Differential RNA expression log_2FC
METTL3	0,13947	-0,31803	-0,27174
METTL14	0,363481	-0,69032	-0,08636
WTAP	0,222356	-0,36839	0,548904
ALKBH5	-0,36141	0,014856	0,120246
FTO	0,271047	-0,01088	-1,81771

It is known that the writers and erasers can shuttle between the nucleus which is the main place of action and the cytoplasm [228]. Reasoning that if the localization is affected upon treatment that would also impact m^6A levels, we next carried out immunofluorescence experiments to determine the localization of these proteins. We detected the distribution of the writers in both the cytoplasm and nucleus as reported in literature and treatment with cis-Pt under the studied conditions did not affect the localization of the m^6A writers (Fig 4.9).

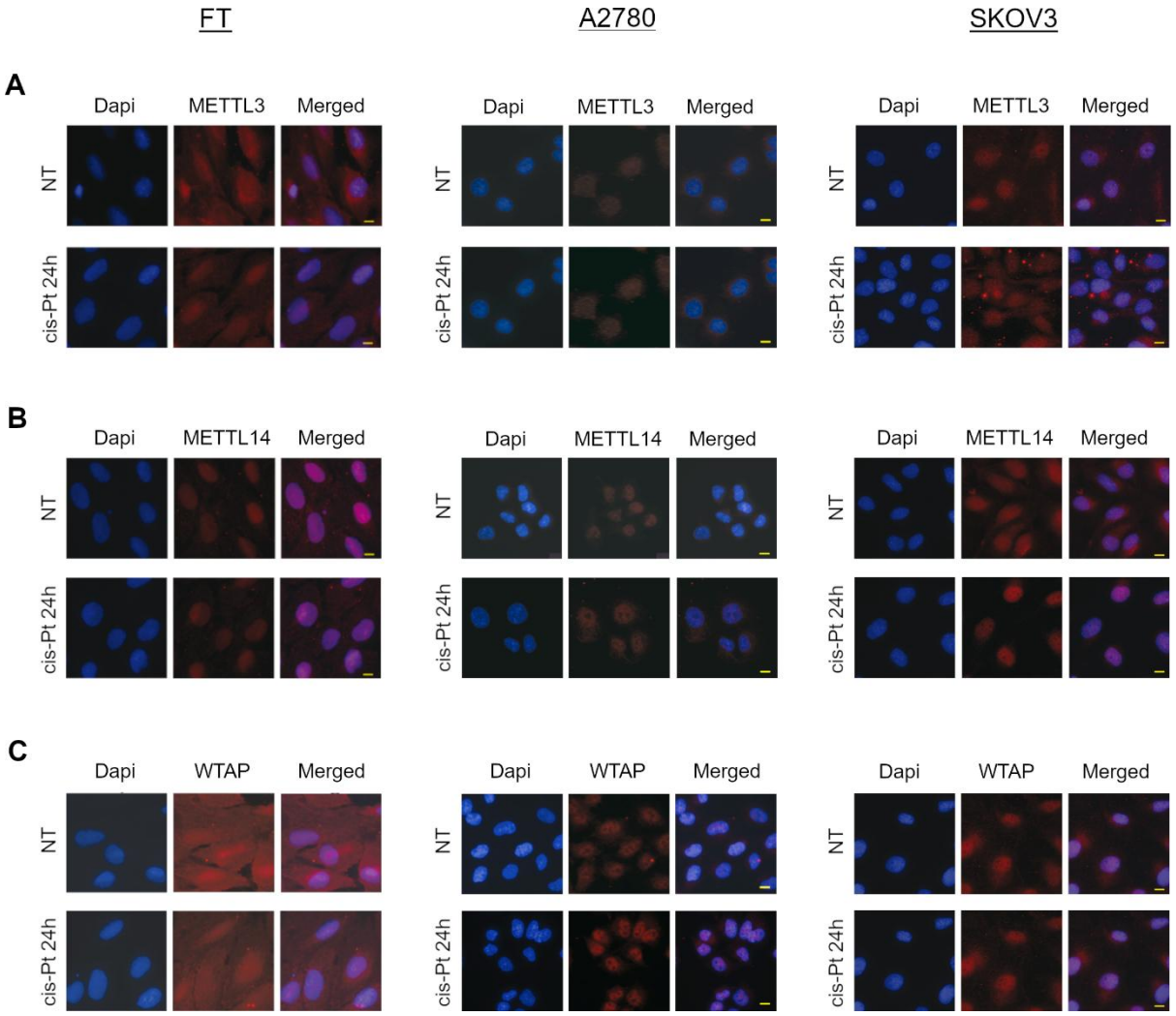

Figure 4.7 ***Localisation of m^{6}A writers is not affected cis-Pt treatment.*** *Untreated (NT) or cells treated with cis-Pt for 24h were fixed on slides and probed with antibodies (red) against [A] METTL3, [B] METTL14 and [C]WTAP to detect whether they were located in the nucleus or cytoplasm and whether treatment affected their localization, nuclei were counterstained with DAPI (blue). Scalebar shown corresponds to 10μM.*

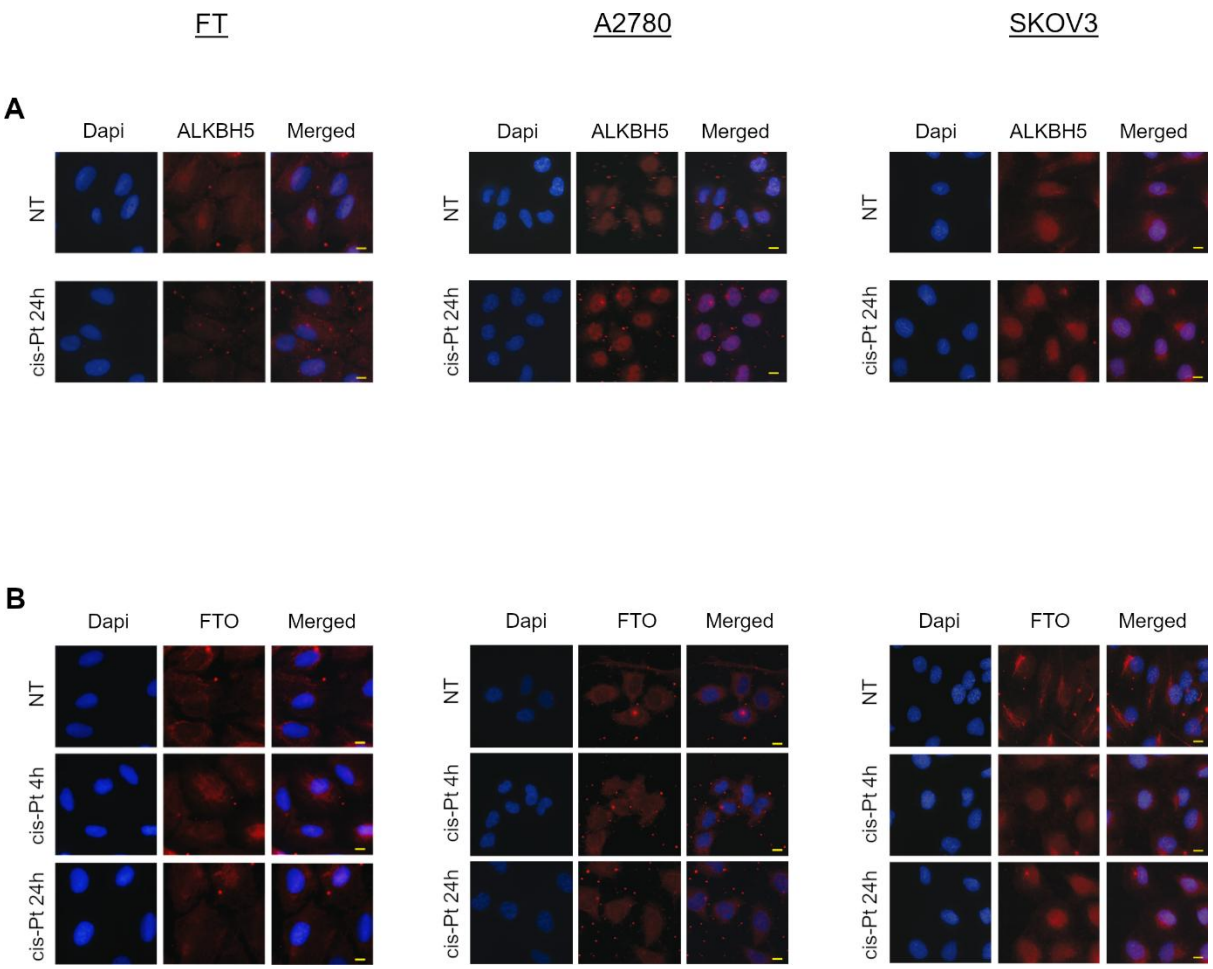

Figure 4.8 ***FTO is concentrated in the nucleus when SKOV3 cells are treated with cis-Pt.*** *Untreated (NT) or cells treated with cis-Pt for 24h were fixed on slides and probed with antibodies (red) against [A] ALKBH5 and [B] FTO to detect whether they were located in the nucleus or cytoplasm and whether treatment affected their localization, nuclei were counterstained with DAPI (blue). Immunofluorescence showed that in SKOV3 cells only FTO was more concentrated in the nuclear/perinuclear region after treatment with cis-Pt. Scalebar shown corresponds to 10μM.*

Noteworthy here was that in the SKOV3 cells, we see the m^6A distributed in both the nucleus and the cytoplasm under normal conditions but when treated with cis-Pt, m^6a appears to have concentrated in the nuclear and peri-nuclear region. This is not the case with the other two cell lines, A2780 and FT. This movement of the FTO into the nucleus was also observed at an earlier time point i.e. 4h post cis-Pt treatment confirming that it is no artifact but an effect of cis-Pt, and was seen only in the SKOV3 cells. It is known that FTO could mediate demethylation through different substrates namely m^6A or m^6Am in the cytoplasm or nucleus [229]. Concentrating the m^6A into the nucleus might be related to specific substrate selection and further downstream signaling. However, this is speculative and further evidence to support this is necessary.

4.3 Discussion

Here we show that cis-Pt leads to very different responses in the A2780 cell line as compared to SKOV3 cells. Cancer is a multifaceted disease, and no two cancers are the same, even within the same cancer the heterogeneity can be very high. Just as different as the cancers themselves are, the regulation of drug activity and the molecular mechanisms involved thereby can be very diverse and multifactorial with interdependent or completely independent factors involved. It is therefore no surprise that the cells we studied respond differently to cis-Pt. We showed here that prolonged exposure to cis-Pt reduces the levels of amino-acylated tRNAs. Differential gene analysis did not show any alteration in the expression levels of tRNA synthetases. Researchers have shown a positive correlation between expression of SLFN11 and sensitivity of tumor cells to DNA damaging agents (DDA s)[163], and could possibly be a reason for the sensitivity of A2780 cells, but we did not detect any differences in the SCHLFN11 gene upon cis-Pt treatment in these cells. Furthermore, we did not observe any changes in the metabolites (data not shown) which could explain these reduced tRNA levels. Understanding the exact cause and effect of the observed reduction in tRNA levels remains to be studied. Surprisingly, the reduction in charged tRNAs does not elicit the classical GCN2 activation (Fig 4.5). Activation of the ISR in response to stressors generally occurs within minutes of exposure to stress [107] and GCN2 activation is a cyclical process and it could well be that the time point used in this study does not coincide with this activation time hence we were unable to capture it here. Unlike that observed in SKOV3 cells, we do not detect massive ribosome stalling at the TTA codons. Mapping the ribosomal occupancy on codons indicates nominally increased dwell time of ribosomes on codons with adjacent G's, C's or GC's when treated with cis-Pt. The difference compared to the untreated cells is however marginal and cannot be used to draw further conclusions. Guanines are generally known as the most common sites for cis-Pt adducts mainly binding to the N-7 of guanine residues forming intra-strand crosslinks between adjacent guanines on DNA [230] and could be the way cis-Pt affects the A2780 cells. A closer look at the genes upregulated after cis-Pt treatment showed that many genes such as the tp53i3, tp53inp1, cdkn1A are upregulated. All of these are induced by the tp53 gene which could potentially regulate apoptosis due to DNA damage. Bax, a member of the BCL2 family involved in apoptotic pathway is also upregulated in A2780 cells when subjected to cis-Pt treatment. P53 is the direct regulator of the bax gene. Upregulation of these genes indicates that DNA damage, which is indeed the main mode of action of cis-Pt, causes the cells to succumb to the deleterious effects of the drug most likely mediated through the p53.

We also observed that cis-Pt caused a reduction of m^6A levels in A2780 but with no change in the expression or localization of its main writers and erasers. Here we used total RNA for the m^6A studies but determining the specific transcripts that are affected will be interesting too.

Here we report that cis-Pt does not trigger the same mechanisms in A2780 cells like that seen in SKOV3 cells. Although we have not yet characterized the exact factors/ pathways underway in the A2780 cells to counteract the effects of cis-Pt, we do see indications of the DNA damage induced apoptosis, possibly being the reason for the susceptibility to the drug. However, more experimental data is required to substantiate this. But the changes in RNA we observed in SKOV3 were not seen in A2780. Many factors could cause this but these are not addressed in this work. Among them is also the fact that the two cell lines have a different doubling time, the different stages that the cell lines are in could also have an impact on the responses which need to be addressed. More importantly it was observed that the cell line has been shown to having a different origin [231] and this can be a major cause of the differences seen. Hence comparing it to SKOV3, might not be optimal. Thus, we did not pursue further experiments using A2780.

Additionally, we also uncovered that in SKOV3 cells, upon cis-Pt treatment affected the expression levels and the localization of FTO. FTO most commonly considered to play a role in the reversal of m^6A modification has also been shown to affect m^6Am. Relier et al (2021) demonstrated that low FTO expression was associated with elevated m^6Am level in mRNA which in turn enhanced in vivo tumorigenicity and chemoresistance [232]. FTO also exhibits differential substrate preferences in nucleus versus cytoplasm and has shown to have substrates other than the m6A modifications and can also affect various RNA species [233]. This shuttling between the nucleus and cytoplasm and demethylation potential of FTO could affect transcript specific gene expression. Whether it has a role in the carcinoma and/ resistance phenotype in ovarian cancer would be interesting to look at.

4.4 Materials and Methods

4.4.1 Cell line

A2780 cells were cultured in RPMI 1640 (Panbiotech) medium supplemented with 10% fetal bovine serum and 2 mM glutamine at 37°C under a humidified environment with 5% CO_2.

4.4.2 Polysome Profiling, RNA extraction and RNA-seq & Ribo-seq

Approximately 15 million cells were used for each experiment. Untreated cells or cells treated with cis-Pt for 4h or 24h were harvested in polysome lysis buffer (10 mM Tris.HCl (pH 7.4), 5 mM MgCl2, 100 mM KCL, 1% Triton X-100) supplemented with 100 µg/ml cycloheximide and 2mM DTT. Samples were layered onto a 5 ml sucrose gradient and then centrifuged for 1.5 h at 148,900xg (Beckman Coulter, SW 55Ti rotor) at 4°C. The gradients were fractionated on a piston gradient fractionator (Biocomp) and the absorbance at 254nm was recorded.
The monosome fractions were collected and RNA was extracted by adding 0.1 volume of 10% SDS, one volume of acidic phenol-chloroform (5:1, pH 4.5) preheated to 65°C and then incubated at 65°C for 5 min. Thereafter the samples were cooled on ice for 5 min and centrifuged at 21,000xg for 5 min to separate different phases. Equal volume of acid phenol-chloroform was added to the aqueous phase, separated by centrifugation and supplemented with an equal volume of chloroform:isoamyl alcohol (24:1). Upon separation, the aqueous phase was supplemented with 0.1 vol 3M NaOAc (pH 5.5) and an equal volume of isopropanol. Samples were precipitated for 3h at -20°C. RNA was pelleted by centrifugation at 21,000xg at 4°C, and resuspended in DEPC-H_2O. The isolated RNA was then fragmented in alkaline fragmentation buffer (0.5 vol 0.5 M EDTA, 15 vol 100 mM Na2CO3, 110 vol 100 mM NaHCO3) and subjected to cDNA library preparation as previously described [192].

For Ribo-seq, cleared cell lysates were digested with RNase I (15 U; Lucigen) and layered onto sucrose gradients to collect the monosomes. RPFs were extracted and libraries were prepared as described previously [192] [193]

4.4.3 Analysis of the RNA seq and Ribo seq data

Sequenced reads were trimmed (fastx-toolkit v0.0.13.2; quality threshold=20) and depleted from the adapter sequences (cutadapt v1.8.3; minimal overlap=1 nt). The remaining reads were mapped to the human genome (GRCh38.p13) using STAR v2.5.4b 52 (--outFilterMultimapNmax 1 --outFilterMismatchNmax 1). Uniquely mapped reads were normalized to reads per million mapped reads (RPM), or reads per kilobase per million mapped reads (RPKM). Independent biological replicates of SKOV3 untreated show high reproducibility (R2=0.783, Pearson correlation coefficient), thus, the replicates were merged into one metagene set using samtools v1.7. To identify the ribosomal A site within the RPFs, the RPFs were binned into groups of identical read length and then each bin aligned individually to the start codon thus identifying the P-site 22,53,54, using the calibration tool https://github.com/AlexanderBartholomaeus/MiMB_ribosome_profiling). Briefly, bins with RPFs of the same size were plotted individually covering the start codon region including 50 nt upstream and downstream of it, which is used to determine the individual offset distance between the 5' end of the RPF and the start codon in the ribosomal P site, and by adding 3 nt to the A site. We considered six bins for calibration (29-34 nt length).

For each transcript, all A-site codon occupancies are summed up and normalized on the transcript background as described [171]. The comparison between A-site codon occupancy (frequency) between untreated and cis-Pt treated cells, the A-site codon occupancy across all transcripts for treated cells were divided by the those for untreated cells and presented as the differential A-site codon frequency [172].

4.4.4 tRNA microarrays

Comparative microarray analysis was performed to quantify the absolute tRNA amount and the fraction of aminoacyl-tRNAs using protocols described earlier140 161. To determine the fraction of aminoacyl-tRNAs, total RNA was extracted from cells using acidic phenol (Roth, pH 4.5), which preserves the aminoacyl group at the 3'tRNA end. Extracted total RNA was split into 2 aliquots, one aliquot was treated with periodate to oxidize non-aminoacylated tRNAs leaving the aminoacyl-tRNAs intact. Thereafter, both aliquots were deacylated by incubating with 125 mM Tris-HCl, pH = 9.0 containing 0.1 M EDTA and 0.5% (w/v) SDS at room temperature for 45 minutes, followed by a treatment with an equal volume of 1M NaOAc, pH = 5.5. The single stranded 3' NCCA ends of the deacylated tRNAs were then ligated to a

fluorescently labelled RNA/DNA stem loop oligonucleotide; the oxidized sample with a Cy3-labelled oligo and the non-oxidized control sample with an Atto647-labelled oligonucleotide respectively.

For tRNA abundance, total RNA was isolated with TriReagent (Sigma Aldrich), which simultaneously deacylates all tRNAs. tRNAs were ligated to a Cy3-labelled RNA/DNA hybrid oligonucleotide. For comparison, total RNA from HEK cells was isolated and labeled with Atto647-labeled oligonucleotide.

Labeled tRNA samples were then loaded onto a microarray consisting of 40 full-length tDNA probes recognizing all nuclear encoded human isoacceptor tRNAs and hybridized for 16 h at 60°C. Fluorescence signals of microarrays were recorded with a GenePix 4200A scanner (Molecular Devices) and statistically analyzed with in-house scripts in Python (version 3.7.0) [182]. A detailed protocol is available at dx.doi.org/10.17504/protocols.io.hfcb3iw.

4.4.5 Dot blot

Cells were cultured with and without cis-Pt treatment. After 24h of cis-Pt treatment cells were harvested and total RNA was extracted using TRIzol reagent. Equal amounts of total RNA (~2µg) for each condition were spotted onto a nylon membrane. The RNA was crosslinked by exposing it to UV (254nm). The membrane was then blocked in 5% fat free milk in TBST for 1h at R.T. The membrane was then incubated with the m6A antibody overnight at 4°C. The membrane was then washed in TBST and subsequently incubated with a HRP conjugated secondary antibody for 1h at R.T. Detection was carried out by chemiluminescence.

4.4.6 Immunoblots

Cells were grown in rich medium containing 10% FBS and lysed with RIPA buffer (150 mM NaCl, 1% IGEPAL CA-630, 0.5% sodium deoxycholate, 0.1% SDS (sodium dodecyl sulphate), 50 mM Tris-HCl, pH 8.0) containing 25Xcomplete or RPE buffer [191]. Cell lysates were separated on SDS-PAGE, transferred onto a PDVF membrane (Merck Millipore) and incubated with a primary antibody (as seen in table 3.1) overnight at 4°C. the membrane was then washed (3X 5mins) with TBST and subsequently incubated with an HRP conjugated secondary antibody for 1-2h at room temperature. The membrane was washed with TBST (3X) and the bands were detected by chemiluminescence. (Bio-Rad Gel Doc XRS+).

Table 4-2 Antibodies used in the study

Target	Source	Dilution	Manufacturer	Cat #
M6A	Rabbit	1:1000	Sysy	202003
METTL3	Rabbit	1:1000	Proteintech	15073-1-AP
METTL14	Rabbit	1:1000	Sigma-Aldrich	HPA038002
WTAP	Mouse	1:1000	Proteintech	60188-1-Ig
ALKBH5	Rabbit	1:1000	Proteintech	16837-1-AP
FTO	Rabbit	1:1000	Proteintech	27226-1-AP
Beta Actin	Mouse	1:1000	Cell signaling technologies	
HRP conjugated anti Rabbit	Goat	1:3000	Biorad	172-1019

4.4.7 Immunofluorescence

Cells were grown in 6 well plates containing coverslips. Cells were grown with and without cis-Pt for 24hs and thereafter cell on coverslips were fixed with 4% paraformaldehyde for 15mins. Following this, cells were permeabilized using 0.5% saponin and subsequently blocked using 1% BSA in PBST for 1h. Samples were incubated for 1h with primary antibodies as tabulated (Table 3.1) washed 3times with PBS and incubated with secondary antibody AlexaFluor 568 for 1h. All incubations were carried out at room temperature. Images were acquired on the Leica microscope (DMi8 platform) and processed by ImageJ.

5 tRNA sequencing using the nanopore platform

RNA sequencing has revolutionized the field of biology, unlocking a wealth of information. The most commonly used RNA sequencing methods today though very precise and informative have limitations such as short read lengths and biases due to reverse transcription and amplification. They do not provide information about the numerous post-transcriptional modifications that RNA molecules harbor. The nanopore sequencing method is an alternative sequencing method with advantages over current methods and has the potential to provide information about the base modifications. Post-transcriptional modifications on RNA have been shown to have various biological functions[209]. Among all RNA molecules, the tRNA molecules are the most complex and most highly modified molecules with very important functions in the cell. We aimed to tailor the nanopore sequencing method and target tRNA molecules that are difficult to sequence by the traditional methods. In this chapter, I present our approach to establish a method to sequence tRNAs and detect the base modifications. We were able to show that indeed tRNA molecules can be sequenced in their entirety using nanopore's simple workflow. The future of sequencing with nanopore looks very promising and with well-trained algorithms detecting and deciphering modifications will soon be a reality.

The experiments presented here were conceptualized and performed by myself and the bioinformatic analysis of the data was performed by Christine Polte, a colleague working in our research group.

5.1 Introduction

The transcriptome of a cell holds rich information and can provide insights into how various biological processes are regulated. Sequencing the RNA in a biological sample provides a detailed and quantitative view of gene expression, alternative splicing, and allele-specific expression thus unlocking a wealth of information [234]. Development of high-throughput next-generation sequencing (NGS) technologies revolutionized the field of transcriptomics enabling detailed analysis of RNA[234]. Most of the currently used sequencing platforms use a sequencing-by-synthesis technique to parallelly sequence millions of small sequences. They employ reverse transcription to synthesize cDNA molecules and PCR amplification to sequence the synthesized products [235].

Nanopore sequencing is an alternate sequencing platform that enables direct sequencing and real-time analysis of DNA or RNA molecules, aiding long read-sequencing and at the same time maintaining the integrity of the molecule being sequenced [235]. Originally used to sequence DNA, the technique has rapidly advanced and has been successfully adapted to sequence RNA molecules allowing researchers the ability to explore the transcriptome of cells in more ways than previously perceived. Oxford Nanopore Technologies' nanopore-based platform detects single molecules of DNA or RNA as they pass through a nanopore, without involving an enzymatic synthesis reaction [235]. The nanopore technology as the name suggests relies on a nanoscale protein pore, or a 'nanopore', which serves as a biosensor [236]. The nanopores are embedded in electrically resistant synthetic polymer membranes. In an electrolytic solution, a constant voltage is applied which produces an ionic current through the nanopores, the electric potential guides the DNA/RNA molecules from a negatively charged 'cis' side to the positively charged 'trans' side through these nanopores[236]. Engineered proteins, called motor proteins, are attached to the DNA/RNA molecules during the library preparation which regulate the movement of the bound polynucleotide at a consistent rate through the pores. The motor proteins control the speed of translocation as well as help unwind the DNA or DNA/RNA duplexes into single stranded molecules that can pass through the nanopore. When a polynucleotide is captured and advances through a pore in single nucleotide steps it creates perturbations of the nanopore current and these changes to the ionic current as molecules translocate corresponds to the nucleotide sequence in the sensing area at a given time point. A recurrent neural network (RNN) algorithm trained with known nucleotides converts the resulting current series into base sequences [2, 4 236 238]. The sequencing takes place on flow cells. The MinION is a pocket size sequencing device. Technically, such a minION flow cell contains 512 channels with 4 nanopores in each channel, with a total of 2,048 nanopores available to sequence DNA or RNA molecules. They are embedded in an electrically resistant polymer membrane and connected to a sensor chip. Each individual channel is linked to a separate electrode in the sensor chip and measured by the application-specific integration circuit (ASIC). A constant voltage is applied across the membrane which creates an ionic current across the nanopore and as nucleotides pass through this, the current changes which is then recorded [236].

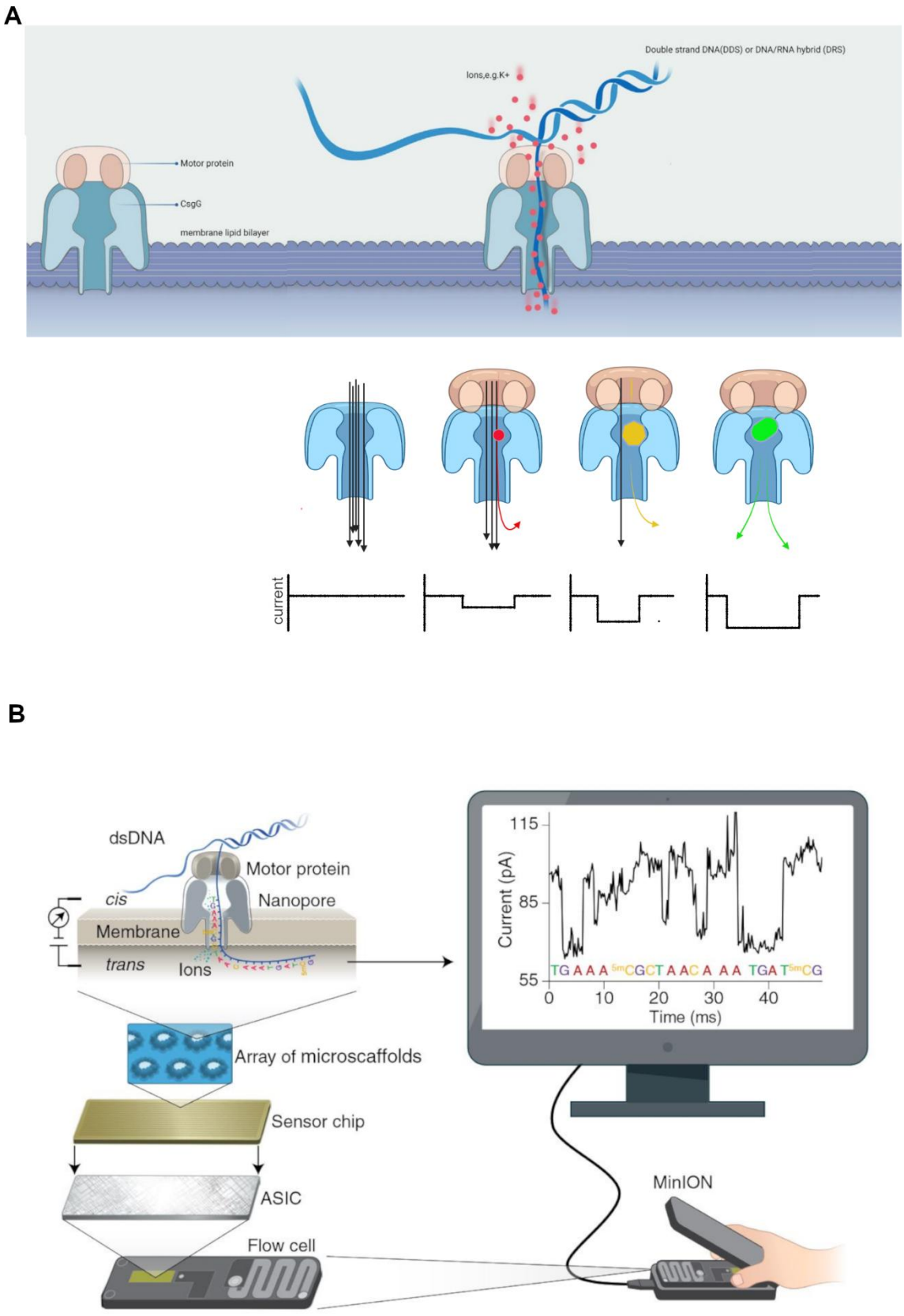

Figure 5.1 ***Principle of the nanopore technology.*** *[A] Schematic representation of how the RNA/ DNA molecules ratchet through the nanopore causing a deflection of ionic current. Adapted and modified from*[239]*. [B] Nanopore sequencing on the Minion and assembly of nanopores on the minion flowcell which is the basic unit where sequencing takes place, adapted from* [236].

The most commonly used strategy for RNA sequencing involves either polydeoxythymidine (poly(dT)) priming or fragmentation of RNA followed by cDNA synthesis with random hexamer priming. Such experiments completely rely on the accurate conversion of RNA to DNA. Library preparation for sequencing these cDNA strands generally involves a PCR step. This however introduces biases. Not all transcripts amplify with the same efficiency causing loss of some and excess amplification of some thus distorting the understanding of the genuine abundance of the RNA species. In addition, as standard sequencing techniques rely on converting the RNA to cDNA before sequencing, information about the modifications are lost. The Nanopore approach provides promising advantages over other RNA-seq strategies; overcoming the limitations of the widely used sequencing by synthesis methods. It does not require RNA to be converted to cDNA in order to be sequenced thus maintaining the integrity of the RNA molecule itself. It allows sequencing of long molecules in their entirety without the need to cut into smaller fragments and arrange in a sequential manner. Amplification of the target molecule is not required thereby eliminating the PCR bias. And the base modifications are preserved.

tRNAs, the most numerous RNA species in living cells, are non-coding RNA molecules playing an important role in the process of translation. Mature tRNAs are composed of ~70–90 nucleotides and exhibit a characteristic cloverleaf secondary structure and further folds into an L-shaped tertiary structure [240]. Besides the structural complexity, other factors such as the presence of tRNA sequence variants known as isoacceptors and isodecoders, base modifications, the versatility of protein binding partners, dynamic tissue specific abundance and expression, tRNA fragmentation events together add an incalculable complexity associated with the biology of these small molecular entities [241] [242]. Although tRNAs are ubiquitous molecules, tRNA expression has been shown to differ across human tissues [243]. Dysregulation of tRNA levels and modifications has been implicated in a wide range of human diseases such as mitochondrial diseases, neurological disorders and cancer [244] [245]. Moreover, researchers have pointed out that tRNA levels are not static, but rather dynamic in nature, both under normal health and disease conditions [246]; tRNA levels vary greatly across different cancer types [247] [248] [249] [250]. It is evident that tRNA abundance, expression and modifications can influence various biological processes. Base modifications are abundant and critical to tRNA function. In the mammalian tRNA pool nearly 1 in 5 nucleotides are modified and more than 50 unique modifications have been identified in eukaryotes [242]. The modifications have important roles and regulatory functions, these modifications are even suggested to carry more genetic

information than the tRNA gene themselves [251] [244]. Dysregulation of these modifications have been implicated in various diseases including cancer[245]. Our findings detailed in the previous chapters also indicate tRNA modification having a role in resistance to cis-Pt. To understand better the functional and physiological roles of tRNA modifications, a comprehensive analysis of such modification is necessary.

The typical RNA-seq methods are based on ligating oligonucleotides (called adaptors) to the ends of RNAs followed by reverse transcription using a primer complementary to the adaptor ligated at the 3′ end. Unlike most other transcripts this approach does not work well for tRNAs, mainly due to two reasons, namely (i) mature tRNAs have a complex tertiary structure, limiting the efficiency of adaptor ligation and sterically obstructs the cDNA synthesis; (ii) tRNAs are extensively decorated with base modifications which enable proper tRNA folding and affect translational fidelity [252]. Individual tRNAs are unevenly modified, the nuclear encoded tRNAs containing an average of 13 modifications per molecule [244]. Base modifications include 1-methyladenosine (m^1A), 1- methylguanosine (m^1 G), 3- methylcytidine (m^3C), 3-(3- amino-3-carboxypropyl) uridine (acp^3U) and pseudouridine (Ψ) etc [245]. Among these base alterations some such as m^1A and m^1G are considered 'hard-stop' modifications - which block extension by reverse transcriptase resulting in only truncated sequences from the pool of all tRNAs [252].

Anticipating that the advantages nanopore sequencing offers can be harnessed to sequence tRNAs and study the modifications, we decided to use this platform and establish a method to sequence tRNAs and detect modifications. Detailed below is our approach at adapting the basic nanopore workflow.

The basic workflow of the RNA sequencing by the nanopore is depicted schematically in Fig 5.2. The target RNA molecule is isolated, adapters complementary to the 3' end of the target are ligated to the RNA in a first round of ligation followed by reverse transcription for first strand synthesis. Important to note here is that the cDNA synthesized is not the molecule which will be sequenced but it will serve to unwind the secondary structures of the RNA molecules thus enabling smooth movement through the nanopores. Sequencing adapters are then ligated in a second ligation step to the RNA/DNA hybrid molecule and then loaded onto the flowcell for sequencing. The sequencing adapters bear a motor protein which guides the RNA molecule into the nanopores and regulates the speed at which the RNA traverses. The cDNA synthesis

however is optional and one can sequence molecules even without the need of reverse transcription. The method can easily be adapted to sequence specific RNA molecules by using adapters complementary to the 3' end of the molecule of interest.

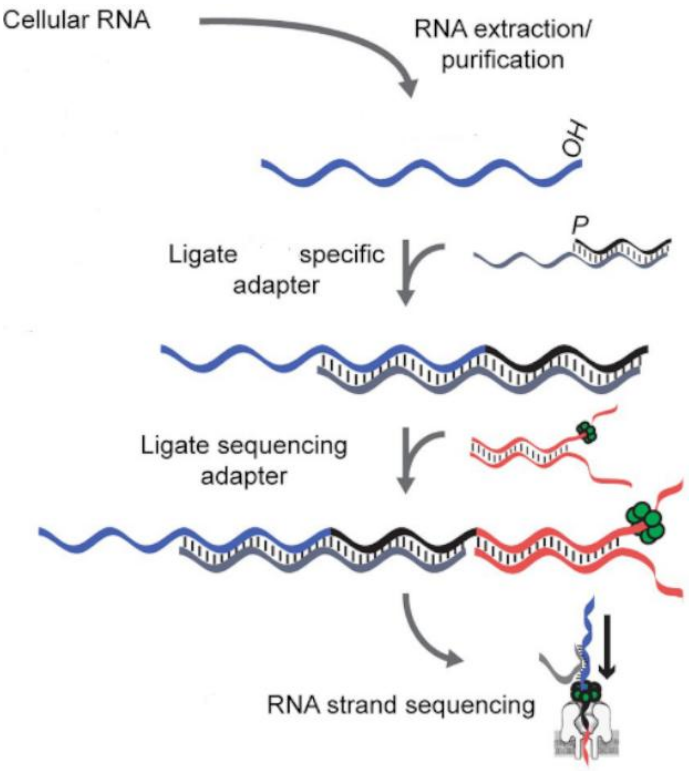

Figure 5.2. ***Basic workflow of the RNA sequencing on the nanopore platform,*** *adopted and modified from* [253]

Approach 1:

As mentioned above, to sequence molecules, we needed to design adapters complementary to the 3' end of the target molecule. For sequence specific RNA sequencing, ONT recommends adapting their predesigned adapters to include ≥10 nucleotides complementary to the 3' end of the target molecule replacing the poly T stretch that they have used (considering complementarity to the poly A tails of mRNAs). The single stranded CCA tail of the tRNAs has been successfully used in our research group to specifically target tRNA ligations in applications such as the tRNA microarrays [254]. Thus, we decided to use the unique feature of the CCA tail of the tRNAs and design adapters with only these 3 nucleotides complementarity, the remaining nucleotide sequence was similar to the standard ONT adapter sequence [253].

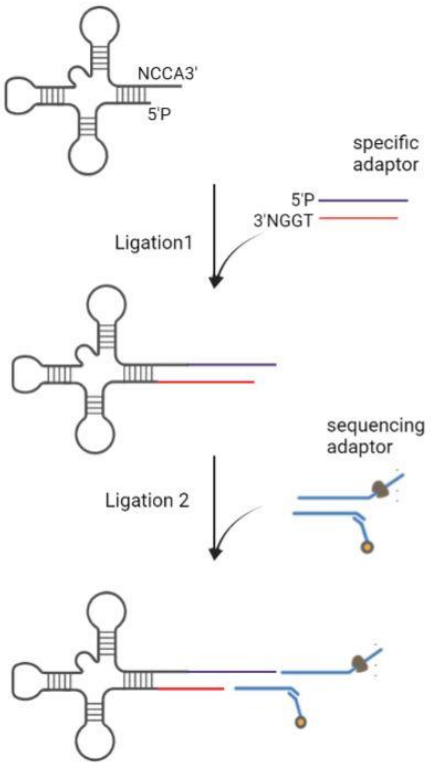

Figure 5.3 ***Workflow for preparation of the tRNAs samples for sequencing****. Schematic representation of subsequent steps involved in preparing the sequencing samples, adapted and modified from* [255].

Method:

Two synthetic oligomers with sequences 5'GGCTTCTTCTTGCTCTTAGGTAGTAGGTTC-3' and 5'GAGGCGAGCGGTCAATTTTCCTAAGAGCAAGAAGAAGCCTGGN 3' to serve as adaptors were purchased from Microsynth. The two adaptors were annealed as described [255]. The tRNAs were heated to 95°C for 2 min to unfold the structure and placed on ice. tRNA samples were first ligated to the splint adapter. The ligation was performed at room temperature for 10 min using T4 DNA ligase. The samples were purified using 3X Ampure RNAClean XP beads (Beckman-Coulter) so as to recover the ligated tRNAs. A second ligation step was then performed to ligate the splint-ligated tRNA (from 1st step) to the RMX Adapter (included in ONT's RNA sequencing kits). The samples were then purified and prepared for loading on the MinION flow cell as detailed in the sequence specific direct RNA sequencing protocol, the ONT SQK-RNA002 protocol [256].

Experiments:

To assess if we could capture and unfold tRNAs allowing their sequencing, initially we used an in vitro transcribed tRNA (alanine) The library preparation was carried out as previously

explained and the sample was sequenced. Following this we also performed a run using an equimolar mix of 4 different tRNAs with the aim of detecting and differentiating between the different species.

Results:

In both the runs, we were able to detect sequences that aligned to the reference sequence, Fig 5.4. In most cases only parts of the obtained reads could be aligned to the reference tRNA sequence. Only few reads among the obtained reads showed an alignment of more than 45 nucleotides when compared with the reference sequence. Although this was a small subset of the total number of reads obtained it was an indication that tRNAs can be captured in this manner (Fig.5.4 A). Unlike in illumine sequencing, where error rate is very low, nanopore sequencing comes with a comparatively high error rate. Multiple sequence alignment tools were difficult to use for our purpose. As it is difficult to use the commonly used alignment tools in this case, we tried a different approach – a pairwise alignment function from Biostrings R package was used to align the reads to each of the reference sequences and the alignment scores thus obtained were used to sort the tRNAs. The highest alignment score was used to assign the reads to either of the 4 groups of the reference sequence. The lack of suitable alignment tool and the very high error rate of the nanopore platform itself made it more difficult to draw inferences from this data set. It was difficult to understand whether the small size of the molecule was not suitable for such sequencing or whether it was a base calling error or simply difficult to sequence regions. Such questions remained to be answered. Not using the available sequence alignment tools, rather using the raw signals generated by the reads will be a better way to decipher the sequences of tRNAs. We noted that in most of the reads which aligned to the references, independent of how much similarity they had to the references, the 3’ and 5’ end sequence information were missing, i.e. the end regions were not being sequenced or read.

We reasoned that the only plausible reason for such a loss at the end regions was proximity to the DNA adaptors used. In order to overcome this problem, we decided to try two alternative approaches, (i) increase the size of our tRNA molecules or (ii) use RNA adaptors instead of the currently used DNA adapters.

Figure 5.4 ***Alignment of sequencing reads.*** *A) Alignment of one single sequenced read to the reference sequence, as the first indication that we that we are able to capture tRNA molecules. B) Subset of reads obtained aligned to the reference sequence using multiple alignment tool.*

Approach 2:

Since we lost bases at the end regions of the tRNAs, we reasoned that extending the tRNA ends would allow us to sequence in a similar manner and even if we did lose the ends, we would lose the added nucleotides but our species of interest, the tRNA itself would be fully sequenced. Aiming to increase the size of the molecule but still keep the protocol simple we decided to extend the 3' end of the tRNAs with a poly(A) tail. This also had an added advantage, namely we could use the standard adaptors provided by ONT for mRNA sequencing as they were complementary to the poly A tail of the mRNAs.

Method:

The poly(A) tailing was carried out using the NEB# M0276 kit, a reaction mix consisting of purified tRNAs, Poly(A) polymerase reaction buffer, ATP and E. Coli Poly(A) Polymerase (as per manufacturer's instruction) was incubated at 37°C for 30mins. 10mM EDTA was added to stop the reaction and the tRNAs were then purified by precipitation. We confirmed the addition by observing a size shift on a polyacrylamide gel. This tRNA now with a poly(A) stretch on the 3' end was ligated to the poly(T) adaptors, followed by ligation of sequencing adaptors and processed for sequencing as per the standard ONT SQK-RNA002 protocol [256].

Results:

These runs did not yield any better results than approach 1. The alignment of reads across the sequence of the tRNA reference remained poor. In contrast to what we expected we did not even detect poly(A) stretches at the 3' end of all reads. Similar experiments with poly(C) added tRNAs also did not improve the sequencing.

Updates from ONT about the nanopore platform confirmed our assumption that the transition between the DNA and RNA bases was indeed a problem and the motor proteins used in ONT kits were not suitable to read both DNA & RNA, but either DNA or RNA. Also, it was updated that homopolymer regions are difficult to assess and cause problems in the sequencing. This explained why our approach with poly(A)/poly(C) addition failed.

Approach 3:

In order to overcome this limitation, we redesigned our adapter to consist of ribonucleotides instead and thereby allow the motor protein to move smoothly along the molecule. During the course of this study, Thomas et al [257] published their success with using a hybrid DNA/RNA hybrid adapter to sequence tRNAs. This approach was promising as it resulted in increasing the size of the tRNA per se as well as having ribonucleotides in the vicinity of the tRNA thus targeting the two major problems we have been facing. We decided to use their strategy and adapted our experiments to protocol they published.

RNA/DNA hybrid adapters were ligated to either end of the tRNAs. This was followed by ligation of sequencing adapters and loaded onto the minion as per manufacturer's protocol (ONT SQK-RNA002 protocol).

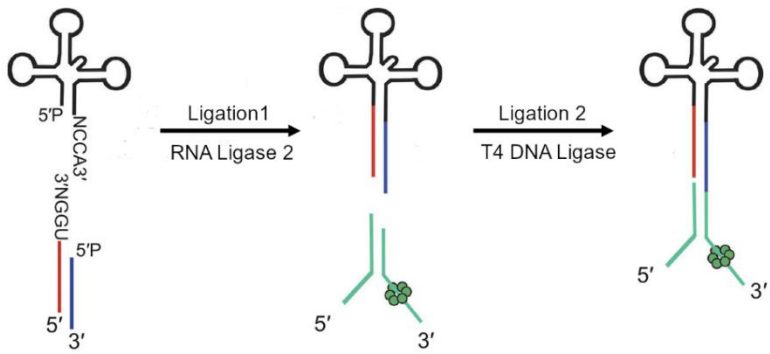

Figure 5.5 ***Sample preparation of tRNAs for nanopore sequencing*** *by two consecutive ligation reactions. An RNA ligase first adds the RNA/DNA hybrid to the tRNAs and in the subsequent round of ligation DNA ligase ligates the sequencing adaptors with the motor protein, adapted and modified from* [257].

5.2 Method

Two synthetic oligomers were purchased from Microsynth. The oligonucleotide that ligates to the 3′ end of the tRNA was 30nt in length, composed of six ribonucleotides followed by 24 DNA nucleotides (5′P- rGrGrCrUrUrCTTCTTGCTCTTAGGTAGTAGGTTC-3′).
The oligonucleotide that ligates to the 5′ end of the tRNA was 24nt in length, composed of six DNA nucleotides followed by 18 RNA nucleotides (5′P-CCTAA-GrArGrCrArArGrArArGrArArGrCrCrUrGrGrN-3′ where N = A/U/C/G). As different tRNAs could have either of the 4 nucleotides as a discriminator base we designed the adapter to contain a mix of all 4 nucleotides at the 3’ end and use one common oligonucleotide instead of 4 separate ones each targeting one of the possible discriminator bases.

The tRNAs were heated to 95 °C for 2 min, allowed to cool for 2 min, then placed on ice for 2 min. tRNA samples were first ligated to the splint adapter. The reaction was carried out at room temperature for 45 min. the reaction constituted of 1× RNA ligase 2 buffer (NEB) supplemented with 5% PEG 8000, 2 mM ATP, 6.25 mM DTT, 6.25 mM $MgCl_2$, and 0.5 units/µL T4 RNA ligase 2 (10,000 units/mL). The splint adapter to tRNA ratio was kept at 1:1.25. After the ligation, gel excision and purification of the product was performed to avoid carry over of any unligated or partially ligated tRNAs. A second ligation step was then performed to ligate the splint-ligated tRNA (from 1st step) to the RMX Adapter (included in ONT’s RNA sequencing kits). The samples were then purified using Ampure RNAClean XP beads (Beckman-Coulter) and prepared for loading on the minION flow cell as detailed in the sequence specific direct RNA sequencing protocol (ONT SQK-RNA002 protocol).

5.3 Results

We started with in vitro transcribed tRNAs as proof of concept experiments. Aiming to check whether our adapters can capture tRNAs with different discriminator bases, we used a mix of 3 tRNAs each with a different discriminator base, namely G, A & U at the position prior to CCA tail. Due to lack of availability we could not include a tRNA with a discriminator C.
The ligation to the adapters worked, but the ligation efficiency was fairly low and we still had a lot of unligated tRNAs (< 50%). However, as our first aim was to verify whether the adapters are able to capture and bind to all tRNAs and whether we are able to sequence the full length tRNAs molecules we decided to go ahead with the ligation in spite of low yield. The ligated

product was excised from the gel and then sequencing adapters were ligated to these. Library preparation was completed and the samples were loaded onto the MinION. The sequencing yielded a total of ~11000 reads which we then used to check for tRNA sequences. Most reads were discarded as they did not pass the quality criteria. We still used the reads knowing that the base callers are not ideal for tRNA sequencing. The reads aligned well to the reference sequences we used and indeed we were able to see that most of the reads covered the entire length of the tRNAs we used. Fig 5.6 shows the alignment of the obtained reads to the reference sequences of the 3 input tRNAs. Using this method, we are indeed able to capture the entire tRNA and to distinguish one tRNA from another.

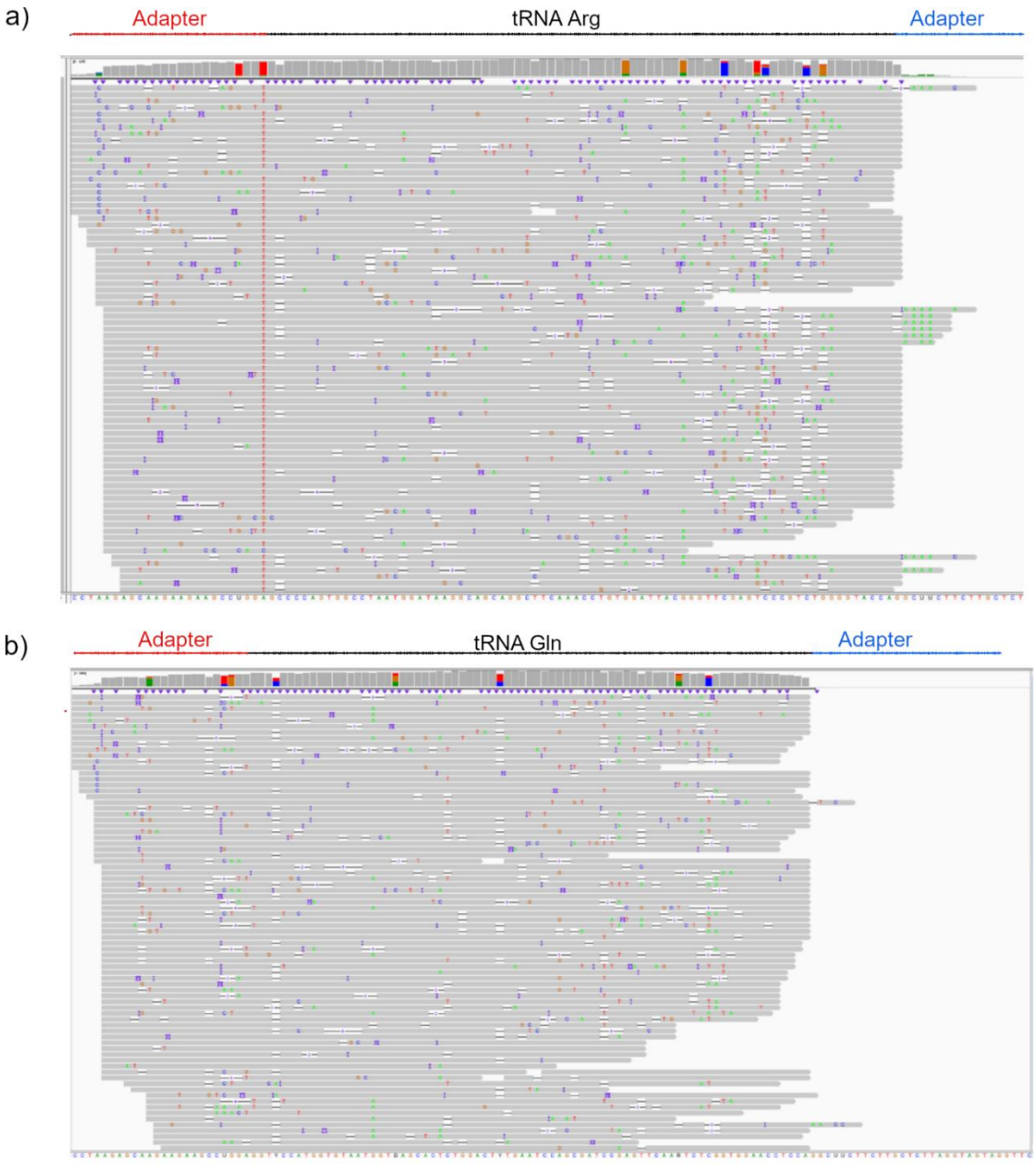

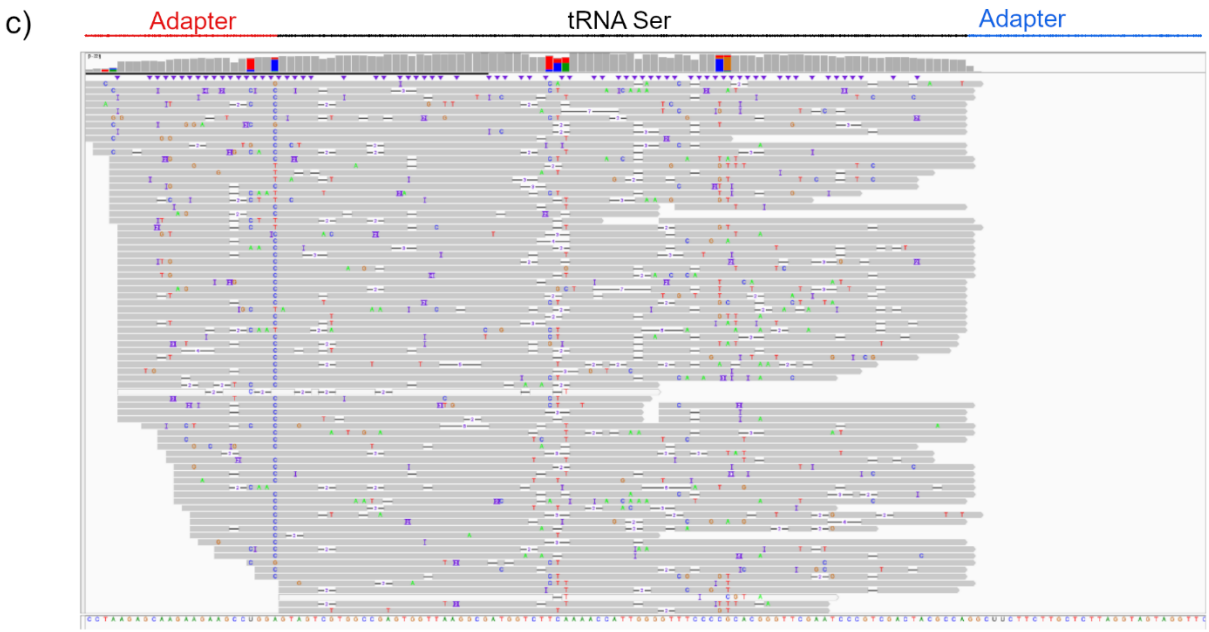

Figure 5.6 ***Alignment of obtained reads to the reference sequences*** *a) tRNA Arg, b)Gln c) tRNA Ser showing that in most cases we are able to capture the entire length of the tRNAs.*

Once we were able to characterize the signals obtained by tRNAs passing through the nanopores we then decided to try and sequence a tRNA with modifications. The same tRNA was then in vitro transcribed again but using Ψ instead of U in the pool of dNTPs. This would imply that all the U's would then be Ψ and by detecting and comparing the signals from the 2 runs we would be able to infer the signal associated with Ψ. The tRNA with its modified bases passed through the pores without blocking the pores and we were able to obtain sequence information. The run though successful did not yield many reads. When comparing the data set with that of the non-modified tRNAs, we did observe some base miscalls at the positions we would expect a Ψ. However, we cannot draw any conclusions based on such a small subset of data. We will need much more reads and multiple replicates to look for signal patterns and for more robust conclusions. Nonetheless we think, this was a good starting step to show that this method can indeed be used for the purpose of detecting modifications as well and all in the same run. Future experiments are planned to carry out more sequencing runs using modified nucleotides and also varying the amount of modifications introduced to the same run.

5.4 Conclusion

Here we showed that the complex tRNA molecules can indeed traverse through the nanopore as individual unfolded strands and the deflection of ionic current caused by this translocation

can be used to infer their nucleotide composition. The ligation of an RNA/DNA hybrid adapter adding ribonucleotides in the close proximity of the tRNA ends enabled end to end sequencing without loss of sequence information towards the ends. Having used a mix of tRNAs we also showed that different tRNAs, which differ only slightly in their sequences can be successfully distinguished. Unfortunately, the data generated was insufficient for more detailed analysis but it definitely serves to confirm proof of concept that tRNAs can be sequenced by this method.

We acknowledge the requirement of various improvements so as to use the nanopore technology more efficiently. One the one hand, the ligation with the adapters needs to be optimized to maximize utilizing the available biological sample. Equally important is to develop better trained algorithms to detect and decipher the modifications. On the other hand, technical improvements to the platform such as to improvement of the accuracy of the base caller or implementation of better pores to improve resolution of the difficult to sequence regions (eg homopolymer regions) will help in the attempts to develop a good sequencing method.

The prospects for a comprehensive sequencing of the complex tRNA molecules on the nanopore platform are very promising. Looking ahead, we believe that the nanopore platform will serve as an indispensable tool to advance our understanding of tRNA biology and uncover the role of tRNA base modifications and their aberrations in context of human diseases.

6 General Discussion

Cis-Pt, is an effective chemotherapeutic drug but development of resistance leads to treatment failure and is the major limitation in the use of this drug. In ovarian cancer, where the disease itself is detected at a very late stage, the development of resistance to the drug has more disastrous effects. As it influences survival and quality of life of patients, improving the response to the drug is an important challenge. Alterations in the ability of cells to repair cis-Pt-induced DNA damage is the most common cause of drug resistance in ovarian cancers [26] [38,42] [161]. But resistance to cis-Pt can occur due to more than one reason and can operate at different cellular levels. Different studies have identified different factors leading to resistance (reviewed in [10]) demonstrating the complexity and multifactorial nature of resistance to the drug. Increased DNA repair, including increased excision of the adducts formed on DNA or increased lesion bypass, is just one aspect. Other mechanisms causing resistance include decreased drug uptake and thus decreased intracellular concentration, increased reflux, increased sequestration by sulfhydryl molecules such as glutathione etc. Dysregulated expression of regulatory proteins involved in signal transduction pathways have also been shown to affect sensitivity to the drug [28]. Here we elucidated a mechanism involving key cellular ribosomal surveillance pathways. We demonstrate that prolonged exposure to cis-Pt leads to activation of GCN2 which provides survival benefits to SKOV3 cells.

6.1 GCN2 acts as a critical nexus in cis-Pt resistance

Here we show that prolonged cis-Pt treatment leads to ribosome stalling at one specific TTA codon in turn leading to collisions which are then sensed by the cell and activates the ZAKα→JNK axis of the MAP kinase. In addition, the collisions also activated the GCN2. As a key regulator of the ISR, GCN2 plays a role in helping cells to overcome stress. We showed that depletion of GCN2 sensitizes cells to cis-Pt. When cells lacking GCN2 are exposed to prolonged cis-Pt treatment, cells lead to ribosome stalling as before, but in the absence of GCN2 the cells are unable to overcome the ribosomal stress leading to continued activation of the JNK which triggers apoptosis. Irrespective of presence or absence of GCN2, the JNK signal is activated, however the activation levels vary and culminate in different consequences. In GCN2 depleted SKOV3 cells, JNK is strongly activated early on and triggers apoptosis as

detected by cleavage of PARP. The activation of GCN2 in wild type cells resolves the cellular stress. This is in line with the previous observation that JNK proteins have a dual role in both apoptotic and antiapoptotic pathways, where a transient activation leads to cell survival but continuous activation leads to apoptosis [138]. In this work we did not distinguish between JNK1 and JNK2. It would also be interesting to check whether isoform specificity has a role here given that they can have distinct and opposite roles as well [130 139 258]. Our observations also add to the growing literature showing that ribosomes are not mere protein synthesizing machines but have important roles in maintaining cellular homeostasis. We showed here that damage to RNA detected by ribosomes are cascaded down by different pathways. Previous work has shown that ISR and RQC converge on ribosome collisions [183]. Meydan & Guydosh (2021) suggested that the context and severity of collisions play a role in determining the fate of collisions and this is modulated by various surveillance pathways [78]. In this study, we elucidate the interplay of RSR and ISR in response to cis-Pt induced ribosome stalling in SKOV3 ovarian cancer cells with GCN2 serving as the critical nexus for the two pathways and conferring survival benefit to SKOV3 cells.

A2780, a cell line derived from an untreated patient of ovarian endometroid adenocarcinoma, when exposed to cis-Pt treatment (under conditions similar to those used for SKOV3) however did not show similar pathways activated. We did not detect ribosome stalling at the TTA or any codon, nor any activation of the GCN2. The response exhibited by these cells likely involves response to DNA damage as seen by dysregulation of genes related to such pathways. Although we initially started experiments using this cell line with a purpose of comparison with SKOV3 cells, it was soon realized that the origin of these cells differs significantly from the SKOV3 [231] and hence a direct comparison may not be ideal. Other than the many possible mechanistic differences, the inherent characteristics of the cells itself could account to different responses and one cannot distinguish. We do present evidence of similar stalling, although to a less extent, in transformed fallopian tube cells supporting the damage caused by cis-Pt as we explained. Other ovarian cancer cell lines need to be looked at to identify whether the role of GCN2 is a common feature of resistant ovarian cancer cells or if this is specific to SKOV3 only.

6.2 Cis-Pt alters natural tRNA modification

The observed ribosome stalling and the downstream effects are very interesting. But the one obvious question that remained was why ribosome stalling was observed only at TTA codon? Using tRNA tailored microarrays we ruled out the possibility that ribosome stalling at the TTA codon and GCN2 activation were linked to leucyl-tRNA^{Leu}(UAA) paucity. Cis-Pt induces damage to the DNA/RNA nucleotides, which could be the reason to impede the ribosomes movement. It has been seen that adjacent pyrimidines in single-stranded RNAs are regions susceptible to form dimers upon exposure to UV irradiation and oxidative agents [113,180]. We speculated the involvement of such cis-Pt associated pyrimidine dimer formation. In FT cells, most codons with adjacent pyrimidines were affected indicating that all such codons are equally susceptible to such pyrimidine dimer formation. But in SKOV3 cells, stalling was pronounced only at the TTA, suggesting that mRNA damage was less likely. Analysis of post transcriptional tRNA modifications and comparison of the tRNA profiles from untreated and treated SKOV3 cells revealed that cis-Pt altered natural modification in only tRNA^{Leu}(UAA); the G26-U27 pair in tRNA^{Leu}UAA showed alteration signals in cis-Pt treated SKOV3 cells. importantly, no other tRNA showed such alteration. Evidenced in literature we found that cytidine or uracil adjacent to naturally occurring ψ is a hotspot for pyrimidine dimer formation (ref). tRNA^{Leu}UAA, carries a ψ at position 28 i.e. adjacent to the position U-27 where we detected alteration signals. These observations indicate that cis-Pt treatment likely forms such dimers in this tRNA and as the tRNA itself is among low-abundance tRNAs[182], any small change would also show profound effects, exactly what we see. Thus, we show that exposure to cis-Pt causes alterations to the chemical modifications in tRNA^{Leu}UAA which is then affects translation and calls for the cells' response mechanisms.

6.3 Cisplatin alters FTO levels in resistant ovarian cancer cells

Chemical modifications on RNA molecules are important and have pervasive roles in cellular functions. m^{6}A is one such important RNA modification with implications in various diseases including cancer [259] [219] and has also been shown to have a role in therapy resistance [260]. In addition to the changes described in the translational machinery and the stress response pathways we also looked at the internal m^{6}A modification. The total m^{6}A levels in SKOV3 cells were unaffected by cis-Pt treatment (Fig 4.4) but a comparison of the major methylases

and demethylases that regulate the m^6A expression revealed that the expression of FTO, an m^6A eraser, was reduced upon cis-Pt treatment. FTO, the first discovered m^6A eraser has been shown to be frequently dysregulated in various types of cancers [261]. Wen et al (2020) showed that FTO downregulation and thereby increased m^6A levels play an oncogenic role in bladder cancer and protects bladder cancer cells from cis-Pt induced cytotoxicity [261]. The published articles however show contradicting roles of FTO and hence despite significant efforts in research, the exact role and mechanism of action of FTO is unclear. Our findings however did not show any alterations in the m^6A levels. In addition to the decreased levels, we also observed that in untreated SKOV3 cells, FTO was distributed both in the nucleus and cytoplasm but upon cis-Pt treatment FTO appeared to be concentrated only in the nuclear and perinuclear region (Fig. 4.8). Given that methylases and demethylases target different RNA species and/or different modifications according to their subcellular localization [228,262], this is an interesting observation and could imply a different role of FTO than just demethylating m^6A. Besides m^6A, FTO has also been reported to demethylate N6, 2'-O-dimethyladenosine (m^6A_m), a modification with an identical chemical structure in the base moiety to m^6A and is found on the second base adjacent to the 5' cap (cap-m^6A_m) in some mRNAs [228]. Relier et al (2021) showed that low FTO expression was associated with elevated m^6A_m level in mRNA which in turn enhanced in vivo tumorigenicity and chemoresistance [232]. Wei et al (2018) demonstrated that the cellular distribution of FTO can be distinct between different cell lines and that FTO can have different substrates. They showed that FTO can have distinct substrate preference in the nucleus versus the cytoplasm; mediating mRNA m^6A and cap-m^6A_m demethylation in cytoplasm but mostly mRNA m^6A demethylation in cell nucleus [233]. Does FTO affect the m^6A_m levels in the SKOV3 cells when treated with cis-Pt and could this have any role in the drug response? More experiments are needed to dive into these aspects. FTO has emerged as a molecule with multifaceted roles and acts on a wide spectrum of substrates. It can bind to mRNA, snRNA and tRNA and can demethylate internal m^6A in mRNA and snRNA, N6,2′-O-dimethyladenosine (m^6A_m) adjacent to the mRNA cap, and N1-methyladenosine (m^1A) in tRNA [262]. Noteworthy here is that FTO can catalyze tRNA demethylation [263]. FTO efficiently demethylates the m^1A modification in tRNAs when present in a loop structure [262]. Could the Leu UAA effect we detailed previously be linked to a possible FTO activity? Wei et al revealed that FTO exhibits a preference to some tRNAs and knockdown of FTO increases the m^1A/G ratios of $tRNA^{Glu}$(CUC), $tRNA^{His}$(GUG), $tRNA^{Gly}$(GCC), $tRNA^{Gly}$(ACC), $tRNA^{Asp}$(GUC), $tRNA^{Lys}$(CUU), $tRNA^{Gln}$(CUG), and $tRNA^{Leu}$(CAA) in 3T3-L1 cells [233]. Leucine is not amongst the known targets but it is also known that FTO can have distinct context specific

targets. It will be interesting to find out if the reduced FTO levels observed in SKOV3 cells have any effect on tRNAs modifications, in this case specially the tRNA ^{Leu} (TTA). As FTO has such diverse roles, how FTO exerts its effect in one cell line need not necessarily be similar to that in another cell line or in a different physiological state. Presence of cis-Pt could potentially trigger other responses as well. It will be interesting to investigate the role of FTO in ovarian cancer cells and specifically in the context of cis-Pt resistance.

6.4 tRNA sequencing

tRNAs are key players in the protein synthesis process, linking the genetic code with the amino acid sequence of proteins. ~70–90 nucleotides in length mature tRNAs exhibit a characteristic cloverleaf secondary structure and further folds into a complex L-shaped tertiary structure [240]. Presence of tRNA sequence variants, base modifications, tissue specific abundance and expression, add to the complexity associated with the biology of these small but vital molecular entities [241] [242]. tRNAs are highly modified post transcriptionally with an average of 13 modified bases in each tRNA. tRNA levels are dynamic both under normal health and disease conditions [246]. Base modifications are abundant and critical to tRNA function. It is evident that tRNA abundance, expression and modifications can influence various biological processes. tRNA levels and their modifications have been implicated in a wide range of human diseases such as mitochondrial diseases, neurological disorders and cancer [244] [245] [247] [248] [249] [250]. Adding to the wealth of literature, our findings (as detailed in Chapter 2) show that alteration of chemical post transcriptional modification of tRNA^{Leu}(TTA) is linked to cis-Pt resistance in ovarian cancer. Methods to detect and further characterize such modifications are required to uncover such and many other possibly unknown roles that the modifications play.

Although advances in technology have improved RNA sequencing, tRNAs sequencing has not developed to the desired extent. Most analysis of tRNAs focus on determining expression patterns or detection of new tRNAs. Short length, the structural complexity, presence of various genes and the modifications pose a significant challenge to sequencing individual tRNA molecules. Typical RNA sequencing methods employ reverse transcription and then sequence the synthesized cDNA. The structural complexity and modifications present on tRNAs cause the reverse transcriptase to stop or completely drop off hindering the synthesis of cDNA and thereby impeding proper sequencing. In recent years, researches have tried to overcome the problems by alternative reverse transcriptases or by additional steps such as demethylase

treatments, bisulfite treatment for 5-methylcytosine or immunoprecipitation for N^6-methyladenine [237] [257]. But all of them are labor intensive. None of the currently used methods can directly detect base modifications or detect multiple modifications on individual strands. The nanopore sequencing method is a fundamentally different technique which reads nucleotides directly along linearized strands without requiring RT or amplification steps. The technique depends on ionic current deflections as nucleotides pass through the nanopore and the current signature generated is translated into nucleotide identify. This permits detection of nucleotides directly from native RNA strand itself whether modified or non-modified as part of the sequencing process itself without requiring additional handling. The method thus has the potential to provide information on the amount of tRNA (abundance) as well as modifications in one single sequencing run at single molecule resolution.

We showed here that the nanopore method can sequence full length tRNAs (detailed in chapter 5). Addition of RNA/DNA hybrid adaptors to either end of the tRNA molecules helped overcome the initial hurdles of missing the end region and allows sequencing individual full length tRNAs. Although we adapted the method from [257], instead of using 4 sets of adaptors each corresponding to tRNAs containing one of the four possible discriminator bases, in our study we designed the oligonucleotide that ligates to the 5' end of the tRNA to include a random mix of ribonucleotides (N) at the 3'end so that it can pair to tRNAs containing either of the discriminator bases, thus needing only 1 adaptor pair. Although the sequencing depth was not very good we obtained reads from all the different tRNAs used indicating that the adaptor is able to capture all tRNAs. We do however acknowledge that the ligation efficiency needs to be proved. As the sequencing method is very different from the currently used techniques, the data analysis also requires to be tuned for such methods. Using the algorithms and base callers and designed for direct RNA sequencing are not ideal for tRNA seq as most of the reads are discarded leading to poor yield. This is only due to a pre-set quality parameter suited for long RNA reads. Relying only on the in-built basecalling algorithms are not suitable for this method of sequencing. The raw signals behold all the information about the nucleotides and we believe ways to harness this information directly from the current signals need to be developed. The passage of nucleobases through the nanopores alters the flow of ions across the membrane and the presence of nucleotide modifications can induce distinct shifts in current intensity and/or in the time the nucleic acid sequence resides in the pore [264]. Tailored means to analyze data obtained from the nanopore reads are required. In recent years, researchers have worked toward the development of experimental and analytical strategies for the detection of RNA

modifications and generated various algorithms and software packages. Some are based on the detection of modification-induced basecalling errors (eg. Epinano, DiffErr, Eligos) and other are based on the analysis of the raw electrical signal (Tombo, Mines, xPore, nanom6A, nanoRMS etc.). To get a first impression here we also resorted to a method based on base calling errors. With more experiments and more data generated, in the future we look forward to dive deeper into the analysis of modifications.

The ability to unfold and translocate biological tRNAs through such nanopores and get sequence information will serve as a first step towards direct and complete analysis of single tRNAs molecules. Unlike the other commonly used methods today, the nanopore method has the advantage of being relatively easy, less labor and time intensive making it suitable for designing more experiments/ replicates. Researchers will be able to adapt the method quickly to suit their specific interests and answer questions related to differential expression in various tissues or under different physiological conditions. Moving from the very first attempts to try and pass tRNAs through an α-hemolysin (α-HL) nanopore [237], to differentiating tRNA from other small RNA molecules [265] to now being able to sequence full length tRNAs as shown by our results as well as Thomas et al [257], it is being realized this method has great potential. The most recent addition to these efforts has explored the raw signals obtained to determine the abundance and modification in tRNA [266]. These findings emphasize that the nanopore platform will serve as an indispensable tool to advance our understanding of tRNA biology.

Not only tRNAs but RNA biology as a whole is undergoing paradigm shifts. Growing number of studies are hinting towards the fact that the functions of RNA do not rely solely on their sequence information. Chemical modifications on the RNA are becoming increasingly important and deciphering the biology of RNA modifications represents one of the next frontiers in the field of molecular biology [267]. Nanopore technology will play a significant role therein.

References

1. Sung, H. *et al.* Global Cancer Statistics 2020: GLOBOCAN Estimates of Incidence and Mortality Worldwide for 36 Cancers in 185 Countries. *CA A Cancer J. Clin.* **71**, 209–249 (2021).

2. Bailar John C, G. H. L. Cancer Undefeated. *N. Engl. J. Med.* **336**, 1569–1574 (2007).

3. Momenimovahed, Z., Tiznobaik, A., Taheri, S. & Salehiniya, H. Ovarian cancer in the world : epidemiology and risk factors. *Int. J. Womens. Health* **11**, 287–299 (2019).

4. Hausman, D. M. What Is Cancer ? *Perspect. Biol. Med.* **62**, 778–784 (2019).

5. Ghosh, S. Cisplatin: The first metal based anticancer drug. *Bioorg. Chem.* **88**, 102925 (2019).

6. Carbone, A. Cancer classification at the crossroads. *Cancers (Basel).* **12**, 10–15 (2020).

7. Nygren, P. What is cancer chemotherapy? *Acta Oncol. (Madr).* **40**, 166–174 (2001).

8. Dasari, S. & Bernard Tchounwou, P. Cisplatin in cancer therapy: Molecular mechanisms of action. *European Journal of Pharmacology* vol. 740 364–378 (2014).

9. Kelland, L. The resurgence of platinum-based cancer chemotherapy. *Nat. Rev. Cancer* **7**, 573–584 (2007).

10. Galluzzi, L., Senovilla, L., Vitale, I., Michels, J., Martins, I., Kepp, O., Castedo, M., Kroemer, G. Molecular mechanisms of cisplatin resistance. *Oncogene* **31**, 1869–1883 (2012).

11. Tchounwou, P. B., Dasari, S., Noubissi, F. K., Ray, P. & Kumar, S. Advances in Our Understanding of the Molecular Mechanisms of Action of Cisplatin in Cancer Therapy. *J. Exp. Pharmacol.* **13**, 303–328 (2021).

12. Andrea Brown, Sanjay Kumar, P. B. T. Cisplatin-Based Chemotherapy of Human Cancers. *J Cancer Sci Ther.* **11**, (2019).

13. Goodsell, D. S. The Molecular Perspective: Cisplatin. *Oncologist* **11**, 316–317 (2006).

14. Ummat, A. *et al.* Structural basis for cisplatin DNA damage tolerance by human polymerase η during cancer chemotherapy. *Nat. Struct. Mol. Biol.* **19**, 628–632 (2012).

15. Mortensen, A. C. L., Mohajershojai, T., Hariri, M., Pettersson, M. & Spiegelberg, D. Overcoming Limitations of Cisplatin Therapy by Additional Treatment With the HSP90 Inhibitor Onalespib. *Front. Oncol.* **10**, (2020).

16. Eidelman, Eric; Twum-Ampofo, Jeffrey; Ansari, Jamal; Siddiqui, M. M. The Metabolic Phenotype of Prostate Cancer. *Front. Oncol.* **7**, (2017).

17. Jordan, Peter and Carmo-Fonseca, M. Cisplatin inhibits synthesis of ribosomal RNA in vivo. *Nucleic Acids Res.* **26**, 2831–2836 (1998).

18. Siddik, Z. H. Cisplatin: Mode of cytotoxic action and molecular basis of resistance. *Oncogene* **22**, 7265–7279 (2003).

19. Melnikov, S. V., Söll, D., Steitz, T. A. & Polikanov, Y. S. Insights into RNA binding by the anticancer drug cisplatin from the crystal structure of cisplatin-modified ribosome. *Nucleic Acids Res.* **44**, 4978–4987 (2016).

20. Hostetter, A. A., Osborn, M. F. & Derose, V. J. RNA-Pt adducts following cisplatin treatment of saccharomyces cerevisiae. *ACS Chem. Biol.* **7**, 218–225 (2012).

21. Makovec, T. Cisplatin and beyond: Molecular mechanisms of action and drug resistance development in cancer chemotherapy. *Radiol. Oncol.* **53**, 148–158 (2019).

22. Osborn, M. F., White, J. D., Haley, M. M. & DeRose, V. J. Platinum-RNA modifications following drug treatment in S. cerevisiae Identified by click chemistry and enzymatic mapping. *ACS Chem. Biol.* **9**, 2404–2411 (2014).

23. Raudenska, M., Balvan, J., Fojtu, M., Gumulec, J. & Masarik, M. Unexpected therapeutic effects of cisplatin. *Metallomics* **11**, 1182–1199 (2019).

24. Qi, L. *et al.* Advances in Toxicological Research of the Anticancer Drug Cisplatin. *Chem. Res. Toxicol.* **32**, 1469–1486 (2019).

25. De Luca, A. *et al.* A structure-based mechanism of cisplatin resistance mediated by glutathione transferase P1-1. *Proc. Natl. Acad. Sci. U. S. A.* **116**, 13943–13951 (2019).

26. Wong-Brown, M.W., van der Westhuizen, A., Bowden, N. A. Targeting DNA Repair in Ovarian Cancer Treatment Resistance. *Clin. Oncol. (R Coll Radiol)* **32**, 518–526 (2020).

27. Lugones, Y., Loren, P. & Salazar, L. A. Cisplatin Resistance: Genetic and Epigenetic Factors Involved. *Biomolecules* **12**, 1–12 (2022).

28. M Kartalou 1, J. M. E. Mechanisms of resistance to cisplatin. *Princ. Pract. Mod. Radiother. Tech. Breast Cancer* **478**, 23–43 (2001).

29. Shriwas, O., Mohapatra, P., Mohanty, S. & Dash, R. The Impact of m6A RNA Modification in Therapy Resistance of Cancer: Implication in Chemotherapy, Radiotherapy, and Immunotherapy. *Front. Oncol.* **10**, 1–7 (2021).

30. Camille V. Trinidad, Ashley L. Tetlow, Leonidas E. Bantis, A. K. G. Reducing Ovarian Cancer Mortality Through Early Detection: Approaches using Circulating Biomarkers. *Cancer Prev Res (Phila).* **13**, 241–252 (2020).

31. Stewart, C., Ralyea, C. & Lockwood, S. Ovarian Cancer: An Integrated Review. *Semin. Oncol. Nurs.* **35**, 151–156 (2019).

32. Longuespée, R. *et al.* Ovarian cancer molecular pathology. *Cancer Metastasis Rev.* **31**, 713–732 (2012).

33. Kossaï, M., Leary, A., Scoazec, J. Y. & Genestie, C. Ovarian Cancer: A Heterogeneous Disease. *Pathobiology* **85**, 41–49 (2018).

34. Davis, Alison; Tinker, Anna V., Friedlander, M. 'Platinum resistant' ovarian cancer: What is it, who to treat and how to measure benefit? *Gynecol. Oncol.* **133**, 624–631 (2014).

35. Chobanian, N. & Dietrich, C. S. Ovarian Cancer. *Surg. Clin. North Am.* **88**, 285–299 (2008).

36. Grisham, R. N., Hyman, D. M. & Iyer, G. Targeted therapies for treatment of recurrent ovarian cancer. *Clin Adv Hematol Oncol* **12**, 158–162 (2014).

37. Matulonis, Ursula A., Sood, Anil K., Fallowfield, Lesley., Howitt, Brooke E., Sehouli, Jalid., Karlan, B. Y. Ovarian cancer. *Nat. Rev. Dis. Prim.* **2**, 1–22 (2016).

38. McMullen, Michelle., Madariaga, Ainhoa., Lheureux, S. New approaches for targeting platinum-resistant ovarian cancer. *Semin. Cancer Biol.* **77**, (2021).

39. Binju, M. *et al.* Mechanisms underlying acquired platinum resistance in high grade serous ovarian cancer - a mini review. *Biochim. Biophys. Acta - Gen. Subj.* **1863**, 371–378 (2019).

40. Li, Julang., Feng, Qiang., Kim, Jong Min., Schneiderman, Danielle., Liston, Peter., Li, Ming., Vanderhyden, Barbara., Faught, Wylam., Fung, Michael Fung Kee., Senterman, Mary., Korneluk, Robert G. and Tsang, B. K. Human ovarian cancer and cisplatin resistance: Possible role of inhibitor of apoptosis proteins. *Endocrinology* **142**, 370–380 (2001).

41. Shen, D. W., Pouliot, L. M., Hall, M. D. & Gottesman, M. M. Cisplatin resistance: A cellular self-defense mechanism resulting from multiple epigenetic and genetic changes. *Pharmacol. Rev.* **64**, 706–721 (2012).

42. Damia, Giovanna and Broggini, M. Platinum Resistance in Ovarian Cancer : Role of DNA Repair. *Cancers (Basel).* **11**, 1–15 (2019).

43. Yang, Ling., Xie, Hong Jian., Li, Ying Ying., Wang, Xia., Liu, Xing Xin., Mai, J. Molecular mechanisms of platinum - based chemotherapy resistance in ovarian cancer (Review). *Oncol. Rep.* **47**, 82 (2022).

44. Schuller, Anthony P and Green, R. Roadblocks and resolutions in eukaryotic translation. *Nat Rev Mol Cell Biol* **19**, 526–541 (2018).

45. Hershey, J. W. B., Sonenberg, N. & Mathews, M. B. Principles of translational control: An overview. *Cold Spring Harb. Perspect. Biol.* **4**, 1–10 (2012).

46. Pestova, Tatyana V., Kolupaeva, Victoria G., Lomakin, Ivan B., Pilipenko, Evgeny V., Shatsky, Ivan N., Agol, Vadim I., Hellen, C. U. T. Molecular mechanisms of translation initiation in eukaryotes. *Proc. Natl. Acad. Sci. U. S. A.* **98**, 7029–7036 (2001).

47. Merrick, W. C. & Pavitt, G. D. Protein synthesis initiation in eukaryotic cells. *Cold Spring Harb. Perspect. Biol.* **10**, 1–22 (2018).

48. Aitken, C. E. & Lorsch, J. R. A mechanistic overview of translation initiation in eukaryotes. *Nat. Struct. Mol. Biol.* **19**, (2012).

49. Sonenberg, N. & Hinnebusch, A. G. Regulation of translation initiation in eukaryotes. *Cell* **136**, 731–745 (2009).

50. Topisirovic, I. & Sonenberg, N. Translational control by the eukaryotic ribosome. *Cell* **145**, 333–334 (2011).

51. Dever, T. E., Dinman, J. D. & Green, R. Translation elongation and recoding in eukaryotes. *Cold Spring Harb. Perspect. Biol.* **10**, 1–20 (2018).

52. Neelagandan, N., Lamberti, I., Carvalho, H. J. F., Gobet, C. & Naef, F. What determines eukaryotic translation elongation: Recent molecular and quantitative analyses of protein synthesis: Determinants of eukaryotic translation. *Open Biol.* **10**, (2020).

53. Dever, T. E. & Green, R. The elongation, termination, and recycling phases of translation in eukaryotes. *Cold Spring Harb. Perspect. Biol.* **4**, 1–16 (2012).

54. Dever, T. E., Dinman, J. D. & Green, R. Translation elongation and recoding in eukaryotes. *Cold Spring Harb. Perspect. Biol.* **10**, 1–19 (2018).

55. Frank, J. & Agrawal, R. K. A ratchet-like inter-subunit reorganization of the ribosome during translocation. **406**, 269–273 (2018).

56. Liu, Jianzhao., Yue, Yanan., Han, Dali., Wang, Xiao., Fu, Y., Zhang, Liang., Jia, Guifang., Yu, Miao., Lu, Zhike., Deng, Xin., Dai, Qing., Chen, Weizhong and He, C. A METTL3-METTL14 complex mediates mammalian nuclear RNA N6-adenosine methylation. *Nat. Chem. Biol.* **10**, 93–95 (2014).

57. Lareau, L. F., Hite, D. H., Hogan, G. J. & Brown, P. O. Distinct stages of the translation elongation cycle revealed by sequencing ribosome-protected mRNA fragments. *Elife* **3**, e01257 (2014).

58. Frank, J. The translation elongation cycle—Capturing multiple states by cryo-electron microscopy. *Philos. Trans. R. Soc. B Biol. Sci.* **372**, 1–10 (2017).

59. Hellen, C. U. T. Translation termination and ribosome recycling in eukaryotes. *Cold Spring Harb. Perspect. Biol.* **10**, (2018).

60. Tuite, M. F. & Stansfield, I. Termination of protein synthesis. 171–181 (1994).

61. Petry, S., Weixlbaumer, A. & Ramakrishnan, V. The termination of translation. *Curr. Opin. Struct. Biol.* **18**, 70–77 (2008).

62. Melnikov, S. *et al.* One core, two shells: Bacterial and eukaryotic ribosomes. *Nat. Struct. Mol. Biol.* **19**, 560–567 (2012).

63. Matzov, D., Bashan, A., Yap, M. F. & Yonath, A. Stress response as implemented by hibernating ribosomes : a structural overview. **286**, 3558–3565 (2019).

64. Davidovich, C., Belousoff, M., Bashan, A. & Yonath, A. The evolving ribosome : from

non-coded peptide bond formation to sophisticated translation machinery. *Res. Microbiol.* **160**, 487–492 (2009).

65. Ramakrishnan, V., Road, H., Kingdom, U. & Heel, V. and the Mechanism of Translation. **108**, 557–572 (2002).

66. Wilson, D. N. & Cate, J. H. D. The structure and function of the eukaryotic ribosome. *Cold Spring Harb. Perspect. Biol.* **4**, 5 (2012).

67. Khatter, Heena., Myasnikov, Alexander G., Natchiar, S Kundhavai., Klaholz, B. P. Structure of the human 80S ribosome. *Nature* **520**, 640–5 (2015).

68. Thomson, Emma., Ferreira-Cerca, Sebastien., Hurt, E. Eukaryotic ribosome biogenesis at a glance. *J. Cell Sci.* **126**, 4815–21 (2013).

69. Piazzi, M., Bavelloni, A., Gallo, A., Faenza, I. & Blalock, W. L. *Signal transduction in ribosome biogenesis: A recipe to avoid disaster*. *International Journal of Molecular Sciences* vol. 20 (2019).

70. Genuth, N. R. & Barna, M. The Discovery of Ribosome Heterogeneity and Its Implications for Gene Regulation and Organismal Life. *Mol. Cell* **71**, 364–374 (2018).

71. Bastide, A. & David, A. The ribosome, (slow) beating heart of cancer (stem) cell. *Oncogenesis* **7**, (2018).

72. Joazeiro, C. A. P. Ribosomal Stalling During Translation : Providing Substrates for Ribosome-Associated Protein Quality Control. 1–26 (2017).

73. Nadya Kondrashov, Aya Pusic, Craig R. Stumpf, Kunihiko Shimizu, A. C. & Hsieh, Junko Ishijima, Toshihiko Shiroishi4, and M. B. Ribosome mediated specificity in Hox mRNA translation and vertebrate tissue patterning. *Cell* **145**, 383–397 (2011).

74. Gnanasundram, S. V. & Fåhraeus, R. Translation stress regulates ribosome synthesis and cell proliferation. *Int. J. Mol. Sci.* **19**, (2018).

75. Mills, Eric W. and Green, R. Ribosomopathies: There's strength in numbers. *Science (80-.).* **358**, (2017).

76. Joazeiro, C. A. P. Mechanisms and functions of ribosome-associated protein quality control. *Nature Reviews Molecular Cell Biology* vol. 20 368–383 (2019).

77. Nicholas T. Ingolia1,3,4, Liana F. Lareau2, and J. S. W. NIH Public Access. *Cell* **147**, 789–802 (2012).

78. Meydan, S. & Guydosh, N. R. A cellular handbook for collided ribosomes: surveillance pathways and collision types. *Curr. Genet.* **67**, 19–26 (2021).

79. Collart, M. A. & Weiss, B. Ribosome pausing, a dangerous necessity for co-translational events. *Nucleic Acids Res.* **48**, 1043–1055 (2020).

80. Yip, M. C. J. & Shao, S. Detecting and Rescuing Stalled Ribosomes. *Trends Biochem. Sci.* **46**, 731–743 (2021).

81. Vind, A. C., Genzor, A. V. & Bekker-Jensen, S. Ribosomal stress-surveillance: three pathways is a magic number. *Nucleic Acids Res.* **48**, 10648–10661 (2020).

82. Juszkiewicz, Szymon., Chandrasekaran, Viswanathan., Lin, Zhewang., Kraatz, Sebastian., Ramakrishnan, V., Hegde, R. S. ZNF598 Is a Quality Control Sensor of Collided Ribosomes. *Mol. Cell* **72**, 469-481.e7 (2018).

83. Park, J., Park, J., Lee, J. & Lim, C. The trinity of ribosome-associated quality control and stress signaling for proteostasis and neuronal physiology. **54**, 439–450 (2021).

84. Garcia-Barrio, M. Association of GCN1-GCN20 regulatory complex with the N-terminus of eIF2alpha kinase GCN2 is required for GCN2 activation. *EMBO J.* **19**, 1887–1899 (2000).

85. Harding, Heather P., Ordonez, Adriana., Allen, Felicity., Parts, Leopold., Inglis, Alison J., Williams, Roger L., Ron, D. The ribosomal P-stalk couples amino acid starvation to GCN2 2 activation in mammalian cells. *Elife* **8**, 1–19 (2019).

86. Inglis, Alison J., Masson, Glenn R., Shao, Sichen., Perisic, Olga., McLaughlin, Stephen H., Hegde, Ramanujan S., Williams, R. L. Activation of GCN2 by the ribosomal P-stalk. *Proc. Natl. Acad. Sci. U. S. A.* **116**, 4946–4954 (2019).

87. Ishimura, R., Nagy, G., Dotu, I., Chuang, J. H. & Ackerman, S. L. Activation of GCN2 kinase by ribosome stalling links translation elongation with translation initiation. *Elife* **5**, e14295 (2016).

88. D'Orazio, K. N. & Green, R. Ribosome states signal RNA quality control. *Mol. Cell* **81**, 1372–1383 (2021).

89. Ikeuchi, K., Izawa, T. & Inada, T. Recent progress on the molecular mechanism of quality controls induced by ribosome stalling. *Front. Genet.* **10**, 1–7 (2019).

90. Cole S. Sitron & Brandman, O. Detection and Degradation of Stalled Nascent Chains via Ribosome-Associated Quality Control. *Annu rev Biochem* 417–442 (2020) doi:10.1146/annurev-biochem-013118-110729.Detection.

91. Brandman, O. & Hegde, R. S. Ribosome-associated protein quality control. *Nat Struct Mol Biol.* **23**, 7–15 (2016).

92. Anda, S., Zach, R. & Grallert, B. Activation of Gcn2 in response to different stresses. *PLoS One* **12**, 1–13 (2017).

93. Donnelly, N., Gorman, A. M., Gupta, S. & Samali, A. The eIF2α kinases: Their structures and functions. *Cell. Mol. Life Sci.* **70**, 3493–3511 (2013).

94. Pakos-Zebrucka, Karolina., Koryga, Izabela., Mnich, Katarzyna., Ljujic, Mila., Samali, Afshin., Gorman, A. M. The integrated stress response. *EMBO Rep.* **17**, 1374–1395 (2016).

95. Tian, Xiaobing., Zhang, Shengliang., Zhou, Lanlan., Seyhan, Attila A., Hernandez Borrero, Liz., Zhang, Yiqun and El-Deiry, W. S. Targeting the Integrated Stress Response in Cancer Therapy. *Front. Pharmacol.* **12**, 1–12 (2021).

96. Castilho, B. A. *et al.* Keeping the eIF2 alpha kinase Gcn2 in check. *Biochim. Biophys. Acta - Mol. Cell Res.* **1843**, 1948–1968 (2014).

97. Gold, L. T. & Masson, G. R. GCN2: roles in tumour development and progression. *Biochem. Soc. Trans.* **50**, 737–745 (2022).

98. Dokládal, Ladislav., Stumpe, Michael., Pillet, Benjamin., Hu, Zehan., Garcia Osuna, Guillermo Miguel., Kressler, Dieter., Dengjel, Jörn., De Virgilio, C. Global phosphoproteomics pinpoints uncharted Gcn2-mediated mechanisms of translational control. *Mol. Cell* **81**, 1879-1889.e6 (2021).

99. Zaborske, J. M. *et al.* Genome-wide Analysis of tRNA Charging and Activation of the eIF2 Kinase Gcn2p*♦. *J. Biol. Chem.* **284**, 25254–25267 (2009).

100. Masson, G. R. Towards a model of GCN2 activation. *Biochem. Soc. Trans.* **47**, 1481–1488 (2019).

101. De Oliveira, Taiana Maia., Korboukh, Victoria., Caswell, Sarah., Holt, Jon J.Winter., Lamb, Michelle., Hird, Alexander W., Overman, R. The structure of human GCN2 reveals a parallel, back-to-back kinase dimer with a plastic DFG activation loop motif. *Biochem. J.* **477**, 275–284 (2020).

102. Ramirez, M., Wek, R C., Vazquez de Aldana, C R., Jackson, B M., Freeman, B., Hinnebusch, A. G. Mutations activating the yeast eIF-2 alpha kinase GCN2: isolation of alleles altering the domain related to histidyl-tRNA synthetases. *Mol. Cell. Biol.* **12**, 5801–5815 (1992).

103. Dong, J., Qiu, H., Garcia-Barrio, M., Anderson, J. & Hinnebusch, A. G. Uncharged tRNA activates GCN2 by displacing the protein kinase moiety from a bipartite tRNA-binding domain. *Mol. Cell* **6**, 269–279 (2000).

104. Qiu, H., Dong, J., Hu, C., Francklyn, C. S. & Hinnebusch, A. G. The tRNA-binding moiety in GCN2 contains a dimerization domain that interacts with the kinase domain and is required for tRNA binding and kinase activation. *EMBO J.* **20**, 1425–1438 (2001).

105. Grallert Beata, B. E. GCN2 , an old dog with new tricks. *Biochem. Soc. Trans.* **41**, 1687–1691 (2013).

106. Harding, Heather P., Ordonez, Adriana., Allen, Felicity., Parts, Leopold., Inglis, Alison J., Williams, Roger L., Ron, D. The ribosomal P-stalk couples amino acid starvation to GCN2 2 activation in mammalian cells. *Elife* **8**, (2019).

107. Wu, C. C. C., Peterson, A., Zinshteyn, B., Regot, S. & Green, R. Ribosome Collisions Trigger General Stress Responses to Regulate Cell Fate. *Cell* **182**, 404-416.e14 (2020).

108. Yan, Liewei L., Zaher, H. S. Ribosome quality control antagonizes the activation of the integrated stress response on colliding ribosomes Article Ribosome quality control antagonizes the activation of the integrated stress response on colliding ribosomes. *Mol. Cell* **81**, 614–628 (2021).

109. Pochopien, Agnieszka A., Beckert, Bertrand., Kasvandik, Sergo., Berninghausen, Otto., Beckmann, Roland., Tenson, Tanel., Wilson, D. N. Structure of Gcn1 bound to stalled

and colliding 80S ribosomes. *Proc. Natl. Acad. Sci. U. S. A.* **118**, (2021).

110. Marton, M. J., Vazquez de Aldana, C. R., Qiu, H., Chakraburtty, K. & Hinnebusch, A. G. Evidence that GCN1 and GCN20, translational regulators of GCN4, function on elongating ribosomes in activation of eIF2alpha kinase GCN2. *Mol. Cell. Biol.* **17**, 4474–4489 (1997).

111. Nakamura, Akito., Kimura, H. A new role of GCN2 in the nucleolus. *Biochem. Biophys. Res. Commun.* **485**, 484–491 (2017).

112. Castilho, Beatriz A., Shanmugam, Renuka., Silva, Richard C., Ramesh, Rashmi., Himme, Benjamin M., Sattlegger, E. Keeping the eIF2 alpha kinase Gcn2 in check. *BBA - Mol. Cell Res.* **1843**, 1948–1968 (2014).

113. Iordanov, M S., Pribnow, D. & Magun, J L., Dinh, T H., Pearson, J A., Chen, S L., Magun, B. E. Ribotoxic stress response: activation of the stress-activated protein kinase JNK1 by inhibitors of the peptidyl transferase reaction and by sequence-specific RNA damage to the alpha-sarcin/ricin loop in the 28S rRNA. *Mol. Cell. Biol.* **17**, 3373–3381 (1997).

114. De, S. & Mühlemann, O. A comprehensive coverage insurance for cells : revealing links between ribosome collisions , stress responses and mRNA surveillance. *RNA Biol.* **19**, 609–621 (2022).

115. Snieckute, Goda., Genzor, Aitana Victoria., Vind, Anna Constance., Ryder, Laura., Stoneley, Mark., Chamois, Sébastien., Dreos, René., Nordgaard, Cathrine., Sass, Frederike., Blasius, Melanie., López, Aida Rodríguez., Brynjólfsdóttir, Sólveig Hlín., Anders, S. Ribosome stalling is a signal for metabolic regulation by the ribotoxic stress response. *Cell Metab.* **34**, 2036–2046 (2022).

116. https://omim.org/entry/609479.

117. Ruggieri, R. *ZAK*. *ZAK* (Encyclopedia of signaling molecules, 2005). doi:10.1007/978-3-319-67199-4.

118. Vind, Anna Constance., Snieckute, Goda., Blasius, Melanie., Tiedje, Christopher., Krogh, Nicolai., Bekker-Jensen, Dorte Breinholdt., Andersen, Kasper Langebjerg., Nordgaard, Cathrine., Tollenaere, Maxim Alexander Xavier., Lund, Anders Henrik., Olsen, Jesp, S. ZAKα Recognizes Stalled Ribosomes through Partially Redundant Sensor Domains. *Mol. Cell* **78**, 700–713 (2020).

119. Firdaus, M. J. *et al.* ZAK a -driven ribotoxic stress response activates the human NLRP1 inflammasome. *Science (80-.).* **335**, 328–335 (2022).

120. Stoneley, Mark., Harvey, Robert F., Mulroney, Thomas E., Mordue, Ryan., Jukes-Jones, Rebekah., Cain, Kelvin., Lilley, Kathryn S., Sawarkar, Ritwick., Willis, A. E. Unresolved stalled ribosome complexes restrict cell-cycle progression after genotoxic stress. *Mol. Cell* **82**, 1–16 (2022).

121. Jandhyala, D. M., Ahluwalia, A., Obrig, T. & Thorpe, C. M. ZAK: A MAP3Kinase that transduces Shiga toxin- and ricin-induced proinflammatory cytokine expression. *Cell. Microbiol.* **10**, 1468–1477 (2008).

122. Ouyang, D. Y., Wang, Y. Y. & Zheng, Y. T. Activation of c-Jun N-terminal kinases by ribotoxic stresses. *Cell. Mol. Immunol.* **2**, 419–425 (2005).

123. Kyriakis, John M., Banerjee, Papia., Nikolakaki, Eleni., Dai, Tianang., Rubie, Elizabeth A., Ahmad, Mir F., Avruch, Joseph., Woodgett, J. R. The stress-activated protein kinase subfamily of c-Jun kinases. *Nature* **369**, 156–160 (1994).

124. Cui, J., Zhang, M., Zhang, Y. Q. & Xu, Z. H. JNK pathway: Diseases and therapeutic potential. *Acta Pharmacol. Sin.* **28**, 601–608 (2007).

125. Kamal S. Abdelrahman · Heba A. Hassan · Salah A. Abdel-Aziz, · Adel A. Marzouk · Atsushi Narumi· Hiroyuki Konno5 · Mohamed Abdel-Aziz. JNK signaling as a target for anticancer therapy. *Pharmacol. Reports* **73**, 405–434 (2021).

126. Solinas, G. & Becattini, B. JNK at the crossroad of obesity, insulin resistance, and cell stress response. *Mol. Metab.* **6**, 174–184 (2017).

127. Qinghua Wu1, 2, 6 & Kuca, K. JNK signaling in cancer cell survival. *Med. Res. Rev.* **39**, 2082–2104 (2019).

128. Liu, J. & Lin, A. Role of JNK activation in apoptosis: A double-edged sword. *Cell Res.* **15**, 36–42 (2005).

129. Papa, S., Choy, P. M. & Bubici, C. The ERK and JNK pathways in the regulation of metabolic reprogramming. *Oncogene* **38**, 2223–2240 (2019).

130. Bode, A. M. & Dong, Z. The functional contrariety of JNK. *Mol. Carcinog.* **46**, 591–598 (2007).

131. Gkouveris, I. & Nikitakis, N. G. Role of JNK signaling in oral cancer: A mini review. *Tumor Biol.* **39**, (2017).

132. Hammouda, M. B., Ford, A. E., Liu, Y. & Zhang, J. Y. The JNK Signaling Pathway in Inflammatory Skin Disorders and Cancer. *Cells* **9**, 1–22 (2020).

133. Karin, M. & Chang, L. Mammalian MAP kinase signaling cascades. *Nature* **410**, 37–40 (2001).

134. Sabapathy, K. Role of the JNK Pathway in human diseases. *Prog. Mol. Biol. Transl. Sci.* **106**, 145–169 (2012).

135. Qinghua Wu, Wenda Wu, Vesna Jacevic, Tanos C. C. Franca, X. W. and K. K. Selective inhibitors for JNK signalling: a potential targeted therapy in cancer. *J. Enzyme Inhib. Med. Chem.* **35**, 574–583 (2020).

136. Tournier, C. The 2 Faces of JNK Signaling in Cancer. *Genes and Cancer* **4**, 397–400 (2013).

137. La Marca, J. E. & Richardson, H. E. Two-Faced: Roles of JNK Signalling During Tumourigenesis in the Drosophila Model. *Front. Cell Dev. Biol.* **8**, 1–20 (2020).

138. Lamb, J. A., Ventura, J. J., Hess, P., Flavell, R. A. & Davis, R. J. JunD mediates survival

signaling by the JNK signal transduction pathway. *Mol. Cell* **11**, 1479–1489 (2003).

139. Kanaga Sabapathy, K. H., Nam, S. Y., Anton Bauer, M. K. & Wagner, and E. F. Distinct Roles for JNK1 and JNK2 in Regulating JNK Activity and c-Jun-Dependent Cell Proliferation University of California at San Diego. **15**, 713–725 (2004).

140. Fei Chen. JNK-induced apoptosis, compensatory growth and cancer stem cells. *Cancer Res.* **72**, 379–386 (2012).

141. Pan, C.-W. & , Hailong Liu , Yu Zhao , Chenchen Qian , Liguo Wang, J. Q. JNK2 downregulation promotes tumorigenesis and chemoresistance by decreasing p53 stability in bladder cancer. *Oncotarget* **7**, 35119–35131 (2016).

142. Xiaodong Tian., Traub, Benno. Jingwei Shi., Nadine Huber., Stefan Schreiner., Guowei Chen., Shaoxia Zhou., Doris Henne-Bruns., Uwe Knippschild., M. K. c-Jun N-terminal kinase 2 suppresses pancreatic cancer growth and invasion and is opposed by c-Jun N-terminal kinase 1. *Cancer Gene Ther.* **29**, 73–86 (2022).

143. Dhanasekaran, D. N. & Premkumar Reddy, E. JNK-signaling: A multiplexing hub in programmed cell death. *Genes and Cancer* **8**, 682–694 (2017).

144. Mamatha Bhat, Nathaniel Robichaud, Laura Hulea, Nahum Sonenberg, J. P. and I. T. Targeting the translation machinery in cancer. *Nat. Rev. Drug Discov.* **14**, 261–278 (2015).

145. Shi-Long Jiang, Jun-Luan Mo, Ji Peng, Lin Lei, Ji-Ye Yin, Hong-Hao Zhou, Zhao-Qian Liu, W.-X. H. Targeting translation regulators improves cancer therapy. *Genomics* **113**, 1247–1256 (2021).

146. Silvera, D., Formenti, S. C. & Schneider, R. J. Translational control in cancer. *Nat. Rev. Cancer* **10**, 254–266 (2010).

147. Smith, R. C. L. *et al.* Translation initiation in cancer at a glance. *J. Cell Sci.* **134**, 1–9 (2021).

148. Truitt, M. L. & Ruggero, D. New frontiers in translational control of the cancer genome. *Nat. Rev. Cancer* **16**, 288–304 (2016).

149. Song, P., Yang, F., Jin, H. & Wang, X. The regulation of protein translation and its implications for cancer. *Signal Transduct. Target. Ther.* **6**, (2021).

150. Fabbri, L., Chakraborty, A., Robert, C. & Vagner, S. The plasticity of mRNA translation during cancer progression and therapy resistance. *Nat. Rev. Cancer* **21**, 558–577 (2021).

151. Vaklavas, C., Blume, S. W. & Grizzle, W. E. Translational dysregulation in cancer: Molecular insights and potential clinical applications in biomarker development. *Front. Oncol.* **7**, (2017).

152. Chen, Wei., Ma, Lin., Bian, J., Feng, Su., Cao, Dan., Chen, Y., Yang, Jie., Zhang, Jin., Hua, Z. C. & Yin, W. Involvement of general control nonderepressible kinase 2 in cancer cell apoptosis By posttranslational mechanisms. *Mol. Biol. Cell* **26**, 1044–1057 (2015).

153. Furnish, Madison., Boulton, D. P. & Genther, Victoria., Grofova, Denisa., Ellinwood, Mitchell Lee., Romero, Lina., Lucia, M. Scott., Cramer, Scott D., Caino, M. C. MIRO2 Regulates Prostate Cancer Cell Growth via GCN1-Dependent Stress Signaling. *Mol. Cancer Res.* **20**, 607–621 (2022).

154. Wang, Yugang, Ning, Yu., Alam, Goleeta N., Jankowski, Brandon M., Dong, Zhihong., Nör, Jacques E., Polverini, P. J. Amino acid deprivation promotes tumor angiogenesis through the GCN2/ATF4 pathway. *Neoplasia (United States)* **15**, 989–997 (2013).

155. C Rey, B Faustin, I Mahouche, R Ruggieri, C Brulard, F Ichas, I Soubeyran, L Lartigue, and F. D. G. The MAP3K ZAK , a novel modulator of ERK-dependent migration , is upregulated in colorectal cancer. *Oncogene* **35**, 3190–3200 (2016).

156. Linna Li, Ning Su, Ting Zhou, Dayong Zheng, Zheng Wang, Haoyu Chen, S. Y. and W. L. Mixed lineage kinase ZAK promotes epithelial-mesenchymal transition in cancer progression. *Cell Death Dis.* **9**, (2018).

157. Liu, Jinfeng, Mccleland, Mark Stawiski, Eric W Gnad, Florian Mayba, Oleg Haverty, P. M. *et al.* reveals ZAK isoform usage in gastric cancer. *Nat. Commun.* **5**, (2014).

158. Wagner, E. F. & Nebreda, Á. R. Signal integration by JNK and p38 MAPK pathways in cancer development. *Nat. Rev. Cancer* **9**, 537–549 (2009).

159. Jiang, S. L. *et al.* Targeting translation regulators improves cancer therapy. *Genomics* **113**, 1247–1256 (2021).

160. Lelong, E. I. J. *et al.* Prostate cancer resistance leads to a global deregulation of translation factors and unconventional translation. *NAR Cancer* **4**, 1–21 (2022).

161. Huang, R. & Zhou, P. *DNA damage repair : historical perspectives , mechanistic pathways and clinical translation for targeted cancer therapy*. *Signal Transduction and Targeted Therapy* (Springer US, 2021). doi:10.1038/s41392-021-00648-7.

162. Moran, B., Idan, D., David, E. & Alexander, L. Enhanced ROS Production in Oncogenically Transformed Cells Potentiates c-Jun N-Terminal Kinase and p38 Mitogen-Activated Protein Kinase Activation and Sensitization to Genotoxic Stress. *Mol. Cell. Biol.* **21**, 6913–6926 (2001).

163. Li, Manqing., Kao, Elaine., Malone, D., Gao, Xia., Wang, Jean Y J., Diego, S. & Jolla, La., Jolla, La., Diego, San., Jolla, L. DNA damage-Induced cell death relies on SLFN11-dependent cleavage of distinct type II tRNAs. *Nat Struct Mol Biol.* **25**, 1047–1058 (2019).

164. Persons, D. L., Yazlovitskaya, E. M., Cui, W. & Pelling, J. C. Cisplatin-induced activation of mitogen-activated protein kinases in ovarian carcinoma cells: Inhibition of extracellular signal-regulated kinase activity increases sensitivity to cisplatin. *Clin. Cancer Res.* **5**, 1007–1014 (1999).

165. Sullivan, L. B., Gui, D. Y. & Van Der Heiden, M. G. Altered metabolite levels in cancer: Implications for tumour biology and cancer therapy. *Nat. Rev. Cancer* **16**, 680–693 (2016).

166. Vander Heiden, M. G. & DeBerardinis, R. J. Understanding the Intersections between Metabolism and Cancer Biology. *Cell* **168**, 657–669 (2017).

167. Butler, M., van der Meer, L. T. & van Leeuwen, F. N. Amino Acid Depletion Therapies: Starving Cancer Cells to Death. *Trends Endocrinol. Metab.* **32**, 367–381 (2021).

168. Parzych, K., Saavedra-García, Paula, Gabriel N. Valbuena, Hibah A. Al-Sadah, Mark E. Robinson, L. P., Kuzeva, D. M., Ruiz-Tellez, Angie, Sandra Loaiza Viktoria Holzmann Caputo, Valentina, D. C. J. & Kaiser, Martin F. Anastasios Karadimitris, Eric W-F Lam, Eric Chevet, Niklas Feldhahn, H. C. K. H. W. A. The coordinated action of VCP/p97 and GCN2 regulates cancer cell metabolism and proteostasis during nutrient limitation. *Oncogene* **38**, 3216–3231 (2019).

169. Sejeong Shin, Gwen R. Buel, Laura Wolgamott, David R. Plas, John M. Asara, John Blenis, and S.-O. Y. ERK2 mediates metabolic stress response to regulate cell fate Sejeong. *Mol Cell* **59**, 382–398 (2015).

170. Tameire, F. *et al.* ATF4 couples MYC-dependent translational activity to bioenergetic demands during tumour progression. *Nat. Cell Biol.* **21**, 889–899 (2019).

171. Ishimura, Ryuta., Nagy, Gabor., Dotu, Ivan., Zhou, Huihao., Yang, Xiang Lei., Schimmel, Paul., Senju, Satoru., Nishimura, Yasuharu., Chuang, Jeffrey H., Ackerman, S. L. Ribosome stalling induced by mutation of a CNS-specific tRNA causes neurodegeneration. *Science (80-.).* **345**, 455–459 (2014).

172. Zuko, Amila., Mallik, Moushami., Thompson, Robin., Spaulding, Emily L., Wienand, Anne R., Been, M., Tadenev, Abigail L.D., van Bakel, Nick., Sijlmans, Céline., Santos, Leonardo A., Bussmann, J. & Catinozzi, Das, Sarada., Kulshrestha, Divita., Burgess, Robert W., Ignatova, Zoya., Storkebaum, E. tRNA overexpression rescues peripheral neuropathy caused by mutations in tRNA synthetase. *Science (80-.).* **373**, 1161–1166 (2021).

173. Ahmed, N. & Stenvers, K. L. Getting to know ovarian cancer ascites : opportunities for targeted therapy-based translational research. *Front. Oncol.* **3**, 1–12 (2013).

174. Hua, W., Christianson, T., Rougeot, C., Rochefort, H. & Clinton, G. M. SKOV3 ovarian carcinoma cells have functional estrogen receptor but are growth-resistant to estrogen and antiestrogens. *J. Steroid Biochem. Mol. Biol.* **55**, 279–289 (1995).

175. Albert, Benjamin., Kos-Braun, Isabelle C., Henras, Anthony K., Dez, Christophe., Rueda, Maria Paula., Zhang, Xu., Gadal, Olivier., Kos, Martin., Shore, D. A ribosome assembly stress response regulates transcription to maintain proteome homeostasis. *Elife* **8**, 1–24 (2019).

176. Elizabeth V Nguyen 1 2 , Kaisa Huhtinen 2 2 , Young Ah Goo 3 , Katja Kaipio 2 , Noora Andersson 4 , Ville Rantanen 5 , Johanna Hynninen 6 , Riitta Lahesmaa 1 , Olli Carpen 2 4, D. R. G. Hyper-phosphorylation of Sequestosome-1 Distinguishes Resistance to Cisplatin in Patient Derived High Grade Serous Ovarian Cancer Cells. *Mol. Cell. Proteomics* **16**, 1377–1392 (2017).

177. Sung, M. K., Reitsma, J. M., Sweredoski, M. J., Hess, S. & Deshaies, R. J. Ribosomal proteins produced in excess are degraded by the ubiquitin-proteasome system. *Mol. Biol.*

Cell **27**, 2642–2652 (2016).

178. Zencir, S., Dilg, D., Rueda, M. P., Shore, D. & Albert, B. Mechanisms coordinating ribosomal protein gene transcription in response to stress. *Nucleic Acids Res.* **48**, 11408–11420 (2020).

179. Sang, G. P., Schimmel, P. & Kim, S. Aminoacyl tRNA synthetases and their connections to disease. *Proc. Natl. Acad. Sci. U. S. A.* **105**, 11043–11049 (2008).

180. Iordanov, M. S. *et al.* Ultraviolet radiation triggers the ribotoxic stress response in mammalian cells. *J. Biol. Chem.* **273**, 15794–15803 (1998).

181. Marchand, V. *et al.* AlkAniline-Seq: Profiling of m7 G and m3 C RNA Modifications at Single Nucleotide Resolution. *Angew. Chemie Internatioanl Ed.* doi:10.1002/anie.201810946.

182. Polte, C. *et al.* Assessing cell-specific effects of genetic variations using tRNA microarrays. *BMC Genomics* **20**, 1–12 (2019).

183. Yan, L. L. & Zaher, H. S. Ribosome quality control antagonizes the activation of the integrated stress response on colliding ribosomes. *Mol. Cell* **81**, 614-628.e4 (2021).

184. Meydan, S. & Guydosh, N. R. Disome and Trisome Profiling Reveal Genome-wide Targets of Ribosome Quality Control. *Mol. Cell* **79**, 588-602.e6 (2020).

185. Passarelli, M. C. *et al.* Leucyl-tRNA synthetase is a tumour suppressor in breast cancer and regulates codon-dependent translation dynamics. *Nat. Cell Biol.* **24**, 307–315 (2022).

186. Washington, C. R. & Moore, K. N. PARP inhibitors in the treatment of ovarian cancer: A review. *Curr. Opin. Obstet. Gynecol.* **33**, 1–6 (2021).

187. Jäckle Herbert, K. K. PHOTOSENSITIZED FORMATION OF RNA-PROTEIN CROSSLINKS IN AN INSECT EGG (S M I T T Z A SPEC ., CHIRONOMIDAE , DIPTERA)*. *Photochem. Photobiol.* **29**, 1039–1040 (1979).

188. Ramabhadran, T. V., Fossum, T. & Jagger, J. IN VIVO INDUCTION OF 4-THIOURIDINE-CYTIDINE ADDUCTS IN tRNA OF E. COLI B/r BY NEAR-ULTRAVIOLET RADIATION. *Photochem. Photobiol.* **23**, 315–321 (1976).

189. Olejniczak, M. & Uhlenbeck, O. C. tRNA residues that have coevolved with their anticodon to ensure uniform and accurate codon recognition. *Biochimie* **88**, 943–950 (2006).

190. Schmeing, T. M., Voorhees, R. M., Kelley, A. C. & Ramakrishnan, V. How mutations in tRNA distant from the anticodon affect the fidelity of decoding. *Nat. Struct. Mol. Biol.* **18**, 432–437 (2011).

191. Silva, R. C., Castilho, B. A. & Sattlegger, E. A Rapid Extraction Method for mammalian cell cultures, suitable for quantitative immunoblotting analysis of proteins, including phosphorylated GCN2 and eIF2α. *MethodsX* **5**, 75–82 (2018).

192. Kirchner, S. *et al.* Alteration of protein function by a silent polymorphism linked to tRNA abundance. *PLoS Biol.* **15**, (2017).

193. Dobin, A. *et al.* STAR: ultrafast universal RNA-seq aligner. *Bioinformatics* **29**, 15–21 (2013).

194. Marchand, V., Bourguignon-Igel, V., Helm, M. & Motorin, Y. Mapping of 7-methylguanosine (m7G), 3-methylcytidine (m3C), dihydrouridine (D) and 5-hydroxycytidine (ho5C) RNA modifications by AlkAniline-Seq. *Methods Enzymol.* **658**, 25–47 (2021).

195. Galvanin, A. & Lilia Ayadi, Mark Helm, Yuri Motorin, V. M. Mapping and Quantification of tRNA 2'-O-Methylation by RiboMethSeq. *Methods Mol Bio* **1870**, 273–295 (2019).

196. Pichot, F., Marchand, V., Helm, M. & Motorin, Y. Non-redundant trna reference sequences for deep sequencing analysis of trna abundance and epitranscriptomic rna modifications. *Genes (Basel).* **12**, 1–14 (2021).

197. Nagayoshi, Y. *et al.* Loss of Ftsj1 perturbs codon-specific translation efficiency in the brain and is associated with X-linked intellectual disability. *Sci. Adv.* **7**, (2021).

198. Dimitrova, D. G. *et al.* The ribose methylation enzyme FTSJ1 has a conserved role in neuron morphology and learning performance. *bioRxiv* 2021.02.06.430044 (2021).

199. Marchand, V., Bourguignon-Igel, V., Helm, M. & Motorin, Y. Analysis of pseudouridines and other RNA modifications using HydraPsiSeq protocol. *Methods* **203**, 383–391 (2022).

200. Ingen, E. Van *et al.* C / D box snoRNA SNORD113-6 / AF357425 plays a dual role in integrin signalling and arterial fibroblast function via pre-mRNA processing and 2 O-ribose methylation. *Hum. Mol. Genet.* **31**, 1051–1066 (2022).

201. Love, M. I., Huber, W. & Anders, S. Moderated estimation of fold change and dispersion for RNA-seq data with DESeq2. *Genome Biol.* **15**, 550 (2014).

202. Public Health England. Cell line profile. *Eur. Collect. Authenticated Cell Cult.* **60**, 4–5 (2016).

203. Mezencev, R. Interactions of Cisplatin with non-DNA Targets and their Influence on Anticancer Activity and Drug Toxicity: The Complex World of the Platinum Complex. *Curr. Cancer Drug Targets* **14**, 794–816 (2015).

204. Fuertes, M., Castilla, J., Alonso, C. & Pérez, J. Cisplatin Biochemical Mechanism of Action: From Cytotoxicity to Induction of Cell Death Through Interconnections Between Apoptotic and Necrotic Pathways. *Curr. Med. Chem.* **10**, 257–266 (2012).

205. Becker, J. P., Weiss, J. & Theile, D. Cisplatin, oxaliplatin, and carboplatin unequally inhibit in vitro mRNA translation. *Toxicol. Lett.* **225**, 43–47 (2014).

206. Roundtree, I. A., Evans, M. E., Pan, T., He, C. & Program, S. T. Dynamic RNA modifications in gene expression regulation Ian. *Cell* **169**, 1187–1200 (2017).

207. Gilbert, W. V & Bell, T. A. Messenger RNA modifications: Form, distribution, and function. **352**, (2016).

208. Jonkhout, N. *et al.* The RNA modification landscape in human disease. *RNA* **23**, 1754–1769 (2017).

209. Barbieri, I. & Kouzarides, T. Role of RNA modifications in cancer. *Nat. Rev. Cancer* **20**, 303–322 (2020).

210. Frye, M., Jaffrey, S. R., Pan, T., Rechavi, G. & Suzuki, T. RNA modifications: What have we learned and where are we headed? *Nature Reviews Genetics* (2016) doi:10.1038/nrg.2016.47.

211. Mathlin, J. & Pera, L. Le. A Census and Categorization Method of Epitranscriptomic Marks. (2020) doi:10.3390/ijms21134684.

212. Zaccara, S., Ries, R. J. & Jaffrey, S. R. Reading, writing and erasing mRNA methylation. *Nat. Rev. Mol. Cell Biol.* **20**, 608–624 (2019).

213. Fang, Z. *et al.* Role of m6A writers, erasers and readers in cancer. *Exp. Hematol. Oncol.* **11**, 1–20 (2022).

214. Huang, H., Weng, H. & Chen, J. Review m 6 A Modification in Coding and Non-coding RNAs : Roles and Therapeutic Implications in Cancer. *Cancer Cell* **37**, 270–288 (2020).

215. Wang, T., Kong, S., Tao, M. & Ju, S. The potential role of RNA N6-methyladenosine in Cancer progression. *Mol. Cancer* **19**, 1–18 (2020).

216. Oerum, S., Meynier, V., Catala, M. & Tisne, C. A comprehensive review of m6A/m6Am RNA methyltransferase structures. *Nucleic Acids Res.* **49**, 7239–7255 (2021).

217. Zhang, Y. *et al.* M6A modification in RNA: Biogenesis, functions and roles in gliomas. *J. Exp. Clin. Cancer Res.* **39**, 1–16 (2020).

218. Hong, J., Xu, K. & Lee, J. H. Biological roles of the RNA m 6 A modi fi cation and its implications in cancer. *Exp. Mol. Med.* **54**, 1822–1832 (2022).

219. Zhao, W. *et al.* Epigenetic Regulation of m6A Modifications in Human Cancer. *Molecular Therapy - Nucleic Acids* vol. 19 405–412 (2020).

220. Gu, C. *et al.* RNA m6A Modification in Cancers: Molecular Mechanisms and Potential Clinical Applications. *Innovation* **1**, 100066 (2020).

221. Huang, H., Weng, H., Deng, X. & Chen, J. RNA Modifications in Cancer: Functions, Mechanisms, and Therapeutic Implications. *Annu. Rev. Cancer Biol.* **4**, 221–240 (2020).

222. Sun, T., Wu, R. & Ming, L. The role of m6A RNA methylation in cancer. *Biomed. Pharmacother.* **112**, 108613 (2019).

223. Sun, T., Wu, R. & Ming, L. The role of m6A RNA methylation in cancer. *Biomedicine and Pharmacotherapy* vol. 112 (2019).

224. Chang, L. L. *et al.* Emerging role of m6A methylation modification in ovarian cancer. *Cancer Cell Int.* **21**, 1–16 (2021).

225. Guo, J., Zheng, J., Zhang, H. & Tong, J. RNA m6A methylation regulators in ovarian cancer. *Cancer Cell Int.* **21**, 1–13 (2021).

226. Fukumoto, T. *et al.* N6-methylation of adenosine of FZD10 mRNA contributes to PARP inhibitor resistance. *Cancer Res.* **79**, 2812–2820 (2019).

227. Gao, R. *et al.* m6A Modi fi cation : A Double-Edged Sword in Tumor Development. *Front. Oncol.* **11**, 1–12 (2021).

228. Shi, H., Wei, J. & He, C. Where , When , and How : Context-Dependent Functions. *Mol. Cell* **74**, 640–650 (2019).

229. Wei, J. *et al.* Mediated by FTO in the Cell Nucleus and Cytoplasm Differential m 6 A , m 6 A m , and m 1 A Demethylation Mediated by FTO in the Cell Nucleus and Cytoplasm. *Mol. Cell* **71**, 973-985.e5 (2018).

230. Zeng, W. *et al.* Discovery of cisplatin binding to thymine and cytosine on a single-stranded oligodeoxynucleotide by high resolution FT-ICR mass spectrometry. *Molecules* **24**, 1–15 (2019).

231. Domcke, S., Sinha, R., Levine, D. A., Sander, C. & Schultz, N. Evaluating cell lines as tumour models by comparison of genomic profiles. *Nat. Commun.* **4**, (2013).

232. Relier, S. *et al.* FTO-mediated cytoplasmic m6Am demethylation adjusts stem-like properties in colorectal cancer cell. *Nat. Commun.* (2021) doi:10.1038/s41467-021-21758-4.

233. Wei, J. *et al.* Differential m 6 A, m 6 A m , and m 1 A Demethylation Mediated by FTO in the Cell Nucleus and Cytoplasm. *Mol. Cell* **71**, 973-985.e5 (2018).

234. Kukurba, K. R. & Montgomery, S. B. RNA Sequencing and Analysis. *Handb. Mol. Cell. Methods Biol. Med. Third Ed.* **2015**, 951–969 (2016).

235. Garalde, D. R. *et al.* Highly parallel direct RN A sequencing on an array of nanopores. *Nat. Methods* (2018) doi:10.1038/nmeth.4577.

236. Wang, Y., Zhao, Y., Bollas, A., Wang, Y. & Au, K. F. Nanopore sequencing technology, bioinformatics and applications. *Nat. Biotechnol.* **39**, 1348–1365 (2021).

237. Smith, A. M., Abu-Shumays, R., Akeson, M. & Bernick, D. L. Capture, Unfolding, and Detection of Individual tRNA Molecules Using a Nanopore Device. *Front. Bioeng. Biotechnol.* (2015) doi:10.3389/fbioe.2015.00091.

238. Workman, R. E. *et al.* Nanopore native RNA sequencing of a human poly(A) transcriptome. *Nat. Methods* **16**, 1297–1305 (2019).

239. Xie, S. *et al.* Applications and potentials of nanopore sequencing in the (epi)genome and (epi)transcriptome era. *Innov.* **2**, 100153 (2021).

240. Raina, M. & Ibba, M. tRNAs as regulators of biological processes. **5**, 1–14 (2014).

241. Schimmel, P. The emerging complexity of the tRNA world : mammalian tRNAs beyond protein synthesis. *Nat. Publ. Gr.* **19**, 45–58 (2017).

242. Kirchner, S. & Ignatova, Z. Emerging roles of tRNA in adaptive translation, signalling dynamics and disease. *Nat. Rev. Genet.* **16**, 98–112 (2015).

243. Dittmar, K. A., Goodenbour, J. M. & Pan, T. Tissue-specific differences in human transfer RNA expression. *PLoS Genet.* (2006) doi:10.1371/journal.pgen.0020221.

244. Pan, T. Modifications and functional genomics of human transfer RNA. *Cell Res.* **28**, 395–404 (2018).

245. Suzuki, T. The expanding world of tRNA modifications and their disease relevance. *Nat. Rev. Mol. Cell Biol.* **22**, 375–392 (2021).

246. Abbott, J. A., Francklyn, C. S. & Robey-bond, S. M. Transfer RNA and human disease. **5**, 1–18 (2014).

247. Goodarzi, Hani, Nguyen, Hoang C.B. Nguyen Zhang, Steven, Dill, Brian D., Molina, H. T. S. F. Modulated Expression of Specific tRNAs Drives Gene Expression and Cancer Progression. *Cell* **165**, 1416–1427 (2016).

248. Simms, C. L., Mcloughlin, F., Vierstra, R. D. & Zaher, H. S. Oxidation and alkylation stresses activate ribosome-quality control. *Nat. Commun.* 1–15 doi:10.1038/s41467-019-13579-3.

249. Santos, M., Fidalgo, A., So, A., Oliveira, C. & Santos, M. A. S. tRNA Deregulation and Its Consequences in Cancer. 1–13 (2019) doi:10.1016/j.molmed.2019.05.011.

250. Zhang, Z. *et al.* Global analysis of tRNA and translation factor expression reveals a dynamic landscape of translational regulation in human cancers. *Commun. Biol.* 1–11 (2018) doi:10.1038/s42003-018-0239-8.

251. Zdeněk Paris, Ian M.C. Fleming, and J. D. A. Determinants of tRNA editing and modification: avoiding conundrums, affecting function. *Semin Cell Dev Biol.* **23**, 269–274 (2012).

252. Wilusz, J. E. Removing roadblocks to deep sequencing of modified RNAs. *Nat. Methods* **12**, 821–822 (2015).

253. Smith, A. M., Jain, M., Mulroney, L., Garalde, D. R. & Akeson, M. Reading canonical and modified nucleotides in 16S ribosomal RNA using nanopore direct RNA sequencing. *PLoS One* **14**, 1–15 (2017).

254. Kirchner, S., Rauscher, R. & Czech, A. Microarray-Based Quantification of Cellular tRNAs Epigenetic regulation of stage transitions and commitment to sexual development in Plasmodium View project Investigation into the role of silent mutations in CFTR biogenesis View project. (2017) doi:10.17504/protocols.io.hfcb3iw.

255. Highly parallel direct RNA sequencing on an array of nanopores.

256. https://community.nanoporetech.com/docs/prepare/library_prep_protocols/ss-direct-rna-sequencing-sqk-rna002/v/dss_9081_v2_revr_25may2022/library-preparation?devices=minion.

257. Thomas, Niki K., Poodari, Vinay C., Jain, Miten, Olsen, Hugh E., Akeson, Mark., Abu-Shumays, R. L. Direct Nanopore Sequencing of Individual Full Length tRNA Strands. *ACS Nano* **15**, 16642–16653 (2021).

258. Tafolla, E., Wang, S., Wong, B., Leong, J. & Kapila, Y. L. JNK1 and JNK2 oppositely regulate p53 in signaling linked to apoptosis triggered by an altered fibronectin matrix: JNK links FAK and p53. *J. Biol. Chem.* **280**, 19992–19999 (2005).

259. Melstrom, L. & Chen, J. RNA N 6-methyladenosine modification in solid tumors: new therapeutic frontiers. *Cancer Gene Therapy* (2020) doi:10.1038/s41417-020-0160-4.

260. Liu, Z. *et al.* Biological and pharmacological roles of - m 6 A modifications in cancer drug resistance. *Mol. Cancer* 1–20 (2022) doi:10.1186/s12943-022-01680-z.

261. Wen, L., Pan, X., Yu, Y. & Yang, B. Down-regulation of FTO promotes proliferation and migration, and protects bladder cancer cells from cisplatin-induced cytotoxicity. *BMC Urol.* **20**, 39 (2020).

262. Relier, S., Rivals, E. & David, A. The multifaceted functions of the Fat mass and Obesity-associated protein (FTO) in normal and cancer cells. *RNA Biol.* **19**, 132–142 (2022).

263. Wei, J. *et al.* Differential m 6 A , m 6 A m , and m 1 A Demethylation Mediated by FTO in the Cell Nucleus and Cytoplasm. *Mol. Cell* **71**, 973-985.e5 (2018).

264. Leger, A. *et al.* RNA modifications detection by comparative Nanopore direct RNA sequencing. *Nat. Commun.* **12**, 1–17 (2021).

265. Wang, Y. *et al.* Structural-profiling of low molecular weight RNAs by nanopore trapping/translocation using Mycobacterium smegmatis porin A. *Nat. Commun.* **12**, 1–14 (2021).

266. Lucas, M. C. *et al.* Quantitative analysis of tRNA abundance and modifications by nanopore RNA sequencing. (2023) doi:10.1038/s41587-023-01743-6.

267. Schaefer, M., Kapoor, U., Jantsch, M. F. & Schaefer, M. Understanding RNA modifications : the promises and technological bottlenecks of the ‘ epitranscriptome ’. (2017).

268. https://gestis.dguv.de/data?name=010520 (2023).

List of hazardous substances

The table below gives an overview of the substances which were used during this dissertation, characterized by GHS pictograms, signal words, hazard and precautionary statements [268].

Substance	Pictogram	Signal word	Hazard statements	Precautionary statements
2-[4-(2-hydroxy-ethyl)piperazin-1-yl] ethane-sulfonic acid (HEPES)		Not a dangerous substance according to GHS		
2-Mercaptoethanol		Danger	301+331, 310, 315, 317, 318, 373, 410	273, 280, 302+352, 304+340, 305+351+338, 308+310
Acetone		Danger	225, 319, 336	201, 305+351+338, 370+378, 403+235
Acrylamide/ Bis-acrylamide		Danger	302+332, 315, 317, 319, 340, 350, 361f, 372	201, 261, 280, 304+340+312, 305+351+338, 308+313
Agarose		Not a dangerous substance according to GHS		
Ammonium acetate		Not a dangerous substance according to GHS		
Ammonium persulfate		Danger	272, 302, 315, 317, 319, 334, 335	220, 261, 280, 305+351+338, 342+311
Ampicillin		Danger	315, 317, 319, 334, 335	261, 280, 305+351+338, 342+311
Bromophenol blue		Not a dangerous substance according to GHS		
Chloramphenicol		Warning	351	280
Chloroform		Danger	302, 331, 315, 319, 351, 361d, 336, 372	261, 281, 305+351+338, 311
Cisplatin		Danger	300, 312, 315, 318, 332, 335, 350	330, 302+352, 304+340, 332+313, 305+351+338, 310, 280
D-Glucose		Not a dangerous substance according to GHS		

Substance	Pictogram	Signal word	Hazard statements	Precautionary statements
Dimethyl sulfoxide		Not a dangerous substance according to GHS		
Dimethyl sulfate		Danger	301, 314, 317, 330, 341, 350	201, 280, 301+330+331, 302+352, 304+340, 305+351+338, 308+310
Dithiothreitol		Warning	302, 315, 319, 335	261, 305+351+338
Ethanol		Danger	225, 319	210, 240, 305+351+338, 403+233
Ethidium bromide		Danger	332, 341	281-308+313
Ethylenediamine-tetraacetic acid		Warning	319, 332, 373	280, 304+340, 312, 305+351+338, 337+313
Folinic acid		Danger	315, 317, 319, 334, 335	261, 280, 305+351+338, 342+311
Formaldehyde		Danger	301+311+331, 314, 317, 335, 341, 350, 370	201, 280, 301+330+331, 303+361+353, 304+340, 305+351+338, 308+P310
Formamide		Danger	315, 360D, 373	201, 314
Glycerol		Not a dangerous substance according to GHS		
Glycin		Warning	315, 319, 335	261, 305+351+338
Hydrogen peroxide (30%)		Danger	302, 318	280, 305+351+338, 313
Isopropyl alcohol		Danger	225, 319, 336	210, 233, 240, 305+351+338, 403+235
LB-Agar		Not a dangerous substance according to GHS		
LB-Medium		Not a dangerous substance according to GHS		
Luminol		Not a dangerous substance according to GHS		
Magnesium acetate		Not a dangerous substance according to GHS		
Magnesium chloride		Not a dangerous substance according to GHS		

Substance	Pictogram	Signal word	Hazard statements	Precautionary statements
Methanol		Danger	225, 301+311+331, 370	210, 233, 280, 301+310, 303+361+353, 304+340+311
MTT (3-(4,5-Dimethyl-2-thiazolyl)-2,5-diphenyltetrazolium bromide)		Warning	315, 319, 335, 341	201, 202, 261, 302 + 352 , 305 + 351 + 338, 308 + 313
p-Coumaric acid		Warning	315, 319, 335	261, 305+351+338
PEG 8000	Not a dangerous substance according to GHS			
Phenol		Danger	301+311+331, 314, 341, 373, 411	260, 280, 301+330+331+310, 303+361+353, 304+340+310, 305+351+338
Phosphoenol-pyruvate	Not a dangerous substance according to GHS			
Potassium acetate	Not a dangerous substance according to GHS			
Potassium chloride	Not a dangerous substance according to GHS			
Potassium dihydrogen phosphate	Not a dangerous substance according to GHS			
RedSafe	Not a dangerous substance according to GHS			
Sodium acetate	Not a dangerous substance according to GHS			
Sodium azide		Danger	300+310, 373, 410	273, 280, 301+310+330, 302+352+310, 391, 501
Sodium chloride	Not a dangerous substance according to GHS			
Sodium dodecyl sulfate		Danger	228, 302+332, 315, 318, 335, 412	210, 261, 280, 301+312+330, 305+351+338+310, 370+378
Sodium hydrogen phosphate	Not a dangerous substance according to GHS			
SYBR Gold		Warning	227	210, 280, 370+378
Tetramethyl-ethylenediamine		Danger	225, 332, 302, 314	210, 280, 305+351+338, 310

Substance	Pictogram	Signal word	Hazard statements	Precautionary statements
Thiamine		Not a dangerous substance according to GHS		
TRIS acetate		Not a dangerous substance according to GHS		
Trisodium citrate		Not a dangerous substance according to GHS		
Triton X-100		Danger	302, 315, 318, 410	264, 273, 280, 301, 312, 302, 352, 305, 351, 338
TRIzol		Danger	301+311+331, 314, 335, 341, 373, 412	201, 261, 264, 280, 273, 301+310, 302+352, 303+361+353, 304+340, 305+351+338
Tween 20		Not a dangerous substance according to GHS		
Urea		Not a dangerous substance according to GHS		
Xylene cyanol FF		Warning	315, 319, 335	261, 305+351+338

Acknowledgement

First and foremost, I would like to express my sincere gratitude to my supervisor, Prof. Zoya Ignatova, for giving me the opportunity to work on this project and for her unwavering support, guidance, and encouragement throughout this journey. I immensely value her contribution, in formulation of the project, the continuous scientific discussions, for providing a stimulating work environment and independence to implement ideas and for being there always whenever I needed her.

I would like to extend my gratitude to Prof Meliha Karsak, who kindly reviewed this work.

I am thankful to my collaborators, whose contributions have made this work possible and the students, Raya, Pablo and Stine, who have supported me during the course of this dissertation. I am deeply grateful to Dr Thomas Gorochowski who introduced me to the world of nanopore sequencing.

A note of thanks to my colleagues, former and present members of the working group. I have had the privilege of working with so many wonderful people and I am grateful for the intellectual exchange, discussions, and debates that have enriched my thinking and broadened my perspective. Times spent with the team will always be cherished. Sincere appreciation to Leonardo Santos, who performed the bioinformatic analysis presented in this work. Thanks to our amazing technicians Christine Polte and Patrick John without whom proper functioning of the lab would be impossible.

Finally, I thank my family for their selfless support, patience, for believing in me and being a constant source of encouragement, which gave me the strength to come all the way through.

Eidesstattliche Versicherung

Hiermit erkläre ich an Eides statt, die vorliegende Dissertation selbst verfasst und keine anderen als die angegebenen Hilfsmittel benutzt zu haben. Ich versichere, dass diese Dissertation nicht in einem früheren Promotionsverfahren eingereicht wurde.

Hamburg, den

Priyanka Nair